THE AXL INHIBITOR TP-0903 AND ARTESUNATE SYNERGISE TO INDUCE REACTIVE OXYGEN SPECIES, DNA DAMAGE AND APOPTOSIS IN TRIPLE NEGATIVE BREAST CANCER CELLS

MIRKO

TERRAGNO

Submitted in partial fulfillment of the requirements for the degree of

Doctor of Philosophy in Biomedical Science

School of Medicine

Nazarbayev University

Supervised by

Dr Eugene Tulchinsky

January 2024

Declaration

I declare that the research contained in this thesis, unless otherwise formally indicated within the text, is the author's original work. The thesis has not been previously submitted to this or any other university for a degree and does not incorporate any material already submitted for a degree.

Signature

Date

15/01/2024

Aknowledgment

The first special thanks is for my supervisor Dr Eugene Tulchinsky. I am grateful to him for giving the opportunity to test the therapeutics and for expanding my theoretical and practical knowledge. I will always remember the opportunity he gave me to do a PhD.

Thanks to Dr Marina Kriajevskaia for her continuous discussion and comparison of opinions.

Thanks to the RAs Nurken Berdigaliyev and Anton Borossenko for their support in the experimental setting.

Thanks to the support from Ilona Malikova and all members of my group I met during these years.

Thanks to LAs for their punctuality in giving what was necessary to conduct experiments.

Table of contents

CHAPTER 4:

List of tables

List of figures

Acronyms

ADR	multidrug resistant
AML	acute myeloid leukemia
AP-1	activating protein 1
ART	artesunate
ATM	ataxia and telangiectasia mutated
Bad	bcl-2 associated agonist of cell death
Bax	bcl-2-associated X protein
Bcl-2	B-cell leukemia/lymphoma 2 protein
Bcl-xl	B-cell lymphoma-extra large
Bim	BH3-only Bim protein
BRCA1/2	breast cancer predisposition gene 1/2
CAT	catalase
CD	cluster of differentiation
CHOP	C/EBP homlogous protein
CI	combination index
CLL	B-cell chronic lymphocytic leukemia
CML	chronic myelogenous leukemia
CRC	colorectal cancer
DHA	dihydroartemisinin
DDR	DNA damage repair
Dox	doxycycline
DSBs	DNA double strand breaks
EGF/EGFR	epidermal growth factor/receptor
EMT	epithelial mesenchymal transition
ER	endoplasmic reticulum
ESRs/PgRs	estrogen /progesterone receptors
ERK	extracellular signal-regulated kinase
Fas	Fas cell surface death receptor
FGF/R	fibroblast growth factor/receptor
GAS6	growth arrest-specific gene 6
GPX	glutathione peroxidase
GSK3 beta	glycogen synthase kinase 3 beta
HCC	hepatocellular carcinoma
HDAC	histone deacetylase
HER2	human epidermal receptor 2
HGF/R	hepatocyte growth factor/receptor
HIF-1 alpha	hypoxia inducible factor alpha
HNSCC	head and neck squamous cell carcinoma
HR	homologous recombination
IL	interleukin
JAK	janus kinase
JNK	C-Jun N-terminal kinase
KRAS	Kristen rat sarcoma viral oncogene homolog
mAb	monoclonal antibody
MAPK	mitogen-activated protein kinase
MDR	multidrug resistance protein
MEK	mitogen-activated extracellular signal-regulated kinase
MET	mesenchymal-to-epithelial transition
MMPs	matrix metalloproteinases

MYB	myeloblastosis viral oncogene homolog
MYC	myelocytomatosis
NAC	N-acetylcysteine
NB	neuroblastoma
NF-k beta	nuclear factor-κB
NRF2	nuclear factor erythroid-derived 2
NSCLC	non-small cell lung cancer
PARP	poly-ADP-ribose-polymerase
PDGF/R	platelet-derived growth factor/receptor
PD1/L1	programmed cell death protein 1/ligand 1
pH2AX	phospho H2A histone family member X
PI3K/AKT	phosphatidylinositol 3-OH kinase/Ak strain transforming
PKC	protein kinase C
Rac	RAS-related C3 botulinum toxin substrate
Rad51	Rad51 recombinase
ROS	reactive oxygen species
RTKs	receptor tyrosine kinases
SOD	superoxide dismutase
STAT	signal transducer and activator of transcription
Src	sarcoma protein kinase
TGF-β	tumor growth factor β
TKIs	tyrosine kinase inhibitors
TNBC	triple negative breast cancer
VEGF/R	vascular endothelial growth factor/receptor
VIM	vimentin
wt	wild type

CHAPTER 1: ABSTRACT

Triple Negative Breast Cancer (TNBC) is an aggressive, often rapidly growing form of breast cancer. TNBC usually displays a basal molecular phenotype that associates with epithelial mesenchymal transition (EMT), a cellular program that confers chemoresistance and metastasis. Approximately 56% of TNBC cases show a basal-like gene expression profile and roughly 46% of TNBC patients have distant metastasis. In general, the absence of molecular targets in TNBC is the main obstacle for the development of an effective therapy. For example, TNBC does not respond to endocrine and anti-human epidermal receptor (HER2) treatments as it does not express estrogen and progesterone receptors (ESR/PgR) and human epidermal receptor 2 (HER2). In addition, though initially TNBC is more responsive to cytotoxic drugs compared to other subtypes, TNBC presents a higher relapse rate. Therefore, new anti-TNBC treatment strategies are urgently needed. Drug combination therapy for TNBC could rely on protocols whereby EMT reversal sensitizes TNBC to anti-cancer compounds that are effective against epithelial tumors. Recently, the anti-malaria compound Artesunate (ART) has been shown to exert cytotoxicity in breast cancer by generating reactive oxygen species (ROS) and DNA double strand breaks (DSBs). However, the effect was more pronounced in tumors of epithelial than mesenchymal origin. In this project, the hypothesis was to verify whether EMT inhibition could sensitize TNBC cell lines to ART cytotoxicity. To address this, two aims were pursued. Aim 1 verified whether receptor tyrosine kinase (RTK) AXL inhibitors TP-0903/R428 and AXL/ZEB1 knockdown sensitised TNBC cell lines to ART-generated ROS, DNA damage and apoptosis. Aim 2 was to test whether TP-0903 and AXL/ZEB1 knockout in TNBC cell lines suppressed expression of superoxide dismutase 1/2 (SOD1/2), glutathione peroxidase 8 (GPX8) and catalase (CAT).

First, ART cytotoxicity was tested in a panel of breast cancer cell lines and it was found that TNBC cell lines with mesenchymal characteristics exhibited reduced apoptotic response to ART treatment. Next, inhibition of the EMT marker AXL did not sensitise TNBC to ART while partial reversion of mesenchymal phenotype in TNBC cell lines by depletion of a master regulator of EMT, ZEB1, significantly increased sensitivity to ART. Likewise, in reverse experiments, ectopic expression of ZEB1 in epithelial MCF-7 cells resulted in ART resistance concomitant with the induction of EMT. ZEB1-mediated survival of ART-treated cells directly correlated with the reduction in ROS and pH2AX levels. In MCF-7/ZEB1 cells, ZEB1 suppressed E-cadherin while activating expression of the two antioxidant genes SOD2 and GPX8. CAT was not affected. These findings suggested that EMT reversal through ZEB1

inhibition could sensitise TNBC to ROS-generating compounds, such as ART, by suppressing ROS detoxification.

Then, it was tested the cooperation between ART and clinically used compounds known to induce mesenchymal-epithelial transition (MET) in breast cancer cells. The two small molecule inhibitors of the RTK AXL, R428 and TP-0903, currently undergoing a number of Phase I and II clinical trials, were chosen. AXL is expressed in most TNBC tissues and cell lines; it is implicated in drug resistance and is known as a determinant of mesenchymal phenotype in breast cancer cells. TP-0903 and not R428 inhibited AXL phosphorylation, reduced expression of the EMT transcription factors Snail, Slug and ZEB1, increased E-cadherin and cooperated with ART in the induction of ROS, pH2AX and apoptosis in TNBC cells. Importantly, the CompuSyn software, that evaluates the type of drug interaction, has shown that in a sequential treatment, TP-0903 synergized with lower ART concentrations to decrease cell viability while in a simultaneous combination TP-0903 synergised with higher ART concentrations.

Overall, my data shown that induction of EMT in epithelial breast cancer cells by ZEB1 is accompanied by suppression of E-cadherin and upregulation of genes involved in the detoxification of ROS. Supposedly, this represents a mechanism of ZEB1-mediated resistance to ROS-producing compound ART in MCF-7 cells. In TNBC cells, ZEB1 knockdown increased E-cadherin and synergised with ART to induce apoptosis but surprisingly ZEB1 knockdown did not reverse expression of SOD2 and GPX8. Similarly, CAT was not decreased. The powerful inducer of MET TP-0903 induced total ROS and suppressed GPX8 and CAT while SOD2 was slightly reduced. A combination of TP-0903 and ART significantly suppressed GPX8 and SOD2. These findings suggested that the synergistic interactions between TP-0903 and ART could involve factors that are different from the ZEB1- antioxidant pathway. However, stably ZEB1 depleted cells had a relevant higher basal total ROS compared to ZEB1 expressing cells.

ART has been shown to generate DNA double strand breaks via ROS. TP-0903, but not ZEB1 knockdown, reduced expression of the DNA damage repair (DDR) Rad51 recombinase (Rad51). This observation was in line with my findings that pre-treatment with TP-0903 followed by ART was more effective than simultaneous treatment of TNBC cells with both agents.

In conclusion, TP-0903 AXL inhibition and ZEB1 knockdown induced MET and sensitised TNBC cells to ART likely via different pathways. The synergistic interaction between TP-0903 and ART suggests that a combination of both componuds could treat

TNBC. However, TP-0903 plus ART significantly enhanced ROS and this could be toxic in highly proliferative tissues of the body. Further research involving mouse models with TNBC will define toxicity/safety of TP-0903/ART combination.

CHAPTER 2: INTRODUCTION

2.1. TNBC

2.1.1. Clinical classification

Breast cancer is a heterogeneous disease that includes several molecular subtypes, luminal A, luminal B, human epidermal receptor 2 (HER2)-positive, triple negative breast cancer (TNBC) and others (Yin et al., 2020). The TNBC subtype is termed triple negative as it does not express estrogen, progesterone receptors (ESR/PgR) and human epidermal receptor 2 (HER2) (De Ruijer et al., 2011) and is generally classified as a single basal-like group (Yin et al., 2020). However, gene expression profiles, histological and clinical assessments of tumor samples revealed that TNBC presents intrinsic heterogeneity (De Ruijer et al., 2011). Most TNBC cases are high-grade, poorly differentiated and show considerable lymphocyte infiltration and poor prognosis (Marotti et al., 2017). Therefore, TNBC is an advanced and invasive breast cancer subtype.

2.1.2. TNBC: genetic and molecular features

Accumulation of gene mutations and dysregulation of signaling pathways have been found in TNBC. Pinilla et al., (2022) reports that approximately 10–20% of TNBC cases have mutations of the DNA damage repair (DDR) genes breast cancer type 1 susceptibility protein 1/2 (BRCA 1/2), Rad51 recombinase (Rad51) and the partner and localizer of BRCA2 (PALB2) (Pinilla et al., 2022). Other DDR related genes mutated are phosphatase and tensin homolog deleted (PTEN), retinoblastoma 1 (RB1) and tumor protein 53 (TP53) (Yin et al., 2020). TNBC presents high expression of: genes regulating the cell cycle, such as myelocytomatosis protein (MYC), phosphatidylinositol 3-OH kinase (PIK3), Kristen rat sarcoma viral oncogene homolog (KRAS), fibroblast growth factor/receptor 1 (FGFR1); genes modulating stemness, such as aldheyde dehydrogenase 1 (ALDHA1), genes associated with the differentiation-related signaling pathways Wnt/beta catenin and transforming growth factor (TGF)-beta (Yin et al., 2020). The RAS/ mitogen-activated protein kinase (MAPK) and Janus Kinase (JAK)/signal transducer and activator of transcription (STAT3) pathways are commonly active in TNBC (Pinilla et al., 2022). In addition, vascular endothelial factor A (VEGF-A) and epithelial growth factor receptor (EGFR) are overexpressed in TNBC (Pinilla et al. 2022). Though many advancements in the molecular characterisation of TNBC have been achieved, further understanding of TNBC molecular complexity is necessary for the design of personalised treatment schemes.

2.1.3. Classification in sub-types

A consensus molecular subtype analysis classified TNBC into the subtypes "stem-like (SL), mesenchymal-like (ML), immunomodulatory (IM) and luminal-androgen receptor (LAR)". The SL subtype presented overexpression of the stemness factors "suppressor of cytokine signaling 1 (SOCS1), octamer-binding transcription factor 4 (OCT4) and nanog homeobox (NANOG)" while MYC overexpressed both in SL and IM subtypes (Kim et al. 2020). Lehmann et al., (2011) conducted a gene expression analysis of 21 breast cancer data sets and they identified six TNBC subtypes, such as "basal-like 1 and 2 (BL1 and BL2), immunomodulatory (IM), mesenchymal, mesenchymal stem-like (MSL), and luminal androgen receptor (LAR)". The BL1 subtype presented overexpression of cell cycle and DNA damage repair regulators while BL2 subtype had higher expression of growth factors. The IM subtype displayed enhanced immune cell response, the mesenchymal and MSL sub-types presented EMT related features and the LAR subtype was associated with an increased activity of androgen-receptor (Lehman et al., 2011). It is important to note that a gene expression analysis can suggest which treatment would be more beneficial to each patient after identification of specific tumor biomarkers.

2.1.4. Epidemiology and treatment

TNBC includes approximately 24% of all breast cancer cases and younger women are more susceptible (median age lower than 50 years) (Marotti et al., 2017). TNBC patients have generally lower overall survival and breast-cancer-specific survival compared to non-TNBC patients (De Ruijer et al., 2011). Parikh et al. (2008) showed that in TNBC the median time to relapse was 1,2 years shorter than that in non TNBC. The overall five-year survival was 81% for TNBC and 91% for non TNBC (Kaplan and Malmgren, 2008). The absence of molecular targets in TNBC is the main issue in the development of an effective therapy (Marotti et al., 2017). In the treatment of TNBC, chemotherapy is frequently combined with surgery and radiation. As for chemotherapy, cytotoxic agents include "antibutulins (paclitaxel, docetaxel), anthracyclines (doxorubicin, epiribucin), alkylating agents (cyclophosphamide), antimetabolites (methotrexate, gemcitabine), and platinums (carboplatin, cisplatin)" (Andreopoulou et al., 2015). The targeted therapies include poly-ADP-ribose-polymerase (PARP1) and EGFR inhibition. The PARP inhibitor olaparib (AZD2281) has been shown efficient in breast cancer with mutated BRCA1/2 genes in a phase I trial while a combination of the PARP inhibitor BSI-201 with gemcitabine and carboplatin increased the overall survival in a randomised phase II trial (de Ruijter et al., 2011). In addition, patients with

metastatic TNBC responded to treatment with "immune-modulating agents, anti-PD-L1 antibody (pembrolizumab) cytotoxic T-lymphocyte antigen 4 (CTLA-4) inhibitors, anti-angiogenic agent bevacizumab, histone deacetylase (HDAC) and PI3K inhibitors" (Andreopoulou et al., 2015; Cortes et al. 2022). However, though TNBC initially responds to anticancer therapies, the extent of relapse is high and therefore, new anti-TNBC strategies are required to treat TNBC more efficiently.

2.2. The RTK AXL: structure, regulation and functions

In cancer, receptor tyrosine kinsases (RTKs) are aberrantly dysregulated to promote tumor growth and metastasis. Generally, tyrosine kinases are of two groups, the receptor tyrosine kinases (RTKs) and the non-receptor tyrosine kinases (NRTK). In comparison to the NRTK that locate into the cytoplasm, the RTKs are inserted into the membrane. The RTK extracellular region is bound by a ligand to induce RTK dimerization and autophosphorylation in correspondence of the intracellular ATP binding domain that also represents a docking site for some cytoplasmic signaling proteins. Activation of such proteins induces a signaling cascade to increase or suppress cellular mechanisms and functions (Paccez et al., 2014). The RTK AXL is a member of the TAM family also including Tyro3 and Mer (Paccez et al. 2014). The AXL gene locates in the chromosome 19 and there are 20 exons encoding the receptor. The exon 10 after alternative splicing can produce two AXL isoforms and the 5'upstream region is GC rich and does not present the TATA and CAAT boxes. The AXL promoter, "from –556 to –182 bp core region", can be bound by specificity proteins transcription factors (Sp) (five binding sites), myeloid zinc finger protein (MZF1) and activator protein (AP-1) (one binding site for each). AXL can be methylated "at the 19 CpG sites located in the AXL promoter region" that decreases AXL expression (Paccez et al., 2014). In addition, AXL expression is suppressed by miR-34a and miR-199a/b (Mudduluru et al., 2011).

The AXL gene encodes a receptor that has a molecular weight of 140 kDa and is ubiquitously present in many cell types. AXL was firstly identified in chronic myelogenous leukemia (CML) (Paccez et al., 2014). The AXL extracellular domain has "two N-terminal immuno-globulin (Ig)-like domains and two fibronectin Type III(FNIII) repeats", reflecting the cadherins and immunoglobines structure (Paccez et al., 2014). "The TAM family-specific KW(I/L)A(I/L)ES sequence" is found in the AXL intracellular domain and is crucial for activation of the kinase activity (Axelrod and Pienta, 2014) (Fig. 1A). AXL binds the ligand vitamin K-dependent protein Growth Arrest-Specific gene 6 (GAS6). GAS6 has the gamma-

carboxy-glutamic acid residues (Gla) in the N-terminal region for cell membrane contact and the laminin G-like domains (LG) in the C-terminal region that bind the Ig-like domains of AXL (Axelrod and Pienta, 2014) (Fig. 1B). After binding GAS6, AXL dimerises and tyrosines Y698, Y702 and Y703 are phosphorylated. Then, the tyrosine Y779, 821 and 866 are phosphorylated generating docking sites for adaptor proteins (Lauter et al., 2019). The AXL/GAS6 signaling can induce STAT, nuclear factor κB (NF-κB) and MAPK pathways that regulate survival, migration and proliferation (Colavito, 2020) (Fig. 2). AXL can also be activated via heterodimerization with other RTKs, such as EGFR, HER2, platelet-derived growth factor receptor (PDGFR) and VEGFR-2 (Ruan et al., 2012) (Fig. 2). In addition, Hafizi et al., (2002) showed that AXL could interact with the C1 domain-containing phosphatase and TENsin homologue (C1-TEN); however, the authors did not mention which signaling pathways could be activated by the AXL/C1-TEN complex. Also, AXL interacted and activated the Elmo proteins to induce the RAS-related C3 botulinum toxin substrate (Rac) mediated cell migration and invasion (Thuraia et al., 2015). In addition to proliferation, survival, migration and invasion, AXL regulates adhesion of 32D myeloid cells (McCloskey et al., 1997).

Overall, dysregulated expression of AXL is pro-oncogenic. AXL overexpression caused transformation of NIH 3T3 cells (Lee et al., 1999) and correlated with high grade tumors and poor prognosis in several cancer types (Gjerdrum et al., 2010). AXL is also an effector of EMT, a cellular program that confers cancer chemoresistance, stemness and invasion (Gjerdrum et al., 2010). As AXL overexpression correlates with oncogenic functions in cancer, AXL could represent an important molecular target for cancer therapy.
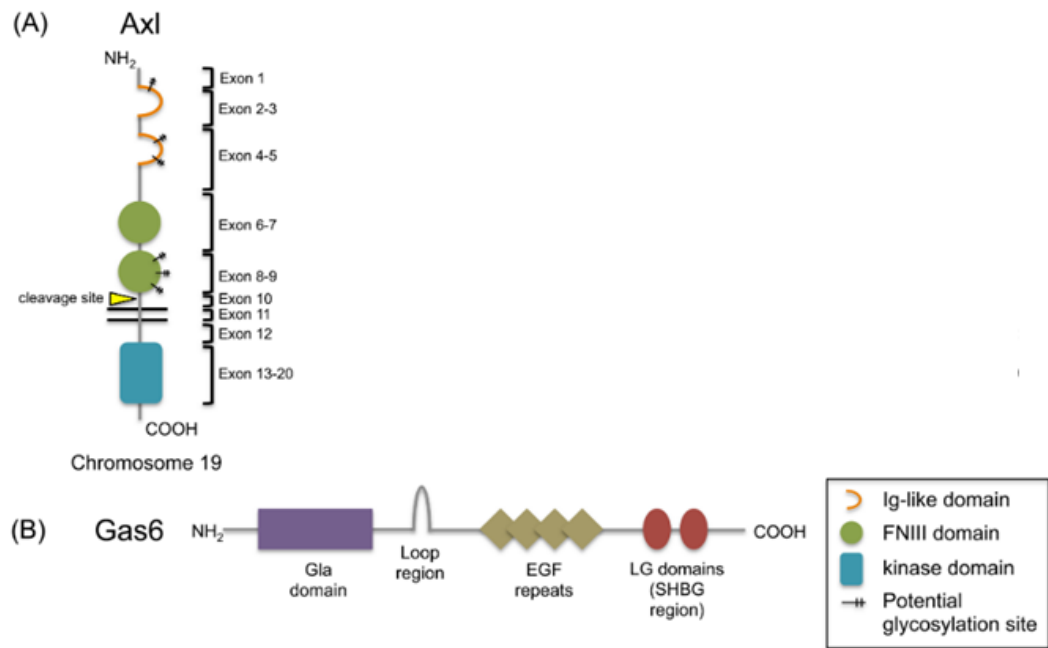
Fig. 1. <u>AXL and GAS6 structure.</u> **A)** The extracellular region of AXL has two Ig-like domains that bind the ligand, and two fibronectin III domains. AXL also shows a cleavage site located outside the membrane. The AXL kinase domain is into the cytoplasm, is encoded by exons 13–20 and presents the amino acid sequence KWIAIES. **B)** Gas6 is composed mainly of the gamma-carboxy-glutamic acid residues (Gla) in the N-terminal region, allowing cell membrane contact, and the LG domains in the C-terminal region, that bind the Ig-like domains of AXL (Axelrod and Pienta, 2014).
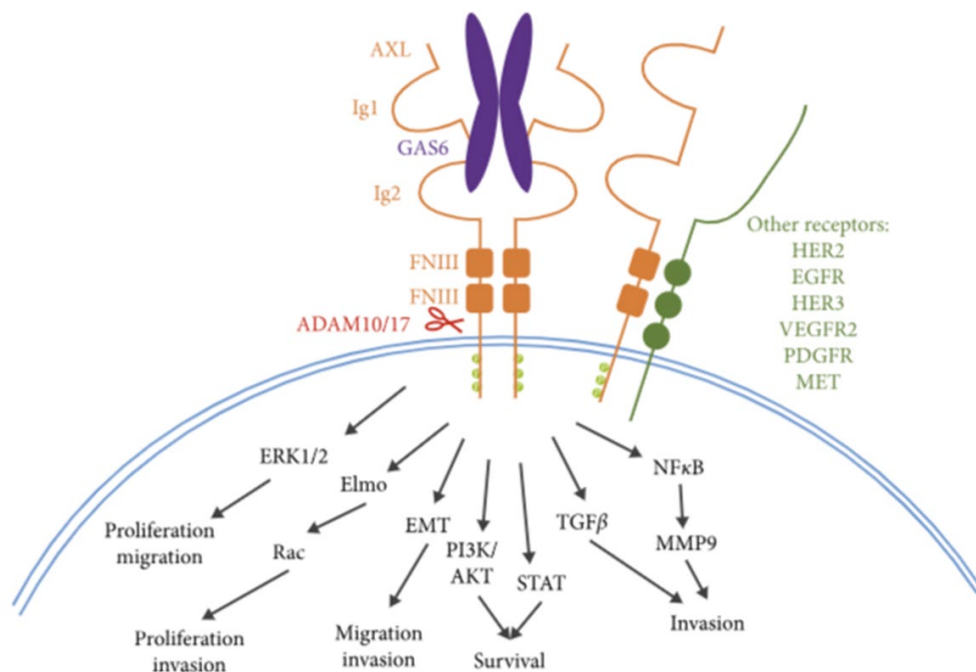
Fig. 2. <u>AXL signaling.</u> After binding GAS6, AXL homodimerizes to induce phosphorylation of the kinase domain that activates multiple pathways involved in cancer growth and metastasis. Also, AXL can interact with some RTKs (Colavito, 2020).

2.2.1. AXL in breast cancer

In cancer, AXL overexpression correlates with poor survival, metastasis and chemoresistance (Paccez et al., 2014). AXL has been found overexpressed in TNBC (Bottai et al., 2016), in inflammatory (Wang et al., 2013) and HER2-positive breast cancers (Goyette et al., 2018). AXL inhibition by the 20G7-D9 anti-AXL monoclonal antibody (mAbs) blocked metastatic capacity in breast cancer (Leconet et al., 2017). Wang et al., (2013) found that tazarotene-induced gene 1 (TIG1) could stabililize AXL that activated NF-κB and matrix metalloproteinase-9 (MMP-9). The AXL inhibitor SGI-7079 decreased proliferation, migration and invasion of IBC cells. In mouse models and human samples, the TGF-β signaling activated AXL to maintain EMT and invasion of HER2+ tumors. The AXL inhibitor R428 decreased both the circulating tumor cells and lung metastases in the HER2+ mouse model (Goyette et al., 2018).

AXL can maintain invasion by inducing EMT. A microarray analysis of gene expression and measurements of RTKs activity found that the MCF-7/multidrug resistant (ADR) cells presented EMT and AXL while the parental sensitive MCF-7 cells had an epithelial phenotype and absence of AXL. In MCF-7/ADR cells inhibition of AXL by siRNA or R428 reduced invasion and sensitised cells to doxorubicin. AXL knockdown significantly repressed ZEB1 by suppressing the AKT/ glycogen synthase kinase 3 beta (GSK3β)/β-catenin pathway and this in turn decreased the capacity of cells to repair DNA damage after doxorubicin treatment (Wang et al., 2016). In breast cancer, AXL correlated with metastasis and shorter patient survival (Gjerdrum et al., 2010). In relation to EMT, Bottai et al., (2016) found that in TNBC cell lines, AXL mediated production of cytokines and chemokines, such as C-C motif chemokine ligand 18 (CCL18) and interleukin 10 (IL-10) that enhanced metastasis and chemoresistance. Asiedu et al., (2014) found that AXL induced EMT in non-tumorigenic breast cells and enhanced growth and chemoresistance of breast cancer stem cells. Thus, AXL modulates various cellular functions to maintain malignant behaviour of breast cancer.

2.2.2. The AXL inhibitor R428

R428 is a small molecule that potently inhibits AXL phosphorylation. R428 blocked AXL phosphorylation on Tyr 821 (Holland et. al., 2010), Tyr 779 (Ludwig et al., 2018) and Tyr 702 (Palisoul et al., 2017). In the Phase I clinical trial that enrolled patients with metastatic breast cancer, R428 synergized with cisplatin to prevent liver and lung metastases (Holland et al., 2010). R428 inhibited the AXL/GAS6 pathway by decreasing *in vitro "*C-C

motif chemokine ligand (CCL2), IL-6, oncostatin M and TGF-beta" (Bottai et al., 2016) while increasing expression of dephosphorylated cyclin-dependent protein kinase cdk1 (CDC2) (Wilson et al., 2014). R428 *in vivo* reduced VEGF and Snail (Holland et al., 2010) and activated the "tumor-infiltrating cluster of differentiation 4 and 8 (CD4$^+$ and CD8$^+$) T cells" (Guo al., 2017). R428 blocked breast cancer metastasis and prolonged survival in breast cancer mouse model (Wang et al. 2016, Holland et al. 2010, Sadahiro et al., 2018, Goyette et al., 2018). In a clinical trial, a combination of R428 and an inhibitor of PD-1 increased survival of non-small cell lung cancer (NSCLC) patients (Felip et al., 2019). In head and neck squamous cell carcinoma (HNSCC), inhibition of AXL restored sensitivity "to erlotinib, cetuximab and radiation" (Giles et al., 2013). In addition, *in vitro* R428 treatment induced apoptosis in the peripheral blood B cells derived from patients with B-cell chronic lymphocytic leukemia (CLL) (Ghosh et al., 2011). Then, R428 can benefit patients with tumors with high expression of AXL.

2.2.3. The AXL inhibitor TP-0903

TP-0903 has been shown to reverse EMT and restore chemosensitivity in colorectal cancer (CRC). TP-0903 cytotoxicity had an IC$_{50}$ ranging 4.5 nM – 123 nM and suppressed Snail and the Wnt/beta-catenin pathway. The Phase I trial that uses TP-0903 in the treatment of patients with CRC is ongoing (clincaltrials.gov, NCT02729298) (Mangelson, Peterson et al., 2019). In the NSCLC cell line H1993, TP-0903 decreased AXL and ZEB1 while increasing E-cadherin. In TNBC cell lines, TP-0903 inhibited HR and synergised with PARP inhibitors to induce cytotoxicity (Balaji et al., 2017). It has been reported how breast cancer is resistant to the immune checkpoint inhibitors (ICIs) and AXL was implicated in such resistance. A combination of anti-PD-1 therapy and TP-0903 highly reduce proliferation of the mouse model 4T1 (resistant to ICIs) by increasing infiltration and activation of dendritic cells in the tumor (Kumagai et al., 2019). AXL has been found constitutively active in the peripheral blood B cells of patients with CLL (Ghosh et al., 2011). In CLL, TP-0903 *in vitro* induced apoptosis by inhibition of AXL, AKT and Bcl-2 while BH3-only Bim protein (BIM) was increased (Sinha et al., 2015). In neuroblastoma (NB) cell lines TP-0903 induced apoptosis and decreased migration, proliferation and intravasation both *in vitro* and *in vivo* (Corallo et al., 2018). In NSCLC cell lines, TP-0903 inhibited EMT, Slug, increased E-cadherin and synergised with the EGFR inhibitor osimertinib *in vivo* (Mangelson, Tyagi et al., 2019). TP-0903 treatment of many ovarian cancer cell lines shown that TP-0903 IC$_{50}$ ranged 33 nM - 840 nM, decreased Snail, Slug and metastasis (Tomimatsu et al., 2019). AXL also

induced resistance to the RTK fms-like tyrosine kinase 3 (FLT3) inhibitors and protein kinase C (PKC) 412 that are used to treat acute myeloid leukemia (AML). TP-0903 inhibited AXL in the AML cell line MOLM13 (resistant to FLT3 inhibitors) and restored sensititvity to PKC412 (Park et al., 2015). TP-0903 is also an enhancer of the CD19 directed chimeric antigen receptor T cell (CART19) therapy (Sakemura et al., 2018). TP-0903 and ruxolitinib, a janus kinase (JAK) inhibitor, synergised to induce cytotoxicity in patient-derived organoids (PDO) from tumors with increased AXL and JAK1 (Taverna et al., 2020). TP-0903 also inhibited EMT and stemness induced by carboplatin, doxorubicin, and paclitaxel (Chi et al., 2021). Then, patients presenting AXL overexpressing tumors could benefit from treatment with the AXL inhibitor TP-0903.

2.3. ZEB1 and its protein structure

The family of ZEB transcription factors includes ZEB1 (named TCF8 or δEF1) and ZEB2 (named SIP1). *ZEB1* gene locates on the chromosome Chr10p11.22 and its protein has 1117 amino acid. Structurally, ZEB1 and ZEB2 are similar. At N-terminal and C-terminal they have two C2H2-type zinc fingers (NZF and CZF) domains by which they bind the "paired CAGGTA/G E-box-like elements" in the promoters of genes especially involved in cell differentiation (Wu et al., 2020). Also, ZEB1/2 have domains that are important for transcriptional activity such as "the CAF/p300 binding domain (CBD), the Smad interaction domain (SID) and the CtBP interaction domain (CID)". In addition, ZEB1/2 have a central Homeodomain (HD) (a POU-like homeodomain) that does not bind DNA (Vandewalle et al., 2009). The schematic representation of ZEB1/2 structure is indicated in Fig. 3.

Fig. 3. <u>ZEB1/2 structure.</u> In the N-terminal and C-terminal there are two zinc finger domains (NZF and CZF); also, centrally is located the Homeodomain (HD). ZEB1/2 can interact with other proteins by the "CAF/p300 binding domain (CBD)" at the N-terminal, the "Smad interaction domain (SID) and CtBP interaction domain (CID)" at the C-terminal. (Wu et al., 2020)

2.3.1. Regulation of ZEB1

ZEB1 expression is induced by STAT3 (Avtanski et al., 2014), insulin-like growth factor 1 (IGF-1)- PKC pathway (Llorens et al., 2016), hepatocyte growth factor (HGF) (Han et al. 2016) and TGF beta, Wnt/beta-catenin, NF-κB, PI3K/AKT, Ras/ extracellular signal-regulated kinase (Erk)" (Chua et al., 2007). ZEB1 is regulated by deubiquitinases (DUBs), such as ubiquitin specific peptidase 51 (USP51) (Zhou, Zhang et al., 2017). The ataxia-telangiectasia mutated (ATM) kinase can prevent degradation of ZEB1 in presence of DNA damage (Zhang, Wei et al., 2014). ZEB1 could induce genes responsive to TGF-beta by interacting with "Smad, p300 and P300/CBP-associated factor (P/CAF) complex" (Postigo et al., 2003). Also, ZEB1 can induce EMT by binding the promoter of E-cadherin gene with the C-terminal binding protein (CtBP) transcriptional co-repressors histone HDAC1/2 resulting in repression of E-cadherin transcription (Zhang, Sun et al., 2015). Activation of ZEB1 needs the functional "ZEB1-Smad3- P/CAF complex" (Kim et al., 2005).

2.3.2. ZEB1 in breast cancer

ZEB1 is overexpressed in TNBC (Karihtala et al., 2013). ZEB1 is involved in many reciprocal loops. The members of miR-200 family, such as miR-200a/b/c, miR-141 and miR-429 can induce epithelisation by binding ZEB1 mRNA in its 3′-untranslated region (UTR) to repress ZEB1 (Gregory et al., 2008). Also, ZEB1 can suppress expression of miR-200s (Burk et al., 2008). The ZEB1/miR-200 loop also is involved in others cellular mechanisms such as survival, apoptosis and proliferation (Vendrell et la., 2012). The ZEB1/ myeloblastosis viral oncogene homolog (MYB) is a second negative feedback loop and considered a determinant of invasion and metastasis in breast cancer. In this loop, ZEB1 repressed transcription of MYB that in turn inhibited ZEB1 expression (Hugo et al., 2013). There are also some positive feedback loops, such the loops ZEB1/CD44s (Preca et al., 2015) and "ZEB1/hyaluronic acid synthase 2 (HAS2)" (Preca et al., 2017).

2.3.3. ZEB1 oncogenic functions
2.3.3.1. Cell plasticity

It has been shown how during inflammation, ZEB1 regulated the switch from a dormant to an active phenotype of metastatic cancer cells (De Cock et al., 2016). ZEB1 also modulated the plasticity of melanoma cells to induce resistance to rapidly accelerated fibrosarcoma (RAF) and/or mitogen-activated extracellular signal-regulated kinase (MEK) inhibitors (Richard et al., 2016).

2.3.3.2. Tumor metastasis and EMT

ZEB1 overexpression in a mouse xenograft model of breast cancer increased metastasis (Zhang et al., 2018). Also, ZEB1 induced IL-6/8 that enhanced tumorigenicity of basal-like breast cancer cells (Katsura et al., 2017). Different transcriptomic analyses found that ZEB1 correlated with EMT, invasion and metastasis (Gheldof et al., 2012). Maturi et al., (2018) found that ZEB1 knockdown by CRISPR-Cas9 affected expression of E-cadherin, polarity genes lethal giant larvae (Lgl2), tumor suppressor homolog 3 (FAT3), polarity-linked regulators such as disks large homolog 2 (DLG2) and the proliferation regulators tissue inhibitors metalloproteinases 3 (TIMP3) and teneurin 2 (TENM2). In breast cancer, single depletion of Snail and Twist did not induce epithelial markers (Tan et al., 2015). To this point, it has been proposed an "epithelial-mesenchymal (E/M) hybrid phenotype" as an intermediate between the epithelial (E) and mesenchymal (M) states (Lu et al., 2013). It was found that Snail/miR-34 pathway could make a transition from E to E/M and also the ZEB1/miR-200 pathway could mediate transition from E/M to M (Zhang, Tian et al., 2014).

2.3.3.3. Chemoresistance

In breast cancer, resistance to chemotherapy has been associated with ZEB1 (Zhang, Sun et al., 2015; Zhang et al., 2018). Zhang et al., (2018) found that ZEB1 induced resistance to epirubicin in a mechanism involving DDR. ZEB1 also correlated with B-cell-lymphoma extra large (Bcl-xl). In this analysis, "the ZEB1/ P300/CBP-associated factor (PCAF) complex" interacted with ATM promoter to induce ATM transcription and activate HR. Bai et al. (2014) found that TGF-β mediated activation of ZEB1 suppressed the "miR-200c/zinc finger protein 217 (ZFN217)/TGF-β/ZEB1 loop" to decrease sensitivity to trastuzumab, an approved targeted therapy for HER2 overexpressing breast tumors. In addition, the beta-catenin/transcription factor 4 (TCF4) pathway activated ZEB1 to mediate DDR (Sanchez-Tillo et al., 2011). Luo et al., (2021) found that in TNBC, the Checkpoint With Forkhead And Ring Finger Domains (CHFR) regulated ZEB1. CHFR is an ubiquitin ligase of ZEB1 and CHFR overexpression and ZEB1 knockdown increased the efficacy of paclitaxel and doxorubicin. In advanced breast and ovarian cancer miRNA-205 and miR-200c, by targeting ZEB1, increased sensitivity to chemotherapy (Cochrane et al., 2009). Also, long coding RNA (lncRNAs) have a role in drug resistance (Bermudez et al., 2019). High expression of lncRNA SET binding factor 1 complex (SBF) induced temozolomide chemoresistance in glioblastoma by ZEB1-dependent pathway; ZEB1 directly induced SBF2 expression to induce double-strand-break DNA repair (Zhang, Yin et al., 2019). EMT induced resistance by increasing

expression of ATP-binding cassette (ABC) transporters that pumps chemotherapeutic drugs out of the cells. In ovarian and lung cancer tissues, EMT activated ZEB1/2 that in turn induced multidrug resistance protein 1 (MDR1) and ABC Subfamily G Member 2 (ABCG2) to mediate resistance to platinum-based drugs (Zhou, Zhu et al., 2017). However, some reports shown that ZEB1 could induce chemoresistance by EMT-independent mechanisms. ZEB1 induced chemoresistance to paclitaxel (Sakata et al., 2017) or cisplatin (Cui et al., 2018) in tumors maintaining epithelial characteristics. ZEB1 induced radioresistance in MCF-7 cells without inducing EMT (Zhang, Wei et al., 2014). These results suggest that ZEB1 modulates chemoresistance in cancer through EMT-dependent and -independent mechanisms.

2.3.3.4. Resistance to radiotherapy

Radiation therapy is less efficient in intrinsically and therapy-induced radioresistant tumors with high DDR capacity. After radiation of breast cancer cells, ATM phosphorylated ZEB1 that in turn stabilised checkpoint kinase 1 (CHK1) by ubiquitinilation of ubiquitin-specific peptidase 7 (USP7)" to activate HR (Zhang, Wei et al., 2014). Also, overexpression of miR-875-5p restored sensitivity to radiation in prostate cancer cell lines and xenografts by inhibiting the EGFR and ZEB1 mediated activation of checkpoint kinase 1 (CHK1) (El Bezawy et al., 2017). Morel et al., (2017) found that ZEB1 in normal stem cells induced the methionine sulfoxide reductase (MSRB3) to protect cells from DNA damage. Also, Prodhomme et al., (2021) found that in claudin-low and basal-like TNBC, ZEB1 directly repressed DNA polymerase theta (POLQ) expression, an enzyme crucial for the theta-mediated end-joining (TMEJ) pathway. As high activity of TMEJ is mutagenic, ZEB1 prevents TMEJ to maintain both stability and integrity of breast cancer cell genome.

2.3.3.5. ZEB1 and antioxidant program

Han et al., (2021) found that ZEB1 induced ROS accumulation by inhibiting glutathione peroxidase 4 (GPX4) transcription in MCF-7 and MDA-MB-231 cells. Also, inhibition of the ZEB1/GPX4 pathway had a therapeutic effect on breast cancer metabolism. Han et al., (2022) found that in breast cancer, ZEB1 directly and positively regulated the expression of the monocarboxylate transporter 4 (MCT4) both *in vitro* and *in vivo* to induce ROS and cancer growth. However, there are not findings showing ZEB1 to activate expression of antioxidant enzymes in cancer.

2.4. Reactive Oxygen Species

ROS are reactive and energetic molecules that can be found as free oxygen radicals and non-radical ROS. The first group contains "superoxide ($O_2\bullet-$), hydroxyl radical ($\bullet OH$), nitric oxide ($NO\bullet$), organic radicals ($R\bullet$), peroxyl radicals ($ROO\bullet$), alkoxyl radicals ($RO\bullet$), thiyl radicals ($RS\bullet$), sulfonyl radicals ($ROS\bullet$), thiyl peroxyl radicals ($RSOO\bullet$), and disulfides ($RSSR$)". The second group includes "hydrogen peroxide (H_2O_2), singlet oxygen ($1O_2$), ozone/trioxygen (O_3), organic hydroperoxides ($ROOH$), hypochloride ($HOCl$), peroxynitrite ($ONO-$), nitrosoperoxycarbonate anion ($O=NOOCO_2-$), nitrocarbonate anion (O_2NOCO_2-), dinitrogen dioxide (N_2O_2), nitronium (NO_2+), and lipid-or carbohydrate-derived carbonyl compounds" (Liou et al., 2010). Of these ROS, superoxide anions, hydrogen peroxide and hydroxyl radicals are the most relevant and investigated in cancer (Liou et al., 2010).

2.4.1. Sources of ROS in the cells and ROS detoxification

The mitochondria is the main producer of superoxide as a product of the oxidative phosphorylation (Ha et al., 2001). Also, peroxisomes can produce superoxide and hydrogen peroxide by xanthine oxidase (Liou et al., 2010). In cancer, ROS can be induced by growth factors and cytokines, such as interferon γ (IFNγ), tumor necrosis factor alpha (TNFα) (Lo et al., 1995), PDGF, insulin, EGF, TGFβ (Minamoto et al., 2000). In addition, macrophages activate TNFα to induce ROS (Storz, 2005); neutrophils and macrophages induced superoxide by the nicotinamide adenine dinucleotide phosphate hydrogen (NAPDH) oxidase (Segal et al., 1997). Also, ROS can be generated by the lipid peroxidation in the cell membrane where the polyunsaturated fatty acids (PUFAs) are susceptible to oxidation. PUFAs can undergo auto-oxidation after interaction with radicals to produce some reactive intermediates, such as malondialdehyde. In addition, PUFAs arachidonic and linoleic acids can be oxidated by the lipoxygenase (LOX) to generate lipid peroxides (Su et al., 2019).

As for mechanisms involved in the ROS detoxification, ROS can be removed by non-enzymatic molecules (glutathione) or antioxidant enzymes (Liou et al., 2010). The metalloenzymes superoxide dismutases (SODs), by using as cofactors "metal ions such as copper (Cu^2+), zinc (Zn^2+), manganese (Mn^2+) or iron (Fe^2+)" can dismutase the "superoxide anion to oxygen and hydrogen peroxide". There are three types of SODs: SOD1, located in the cytoplasm, SOD2 in the mitochondria and SOD3, in the extracellular space. Then, catalase (CAT) can decompose "hydrogen peroxide to water and oxygen"; CAT is mainly located in the cytosol and peroxisomes. Other enzymes, such as peroxiredoxins and thioredoxin, can reduce "hydrogen peroxide, organic hydroperoxides and peroxynitrite". Other enzymes can

use glutathione to remove ROS and they are "glutathione reductase, glutathione peroxidases (GPXs) and glutathione S-transferases (GSTs)" (Liou et al., 2010). In particular, glutathione reduces the disulfide bonds of cysteines in the cytoplasmic proteins and glutathione is oxidized to glutathione disulfide (Liou et al., 2010). The Fig. 4 shows intracellular sources of ROS and which antioxidant enzymes are involved in their removal.
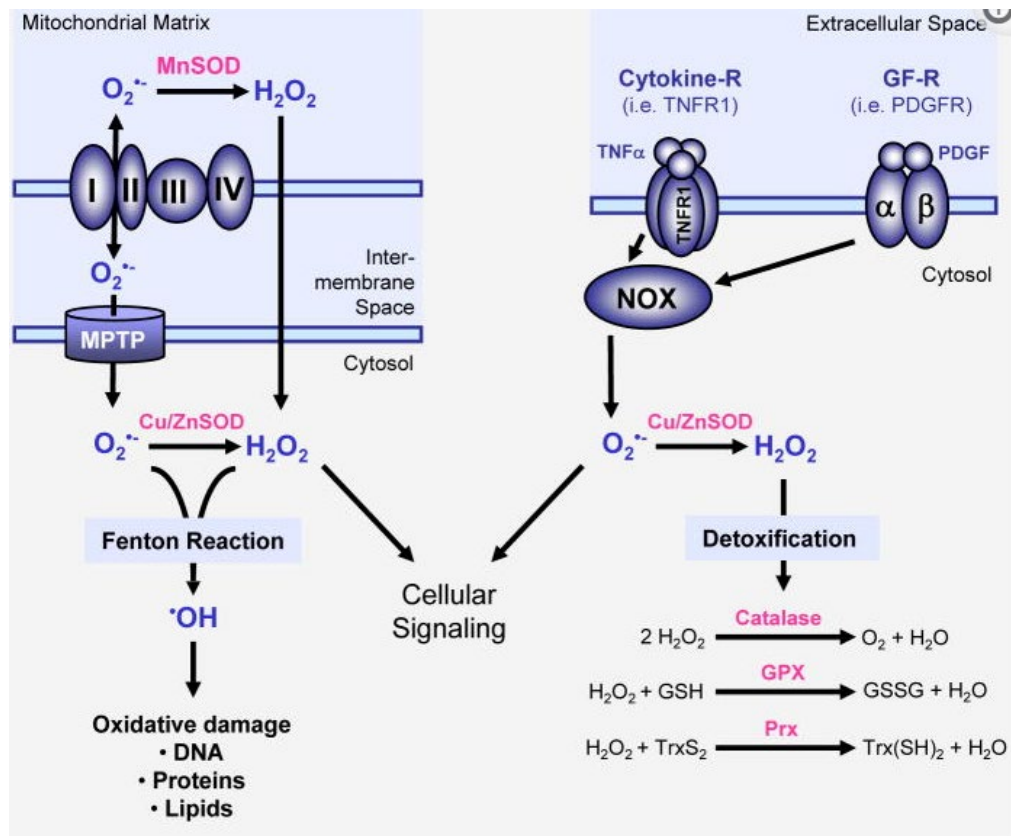
Fig. 4. <u>ROS production and antioxidant mechanisms.</u> Mitochondria are the main contributor of ROS, in partcular superoxide that are released from the electrons transport chain (ECT). The superoxide can be also induced by some growth factors. The superoxide can be dismutated to oxygen and hydrogen peroxide in the mitochondria by SOD2 or can be released in the cytoplasm where they are dismutated by SOD1. In the extracellular space, SOD3 dismutate superoxide. In the lysosomes, hydrogen peroxide can induce hydroxyl radicals in a Fenton reaction or converted to water and oxygen by catalases, glutathione peroxidases and peroxiredoxins. In cancer, both superoxide and hydrogen peroxide can support signaling pathways. (Liou et al., 2010).

2.4.2. ROS mediated regulation of molecular pathways in cancer

ROS are generally elevated in cancer to induce growth and hydrogen peroxide is a highly diffusible ROS and is a second messenger in cellular signaling (Sundaresan et al., 1995). In effect, hydrogen peroxide regulated activity of RTKs and transcription factors by their reversible oxidation (Storz, 2005). In breast cancer, Erk1/2 was activated by hydrogen

peroxide after estrogen metabolism to induce proliferation (Reddy et al., 2007). ROS activated KRAS by oxidation of the cysteine 118 residue (Lander et al., 1997). In many cancer types, activation of Erk1/2 by ROS also increased survival and motility (McCubrey et al., 2007). In MCF-7 and MDA-MB-435 cells, treatment with ROS scavengers or Erk1/2 or MEK inhibitors could induce apoptosis (Ostrakhovitch et al., 2005; Zhou J. et al., 2008). However, treatment with hydrogen peroxide of pancreatic cancer and glioma cells activated Erk1/2 to induce cell death and this could be caused by high basal level of ROS (Osada et al., 2008). This suggests how the role of ROS in regulation of survival is dependent on the type of cancer and the basal amount of ROS. AKT can be also regulated by ROS. AKT can induce survival in cancer by phosphorylation and then inactivation of many substrates, such as BCL-2 associated agonist of cell death (Bad), bcl-2-associated X protein (BAX) and BH3-only BIM protein (BIM) (Brunet et al., 1999). In breast cancer, ROS could activate the PI3K/AKT pathway (Burdick et al., 2003) and EGF. In breast cancer cells, inhibition of the calcium mitochondrial uniporter suppressed ROS and estrogens mediated proliferation (Parkash et al., 2006). In addition, some authors shown that estrogen translocation in the mitochondria increased oxidative stress and proliferation (Reddy et al., 2007; Felty, Singh et al., 2005; Felty, Xiong et al., 2005). In addition, ROS could induce motility and metastasis. In mice, metastasis rate was increased after that carcinoma cells were treated with hydrogen peroxide before intravenous injection (Kundu et al., 1995). Differently from normal cells, tumor cells have independence of anchorage to the extracellular matrix and are resistant to apoptosis. This can be mediated by oxidative stress that activated "autocrine/adhesive signals", such as sarcoma kinase protein (Src) and the EGFR (Liou et al., 2010). In addition, treatment with MMP-3 increased intracellular ROS to activate EMT; N-acetylcysteine (NAC) removed ROS and inhibited EMT (Radisky et al., 2005). Also, in MCF-7 and T-47D breast cancer cells, ROS activated NF-κB to increase metastatic rate (Tobar et al., 2008). It has been reported how under hypoxic conditions, superoxide and hydrogen peroxide mediated accumulation of hypoxia inducible factor 1α (HIF-1α) (Wang et al., 2005). ROS can also induce "multidrug resistance" by increasing expression of the P-glycoprotein (P-gp) and activate the nuclear factor erythroid-derived 2 (NRF2) as a mechanism to remove excess of ROS (Jeddi et al., 2018; Sadeghi et al., 2018). Thus, ROS signaling sustains malignant tumour state by activating various cancer-related pathways.

2.5. Apoptosis

Apoptosis is a highly regulated process that eliminates superfluous and damaged cells during development and normal cell division. Apoptosis is characterized by shrinkage of cells, blebbing of membranes, condensation of chromatin and nuclear fragmentation, formation of apoptotic bodies that are eliminated by "neighbouring cells or macrophages" (Redza and Bates, 2016). Apoptosis is mainly induced by activation "of cysteine-dependent aspartate-specific proteases (caspases)", and in particular, once apoptosis is activated, the procaspases are cleaved to induce their active "proteolytic forms" containing "two cysteine active sites". Then, active caspases can cleave their targets at aspartate residues and there are at least 1000 substrates targeted by caspase 3 and 7, such as PARP, cyclin dependent kinase inhibitor 1 (p21), the "E3 ubiquitin-protein ligase" and "the inhibitor of caspase-activated DNase (ICAD)". Caspases can be initiators such as "caspases 8, 10, 2 and 9" and executors such as "caspases 3, 6 and 7" (Redza and Bates, 2016). Apoptosis can be induced by an extrinsic or an intrinsic (mitochondrial and endoplasmic reticulum) pathway.

2.5.1. Mitochondrial pathway

The most important function of mitochondria is to produce energy. This function is favored by a structure presenting an "outer mitochondrial membrane (OMM)", permeable to molecules up to 5 kDa and an "inner mitochondrial membrane (IMM)" that is impermeable and then capable to form the electrochemical potential necessary for the oxidative phosphorylation. Mitochondria also regulate apoptosis and the "mitochondrial permeability transition pore (MPTP)" is the critical factor for the mitochondria mediated apoptosis (Redza and Bates, 2016). The MPTP complex includes cyclophilin D that binds in the IMM the "adenine–nucleotide–translocator (ANT)" that in turn interacts with the "voltage dependent-anion-channel (VDAC)" in the OMM (Grimm et al., 2012). In presence of high stress, MPTP increases and molecules less than 1.5 kDa can transit into the mitochondrial matrix disrupting the oxidative phosphorylation with a subsequent release of superoxide (Halestrap et al., 2009). Also, an increase of MOMP) activates apoptosis by releasing in the cytosol "cytochrome c, apoptosis inducing factor (AIF) and endonuclease G (endoG)". Then, cytochrome c induces the formation of an apoptosome that includes the "apoptosis activating factor-1 (Apaf-1)" and procaspase 9. Then, cleavage of caspase 9 activates "caspases 3, 6 and 7" (Orrenius et al., 2015). Mitochondrial apoptosis is regulated by members of the BCL-2 family that can be anti-apoptotic, such as "BCL-2, BCL-XL", and pro-apoptotic, such as "BAX" and the "BH3-only proteins BAD, BIM, p53-upregulated modulator of apoptosis (PUMA) and phorbol-12-

myristate-13-acetate-induced protein 1 (NOXA)" (Redza and Bates, 2016). High stress can change the ratio of pro and anti-apoptotic BCL-2 family members in favors of those inducing apoptosis.

2.5.1.1. Caspase 3

Caspase 3 is one of the most important executors of apoptosis. The active form of caspase 3 (cleaved caspase 3, CC3), composed of the two fragments 17 and 19 kDa, cleaves its substrates "between the aspartic acid (D) and the glycine (G) in the substrate DEVDG" (Porter and Ja, 1999). The embryonic stem (ES) cells defective of caspase 3 were resistant to UV irradiation mediated apoptosis (Woo et al., 1998). The neutrophils of bone marrow and mouse fibroblasts defective for caspase 3 were more resistant to apoptosis and cell death that were activated after restoration of caspase 3 (Woo et al., 1998) Also, restoration of caspase 3 in MCF-7 cell line, that does not have this gene, induced "DNA fragmentation and membrane blebbing" after activation of apoptosis (Janicke et al., 1998) In MCF-7 cells, caspase 3 cleaved the "actin binding protein a-fodrin" (Janicke et al., 1998), p21 activated kinase 2 (PAK2) and gelsolin to induce apoptosis (Rudel et al., 1997). Caspase 3 also cleaved the inhibitor of caspase activated DNase (ICAD)-DNA fragmentation factor 45 (DFF) to induce the endonuclease activity of Carbamoyl-Phosphate Synthetase 2, Aspartate Transcarbamylase, And Dihydroorotase (DHOase) that activates DNA fragmentation (Liu et al., 1997). It is important to note that activation of caspase 3 can induce complete apoptosis associated with "cell shrinkage, blebbing, chromatin condensation and DNA fragmentation" only in specific cell types and after treatment with some apoptotic inducers (Porter and Ja, 1999). The discovery of new targets of caspase 3 can clarify which mechanisms are required for caspase 3 mediated apoptosis.

2.5.2. ER and apoptosis

High ER stress can mediate apoptosis by inactivation of BCL-2 located in the ER. Also, C-Jun N-terminal kinase (JNK) activation by inositol requiring protein 1 (IRE-1α) induced inactivation of Bcl-2 in the ER membrane (Sano and Reed, 2013). An inactive Bcl-2 cannot regulate the $Ca^{2}+$ efflux from ER (Breckenridge et al., 2003) that translocates in the mitochondria to activate the mitochondrial permeability transition pore (MPTP) complex and then apoptosis (Orrenius et a., 2015). Also, JNK can activate by phosphorylation Bim located in the ER (Sano et al., 2013). Also, in presence of high ER stress, "the protein kinase r endoplasmic reticulum kinase (PERK)- eukariotic translation initiation factor 2A (eIF2α)-

activating transcription factor 4 (ATF4) pathway" activates C/EBP homlogous protein (CHOP) that induces transcription of apoptotic proteins such as "death receptor 5 (DR5), Bim and p53-upregulated modulator of apoptosis (Puma)" (Sano and Reed, 2013).

2.5.3. Death receptor pathway

Apoptosis can be activated extrinsically by death receptors of "the tumor necrosis factor receptor (TNF-R) family". TNF-Rs include "Death receptor 1 (DR1), DR2, DR3, DR4 (TNF-related apoptosis-inducing ligand (TRAIL)-R1), DR5 (TRAIL-R2) and DR6 (TNF receptor family member 21 (TNFRSF21) (Redza and Bates, 2016). DR2 induces apoptosis by bindng Fas cell surface death ligand (FasL) that causes receptor trimerization (Kaufmann et al., 2012). Then, "the adaptor molecule Fas-associated death domain (FADD)" can form "the death-inducing signalling complex (DISC)" in which FADD activates caspases 8 or 10 (Mahmood and Shukla, 2010). Apoptosis regulated by TRAIL-R1 and R2 is similar to that induced by Fas, but TRAIL is the death ligand. As for TNF-R1 mediated apoptosis, TNF-α activates the TNF-R1 that recruits the "TNF-R-associated adaptor protein with death domain (TRADD)". Association of TRADD with Fas-associated death domain (FADD) and caspase 8 can activate apoptosis by inducing caspases 3, 6 and 7 (Russo et al., 2010).

2.6. ROS and apoptosis
2.6.1. ROS and mitochondrial apoptosis

ROS, including hydrogen peroxide and superoxide, induce release of cytochrome c from mitochondria to activate apoptosis (Redza and Bates., 2016). ROS can induce oxidation of proteins of the mitochondrial permeability transition pore (MPTP) "such as voltage dependent-anion-channel (VDAC), adenosine nucleoside translocase (ANT) and cyclophilin D" to cause "MPTP opening" (Circu et al., 2012). Then, hydrogen peroxide induced "mitochondrial membrane hyperpolarization", translocation of Bax and Bad in the mitochondria and release of cytochrome c (Circu et al., 2010). The mitochondrial ROS could activate JNK that activated pro-apoptotic proteins (West et al., 2006). Circu et al., (2010) found that ROS induced oxidation of cardiolipin, a phospholipid that binds cytochrome c to the inner mitochondrial membrane (IMM) and this caused a release of cytochrome c in the cytosol to induce apoptosis. Also, ROS can induce mitochondrial apoptosis by disrupting the glutathione-glutathione disulfide ratio (Circu et al., 2012).

2.6.2. ROS and ER mediated apoptosis

In the ER the ratio between glutathione and glutathione disulfide is in favor of glutathione disulfide to facilitate folding of ER proteins and formation of disulfide bonds (Redza and Bates, 2016). The "ER oxidoreductin-1 (ERO1)" activates the protein disulfide isomerase (PDI) that induces formation of the disulfide bonds. In particular, electrons from PDI are transferred to flavin adenine dinucleotide (FAD) that once reduced to FADH2 reacts with O_2 to produce hydrogen peroxide. In presence of high ER oxidoreductin-1 (ERO1) activity, high levels of misfolded proteins and hydrogen peroxide induces ER stress (Redza and Bates, 2016). A high level of ROS induced protein misfolding and CHOP activation (Malhotra et al., 2008). In presence of high ER stress, inositol requiring protein 1 (IRE1α) activation could induce apoptosis signal-regulating kinase 1 (ASK1) and p38 to activate CHOP mediated ROS (Zeeshan et al., 2016). Also, JNK activated ER mediated apoptosis (Circu et al., 2010).

2.6.3. ROS and the death receptor pathway

In HeLa cells, hydrogen peroxide increased FasL and caspase 8 to induce mitochondrial apoptosis (Pallepati et al., 2010). In addition, stress conditions could induce "death-associated protein 6 (Daxx)" to interact with Fas and activate apoptosis signal-regulating kinase 1 (ASK-1) and JNK mediated apoptosis (Salomoni et al., 2006).

2.7. ROS for treatment of cancer

In cancer, chemotherapy and radiation can induce apoptosis by ROS. In pancreatic cancer, it has been approved a combination therapy including "gemcitabine, trichostatin A, epigallocate-3-gallate (EGCG), capsaicin and benzyl isothiocyanate (BITC)" that synergise to induce ROS and apoptosis (Liou et al., 2010). The drug Sulindac also induced apoptosis by ROS in the treatment of colon and lung cancer (Marchetti et al., 2009). "Aminoflavone (5-amino-2-(4-amino-3-fluorophenyl)-6,8-difluoro-7-methylchromen-4-one; AF)" was reported to activate caspase 3, ROS and apoptosis in MCF-7 and MDA-MD-468 cells while it did not induce any cytotoxicity in the normal MCF-10A breast cell line (McLean et al., 2008). In breast cancer, other drugs including "IOA, pancratistatin (PST) and triphala (TPL)" act as Aminoflavone to induce apoptosis (Liou et al., 2010). In cancer, chemotherapy induces ROS mediated damage of nuclear and mitochondrial DNA. Then, generation of ROS could be a strategy to induce cytotoxicity in cancer cells. However, an increase of antioxidants or antioxidant mechanisms can be also used as a therapeutic option. This strategy could be

effective in the treatment of metastatic tumors whose ROS levels are low. To this point, "the SOD mimetic EUK-134 or a mimetic of glutathione disulfide named NOV-002" are used in clinics (Liou et al., 2010). Then, both excess of ROS and antioxidants can represent a strategy to treat cancer.

2.8. Rad51 and its functions

Rad51 is a protein involved in the repair of DNA by HR pathway. Rad51 is a member of the "recA/Rad51 gene family" and its regulation is mediated by "BRCA2, partner and localizer of BRCA2 (PALB2) and Rad51 paralogs". A decrease in the functionality of Rad51 or Rad51 regulators induces cancer and "Fanconi anemia (FA)-like syndrome" (Grundy et al., 2020). Rad51 overexpression induced chemoresistance (Grundy et al., 2020). After DSB formation, resected DNA ends form the "3'ssDNA overhangs" that are coated with human replication protein A (RPA). In particular, there are two types of DNA end resections: those short, mediated by "meiotic recombination 11 homolog 1 (MRE11) – Rad recombinase 50 (RAD50) – Nijmegen breakage syndrome 1(NBS1) (MRN) complex with retinoblastoma binding protein 8 (CtIP)" and those long induced by "exonuclease 1 (EXO1) or bloom syndrome- Topoisomerase III- RecQ-mediated genome instability protein 1/2 (BLM–TOPIII–RMI1/2)". Rad51 displaces RPA to form a nucleoprotein filament through "PALB2, BRCA2 and Rad51 paralog sub-complexes". Then, with the support of Rad54, the filament invades an homologous template to find an homologous sequence to form a D-loop structure. After displacement of Rad51, DNA is extended by polymerases that use the repair template to insert nucleotides. Then, after that the "second end of the DSB" is captured, the intermediate filament of DNA can be resoluted or dissoluted producing a crossover or a non crossover product. The resolution of HR is supported by "Hollyday junction 5' flap endonuclease (GEN1) or structure specific endonuclease subunit (SLX1/4)" while dissolution by the "bloom syndrome- Topoisomerase III- RecQ-mediated genome instability protein 1/2 (BLM–TOPIII–RMI1/2)" (Grundy et al., 2020).

2.8.1. Rad51 regulation

As mentioned above, Rad54 supports Rad51 activity. There are many proteins that enhanced Rad51 activity, such as "BRCA2, partner and localizer of BRCA2 (PALB2) and the RAD51 paralogs" (Prakash et al., 2015). The "Rad51 paralogs" (RAD51B, RAD51C, RAD51D)" support Rad51 with the elongation of Rad51 filament (Harris et al., 2018). Rad51 is transcriptionally suppressed by p53. In contrast, Rad51 expression is increased by early

growth response protein (EGR1) (Hine et al., 2014). Also, RTK c-MET (Chabot et al., 2019) and the Polo-like kinase 1 activated Rad51 by phosphorylation (Yata et al., 2012). In cancer, Rad51 is a molecular target as Rad51 overexpression induced resistance to DNA damaging agents (Richardson, 2015; Klein, 2008). The small molecule inhibitor amuvatinib (MP-470) decreased expression of Rad51 while inducing DSBs in glioblastoma (Welsh et al., 2009). The drug halenaquinone prevented the formation of the D-loop between "Rad51 ssDNA filament" and "homologous dsDNA" (Takaku et al., 2011). Then, the antibody 3E10 could target Rad51 (Turchick et al., 2017) and induced sensitisation of tumors to doxorubicin and Ataxia telangiectasia and Rad3-related protein (ATR) inhibitors (Turchick et al., 2019).

2.8.2. Rad51 and breast cancer

Rad51 is generally overexpressed in breast cancer (Maacke et al., 2000). Wiegmans et al., (2014) found that expression of Rad51 protein correlated with TNBC and HER2+ positive breast cancer. In particular, Rad51 associated with lymph nodes metastases, tumors with higher stage, distant metastases and aggressive clinicopathological features. Then, orthotopic implantation of BT-549 cells transfected with Rad51 expression plasmid had higher rate of metastatic burden in the liver compared to empty vector. Maacke et al., (2000) found a correlation between high expression of Rad51 protein and "invasive ductal breast cancer and ductal carcinoma-in-situ" suggesting that Rad51 could be a marker or probably a molecular target in invasive breast cancer.

2.9. Artemisinin

Artemisinin is a biologically active compound extracted from the Artemisia annua L. It is a sesquiterpene lactone with an endoperoxide moiety largely known to have high antimalarial activity. However, artemisinin has reduced bioavailability and its half-life *in vivo* is short (~2.5 h) (Crespo-Ortiz and Wei 2012). The semisynthetic derivatives of artemisinin, such as dihydroartemisinin (DHA), artesunate (ART) and others (Fig. 5) have been produced. In particular, ART is the water soluble derivative and the most common artemisinin derivative used in the antimalarial combination therapy (Crespo-Ortiz and Wei, 2012).
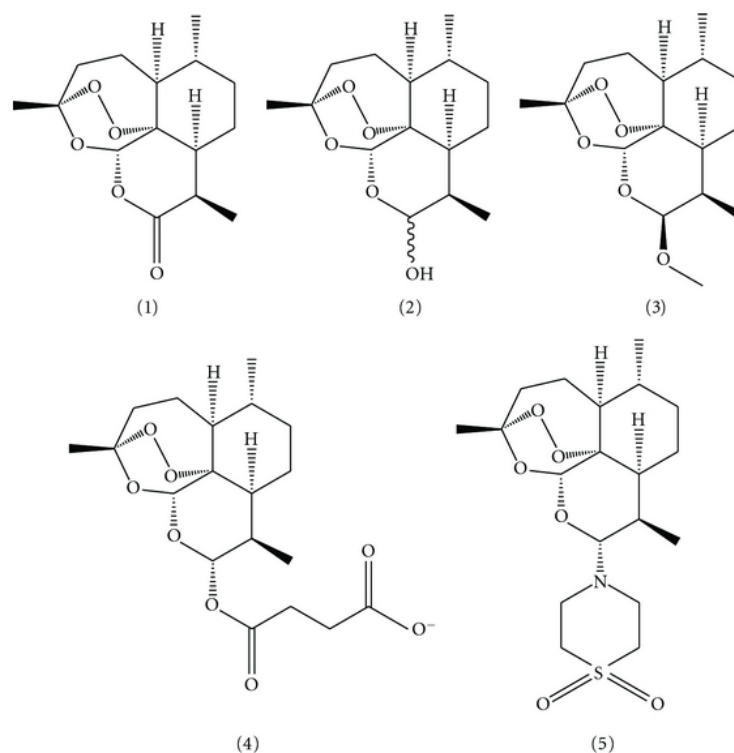
Fig. 5. Artemisinin and its derivatives. In 1) Artemisinin, in 2) dihydroartemisinin (DHA), in 3) artemether, in 4) artesunate (ART) and in 5) artemisone. The molecular structure of the Artemisinin derivatives (Crespo-Ortiz and Wei, 2012).

ART exerts its cancer cytotoxicity by activation of its endoperoxide bridge through ferrous iron (FeII) or heme to produce cytotoxic carbon-centered radicals and ROS that in turn alkylate proteins and damage membrane, lysosomes, ER and genome (Fig. 6). It has been shown that, pre-treatment of cancer cells with iron or holotransferrin (HF) activated artemisinin while pre-treatment with succinylacetone, that inhibits synthesis of heme, decreased DHA cytotoxicity in HL-60 leukemia cells (Mercer et al., 2011). In cancer, pre-treatment wth iron increased artemisinin cytotoxicity by 100x (Lai and Singh, 1995). In effect, inhibition of heme synthesis blocked the activity of some artemisinin dimers in HL-60 cells (Stockwin et al., 2009). Similarly, treatment with desferroxamine (DFO), an iron chelator, rendered artemisinins inactive (Huang et al., 2007). However, in absence of the endoperoxide bridge, the drug still had anticancer activity (Galal et al., 2002). Iron is crucial for cancer growth and the transferrin receptor 1 (TfR1) regulates iron uptake. In breast cancer, transferrin receptors are 10-15x more expressed compared to normal breast cells (Reizenstein, 1991; Habashy et al., 2010). Then, artemisinin can selectively target cancer cells to induce its iron mediated cytotoxicity as indicated in Fig.6.
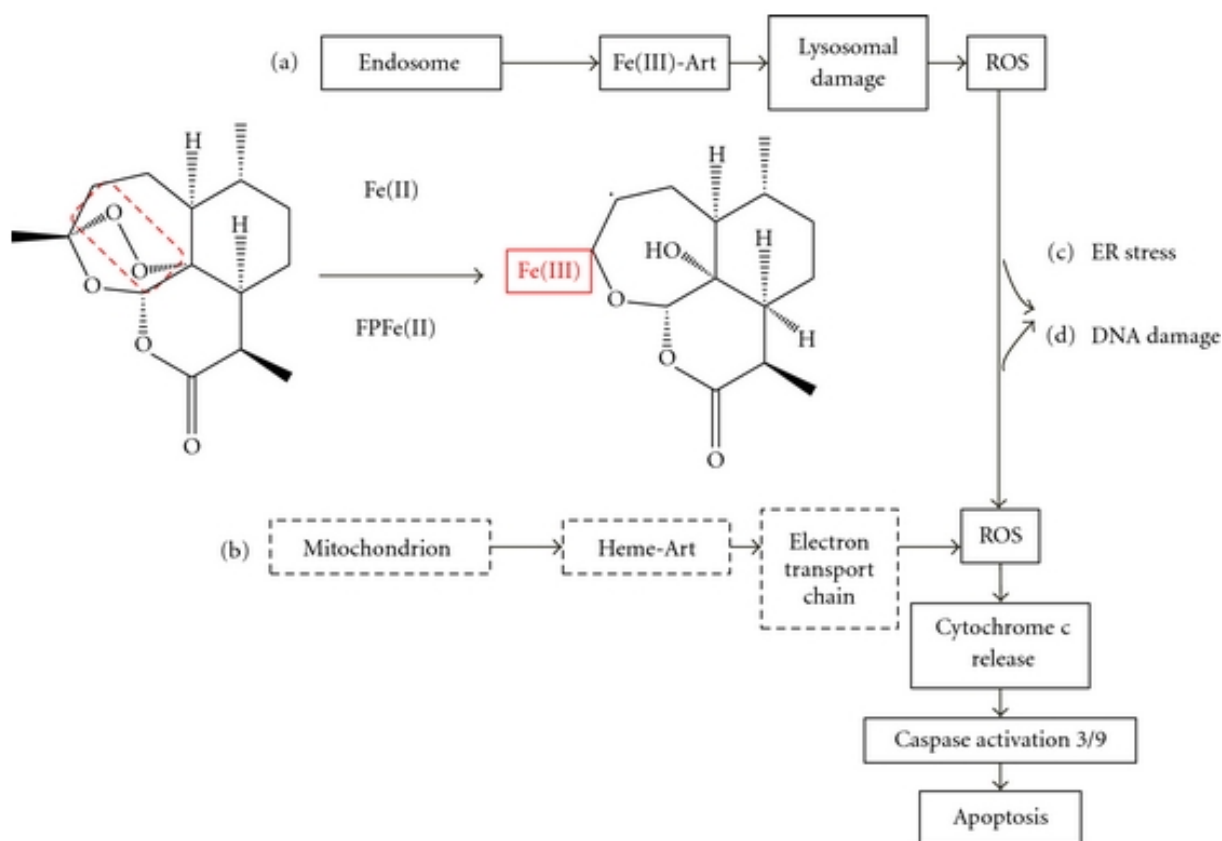
Fig. 6. <u>Artemisinin mode of action.</u> **A)** Artemisinin is internalized together with transferrin, and released in the lysosome. The lysosomal ferrous iron activates artemisinin to generate carbon-centered radicals and ROS, to induce lysosomal and mitochondrial damage and cell death by caspases; **B)** Artemisinin is activated in the mitochondria by heme or heme-bound protein, and its cytotoxic-carbon-centered radicals affects the electron transfer chain (ETC) to induce ROS and apoptosis. ROS production can also affect ER (c) and the genome (d). (Crespo-Ortiz and Wei, 2012).

2.9.1. Artemisinin as anticancer agent

2.9.1.1. Production of ROS and oxidative stress

In cancer, artemisinin is less cytotoxic in presence of high antioxidant activity. In particular, the gamma-glutamylcysteine synthetase induced resistance to ART and its inhibition restored sensitivity (Efferth, Margaret et al., 2003; Michaelis et al., 2010). Interestingly, artemisinin cytotoxicity associated with ROS and blockers of ROS or iron suppressed ART activity (Michaelis et al., 2010). Stockwin et al., (2009) found that dimers of artemisinin had a cytotoxicity 1,000x higher than monomer and ART induced ROS mediated apoptosis. In breast cancer, ART reacted with iron of lysosomes to induce ROS that in turn activated mitochondrial apoptosis (Hamacher-Brady et al., 2011).

2.9.1.2. Effect on cancer growth

A test on 55 cancer cell lines conducted by National Cancer Institute (NCI) found that ART was cytotoxic in many cancer types, including breast cancer (Efferth et al., 2003). From this panel, it was found that ART inhibited cancer growth at G0/G1 and G2/M phases while decreasing cyclin-dependent kinase 2 (CDK2), cell division cycle 25A (CDC25A) and cyclin B1 (Efferth, Sauerbrey et al., 2003). Then, artemisinin decreased CDK transcription (Firestone et al., 2009). ART reduced survival and blocked proliferation at G2/M phase in osteosarcoma cells (Xu et al., 2011). Also, ART inhibited topoisomerase II activity (Youns et al., 2009).

2.9.1.3. Effect on apoptosis

In general, artemisinins activates apoptosis by intrinsic pathway. In osteosarcoma, artemisinins increased the Bax/Bcl2 ratio (Xu et al., 2011) while in lung cancer, DHA and ART induced cytochrome c release, Bax and cleaved caspases 3 and 9 while survivin was highly decreased (Mu et al., 2007). In human endometrial carcinoma (EC) cell line HEC-1B, ART induced apoptosis by activating caspase 3 (Lijuan et al., 2010). In doxorubicin resistant leukemia cell lines, ART induced ROS that mediated apoptosis by activation of caspase 3, 9 and cleaved Parp (Efferth et al., 2007). ART decreased Sirtuin 1 (Sirt1) and induced apoptosis in ovarian cancer (Chen et al., 2019). Also, ART induced apoptosis by increasing Bax, suppressing Bcl-2 while activating caspase 3 and 9 in gastric cancer (Zhang, Luo et al., 2015). In the glioma cell line LN-229, ART induced ROS mediated DSBs to activate apoptosis (Berdelle et al., 2011).

2.9.1.4. Effect on metastasis and invasion

Artemisinin decreased MMP expression and αvβ3 integrins in the melanoma cell lines A375P and A375M (Buommino et al., 2008). Also, artemisinin induced cell adhesion by enhancing E-cadherin while MMP2 was decreased in hepatoma cells (Weifeng et al., 2011). In NSCLC, ART inhibited migration by decreasing MMP2, MMP7, AP-1 and NF-κB (Rasheed et al., 2010). In metastatic colorectal cancer cell lines, ART inhibited EMT by suppressing nuclear translocation of beta-catenin while increasing E-cadherin (Li, Zhang et al., 2008).

2.9.1.5. Effect on angiogenesis

Cancer cells induce angiogenesis. This mechanism is characterised by the generation of new blood vessels that sustain cancer growth with the sufficient blood supply. In CML cells, DHA inhibited VEGF and FGF (Chen et al., 2004) while in glioma ART blocked HIF-1α (Huang et al., 2008). Artemisinins blocked angiogenin (ANG), "the cysteine-rich angiogenic inducer (CYR61)", some metalloproteinases (MMP9, MMP11) and collagens (Anfosso et al., 2006). In pancreatic cancer, DHA inhibited NF-κB and inhibited VEGF, IL-8, cyclooxigenase 2 (COX2) and MMP9 (Wang et al., 2011). In choroidal melanoma, ART blocked VEGFR2, PDGFR, VEGFA and HIF-1α (Geng et al., 2021).

2.9.1.6. Effect on chemoresistant cancer cells

The study conducted by NCI on 55 cancer cell lines found that proteins involved in multi drugs resistance, such as MDR1 did not alter artemisinins cytotoxicity (Efferth, Sauerbrey et al., 2003). In NB cell lines resistant to "vincristin, doxorubicin, cisplastin, topotecan, mephalan and ectoposide", ART sensitivity was not altered (Michaelis et al., 2010). In a doxorubicin resistant leukemia cell line ART cytotoxicity was maintained (Reungpatthanaphong et al., 2002).

2.9.2. Artemisinins toxicity and clinical trials

The NCI analysis conducted on 55 cancer cell lines found that the ART IC$_{50}$ ranged 246 nM-100 μM (Efferth, Sauerbrey et al., 2003). In clinics, measurements from patients with malaria indicated that "plasma peak concentrations" after injection of ART at 200 mg/kg were of 2640 μg/ml (corresponding to 6.88 mM) (Batty et al., 1996). As the plasma peak of ART concentration was approximately three "orders of magnitude" higher than ART IC$_{50}$ values, this suggests that ART at suitable concentrations can be also used to treat tumors. However, cancer treatment could require higher ART concentrations than those used for malaria. Artemisinins have been shown to be toxic only after long-term treatment (Efferth et al., 2010) and treatment with artemisinin for 12 months did not cause relevant side effects (Singh and Verma, 2002). However, treatment of a breast cancer patient with herbal/artemisinin combination (400 mg) induced toxic encephalopathy (Panossian et al., 2005) while in animals, treatment with artemisinin at high concentrations and for more than four weeks caused neurotoxicity (Schmuck et al., 2002). In animals, artemisinins were efficient to block tumors. In HepG2 HCC xenografts, ART at concentrations from 50 to 100 mg/kg/day had low toxicity and cancer growth was inhibited by 79.6% (Weifeng et al., 2011) and also

100 mg/kg/d of DHA inhibited by 60.6% tumor growth (Hou et al., 2008). A few clinical trials have been conducted to check safety and efficacy of artemisinins in cancer. The ARCTIC M33/2 clinical trial on patients with metastatic breast cancer used ART at 200 mg/day for 4 weeks. ART was tolerated and 10/23 patients had stable disease while 5 had cancer progression (von Hagens et al., 2017). A detailed list of *in vivo* studies on animals and clinical trials of artemisinins treatment are reported in the review from Ma et al., (2021).

2.9.3. Artemisinin and breast cancer

In TNBC, DHA decreased cell proliferation, induced apoptosis by reducing phosphorylation of translationally controlled tumor protein (TCTP) and synergised with doxorubicin to increase apoptosis (Lucibello et al., 2015). In MCF-7 cells, artemisinin blocked cell proliferation at G1 phase by inhibition of cyclin-dependent kinase 2/4 (CDK2, CDK4) cyclin E, cyclin D1 and E2F Transcription Factor 1 (E2F1) (Tin et al., 2012). In MCF-7 cells, artemisinin decreased ESR alpha and inhibited cell growth at G1 phase (Sundar et al., 2008). In T4-7D cells, DHA induced apoptosis, inhibited growth at G0/G1 phase, activated caspase 9, Bid and release of cytochrome c (Mao et al., 2013). In MCF-7, T4-7D and MDA-MB-231 cells, ART reacted with lysosomal iron to generate ROS to activate mitochondrial apoptosis (Hamacher-Brady et al., 2011). In MDA-MB-468 and SK-BR-3 cells, ART induced oxidative stress that caused damage of mitochondrial integrity and DNA (Greenshields et al., 2019).

2.7. Hypothesis

In this research project it was hypothesized that EMT inhibition could sensitise TNBC cell lines to ART cytotoxicity.

2.7.1. Aims

Aim 1. To test whether receptor tyrosine kinase (RTK) AXL inhibitors R428/TP-0903 and AXL/ZEB1 knokdowns sensitised TNBC cell lines to ROS, H2AX phosphorylation and apoptosis induced by ART. Aim 2. To test whether R428/TP-0903 and AXL/ZEB1 knockdown in TNBC cell lines suppressed expression of superoxide dismutase 1/2 (SOD 1/2), glutathione peroxidase 8 (GPX8) and catalase (CAT).

A combination therapy is highly appreciated in cancer therapy as multiple drugs act in a synergistic manner to lower therapeutic dosage of each drug, side adverse effects and

incidence of resistance (Mokhtari et al., 2017). In this perspective, TNBC cell lines offer a suitable breast cancer type to test a combination therapy efficacy. It is still unknown whether AXL inhibitors and ART show synergistic effects to suppress TNBC. In addition, sensitisation to ART assumes high relevance as ART exerts its anticancer activity in a multifunctional and pleiotropic manner (Wang, Zhang et al., 2017). In this project, the hypothesis was to verify whether EMT inhibition sensitized TNBC cells to ART cytotoxicity.

In relation to Aim 1 (previously mentioned) TP-0903 and not R428 blocked the mesenchymal phenotype, pAXL 779 and the EMT transcription factors (TFs) Snail, Slug and ZEB1. In a sequential treatment, TP-0903 increased ROS, pH2AX and apoptosis induced by ART. ZEB1 downregulation and not AXL downregulation blocked EMT and increased ART induced ROS, pH2AX and apoptosis.

In relation to Aim 2, ZEB1 overexpression in MCF-7/ZEB1 cells significantly decreased gene expression of *SOD1* while significantly increased that of *SOD2* and *GPX8*. *CAT* was not affected. However, in TNBC cells, ZEB1 knockdown did not decrease GPX8, SOD2 protein expression; also, ZEB1 knockdown did not decrease *CAT* gene expression. In contrast, TP-0903 abrogated *CAT*. TP-0903 also decreased GPX8 and SOD2 protein expression that was further suppressed by ART. In addition, TP-0903 also suppressed Rad51 in TNBC cells but independently of ZEB1.

These results indicated that TP-0903 could sensitise TNBC cells to ART by suppression of antioxidant and DDR enzymes. The synergistic interaction between TP-0903 and ART suggested that a combination of both compounds could treat TNBC.

CHAPTER 3: MATERIALS AND METHODS

3. 1. Materials

3.1.1. Cell lines

In this project were used the non TNBC cell lines MCF-7/ZEB1, T-47D, ZR-75-1, SK-BR-3 and the TNBC cell lines MDA-MB-231/short hairpin (sh) ZEB1, MDA-MB-436, BT-549, Hs 578-T/shZEB1. Also, the TN non tumorigenic HBL-100 cell line was used. Growth of cells occurred in Dulbecco's Modified Eagle Medium (DMEM) medium (Thermo Fisher Scientific, Inc.) with supplement of fetal bovine serum (FBS) (10%), non-essential amino acids (NEAA) and penicillin–streptomycin (PS) (both at 1%). Incubation of cells was at 37°C with CO_2 (5%). Once cells had 80% of confluence, they were detached with 0.05% trypsin, centrifugated at 1000g at 25°C for 5 min, re-suspended in medium and allowed to grow both for the required experiment and for a stock. Cells with the doxycycline (DOX)-inducible ZEB1 expression, MCF-7/ZEB1, were maintained in the presence of absence of 1 μg/ml DOX for 72 h prior the experiments were carried out. To generate MDA-MB-231 and Hs 578-T cells with the stable ZEB1 knockdown (sh), cells were infected with the pLKO.1- PURO lentiviral vectors (Sigma-Aldrich, St. Louis, MO, USA) expressing ZEB1-targeting shRNA or control shRNA. Selection of cells expressing shRNAs was performed in 0.5 μg/ml puromycin-containing DMEM for 7-10 days.

3.1.2. Reagents

The AXL inhibitors R428 (no. HY-15150) and TP-0903 (HY-12963) were bought from MedChemExpress while ART from Sigma-Aldrich (no. A3731). All compounds were in powder and solubilised in dimethyl sulfoxide (DMSO). The stock concentration of each drug was prepared by using the formula V(l) = mass(g)/[MW x Molarity(M)]. In the formula: V(l) the volume of DMSO; m(g) the total weight of the drug in the vial; MW the molecular weight of drug; Molarity(M) the stock concentration wanted. The stock concentration for both AXL inhibitors was 10 mM while that of ART was 100 mM. To prepare a final drug concentration for cell treatment, I used the formula V(μl) = final drug concentration (μM) x final volume (μl) / stock concentration (μM). In the formula: V(μl), the volume to be taken from stock. The DMSO concentration was kept lower than 1 %. Sigma-Aldrich provided the following reagents: phosphate buffered saline (PBS), PS, trypsin, DMSO, NEAA and FBS. With regard to primary antibodies, anti-snail (no. 3879), slug (no. 9585), cleaved caspase 3 (no. 9664),

anti-AXL (no. 8661) were bought from Cell Signaling Technology Inc. (CST). Also, antibodies recognizing anti-pAXL 779 (no. AF2228) and AXL (no. AF154) were bought from R&D Systems. In addition, anti-tubulin (no. T6199), pH2AX (no 05636, clone JBW301) and anti-AXL (no. SAB1409509) were purchased from Sigma-Aldrich and antibodies identifying vimentin (no. 550513), E-cadherin (no. 610181), P-cadherin (no. 610228) from BD Biosciences. The antibody that recognizes ZEB1 was purchased from Santa Cruz (no. sc-515797). Secondary antibodies were obtained from Dako and Abcam. Concerning silencing (si) RNAs, siRNA AXL #1 ([siRNA Details (thermofisher.com)](#)), siRNA AXL #2 ([siRNA Details (thermofisher.com)](#)) were bought from Thermo Fischer. The siRNA ZEB1 #1 ([Zeb1 Mouse siRNA Oligo Duplex (Locus ID 21417) – SR422122 | OriGene](#)) were bought from Origene while siRNA ZEB1 #2 ([siRNA Details (thermofisher.com)](#)) and siRNA ZEB1 #3 ([siRNA Details (thermofisher.com)](#)) from Thermo-Fischer. LTX Lipofectamine with Plus reagent (no. 15338100) was bought from Thermo Fischer.

3.2. Methods

3.2.1. Muse Annexin V assay

In order to check number of apoptotic cells after drug treatment, Muse Annexin V & Dead Cell Assay (no. MCH100105, Sigma-Aldrich) was performed in accordance with instructions from manufacturer ([Muse Oxidative Stress.book (cytekbio.com)](#)). This assay uses Annexin V that identifies phosphatidylserine in the outer membranous layer of apoptotic cells. In brief, 200,000 cells/well were inserted in a 6-well plate and when they had 70%-80% of confluence were treated according to the treatment type and schedule requested. Cells, both adherent and in suspension, were diluted in PBS to 5×10^5 cells/ml before mixing 100μl cell suspension with 100μl Muse™ Annexin V & Dead Cell Reagent. After brief vortexing, samples were incubated for 20 min and their apoptotic profile was analysed through Muse™ Cell Analyzer (Merck Millipore).

3.2.2. Western Blotting

In order to check how protein expression was affected by drug treatment, Western Blot was performed. In brief, 200,000 cells/well were placed in a 6-well plate, and when they had 70%-80% of confluence were treated according to the treatment type and schedule requested. After two washes with PBS, cells lysates were collected in Laemmli buffer 1x, heated at 95°C, sonicated and Pierce Bicinchoninic (BCA) protein assay (Thermo Fisher Scientific, Inc.) was utilised to measure protein concentration. Then lysates mixed with loading buffer

were loaded into sodium dodecyl sulfate (SDS) gels and run with Running buffer 1x, at 120 V, for 80 min. After running, proteins were transferred to polyvinylidene fluoride membrane (Millipore) with Transfer buffer 1x, at 20V, for one day. Then, 5% milk in Tris-buffered saline with 0,1% Tween 20 (TBST) 1x was used to block membranes for 60 min before incubation with primary antibodies at 25°C, for 1 hr. After three 5 min TBST washes, secondary antibodies were applied at 25°C for 1 hr and protein expression was detected by Super Signal horse peroxidase (HRP) chemiluminescent substrates (Thermo Fisher Scientific, Inc.). The images were taken by the ChemiDoc machine. Tubulin was used to maintain equal loading among samples.

3.2.3. MTT/MTS assay

In order to verify how ART influenced cell viability in TNBC (except the BT-549 cell line) and non TNBC cell lines, the cell proliferation [3-(4,5-Dimethylthiazol-2-yl)-2,5-Diphenyltetrazolium Bromide] Assay (MTT) (no. 11465007001, Sigma-Aldrich) was used according to instructions from manufacturer ([11465007001.pdf (sigmaaldrich.com)](11465007001.pdf)). MTT assay is a colorimetric assay based on the reduction by NADPH oxidoreductase enzymes of the soluble tetrazolium MTT to the insoluble formazan that has a purple color. MTT assay measures the metabolic activity of cells as an indication of cell proliferation and cytotoxicity. In sum, 15,000 cells/well were placed in a 96-well plate (approximately 70% of confluence) and treated for three days with ART ranging 20 µM - 320 µM. A positive control (untreated cells), vehicle control (cells with DMSO only) and blank (medium only) were also included. After three days, medium was removed, MTT was inserted and left at 37°C until the formazan product with a clear purple color was formed. Then, 200 µl DMSO was added and absorbance values were determined at 570 nm. After subtracting blank absorbance, cell viability was determined by dividing absorbance of samples treated with drugs by absorbance of control before multiplying by 100. The IC_{50} was calculated in a log scale. In particular, in a XY tab of the GraphPrsim 9.0 program, the linear values of concentrations (X values) and absorbance (Y values) were inserted. Then, X and Y values were normalized by using a log transformation. After, in a nonlinear regression analysis, the "log(inhibitor) vs. response - Variable slope (four parameters)" function allowed to calculate the IC_{50} in a logarithmic scale. ART cytotoxicity in BT-549 cells was measured by the MTS (3-(4,5- dimethylthiazol-2-yl)-5-(3-carboxymethoxyphenyl)-2-(4-sulfophenyl)-2H-tetrazolium) assay and instructions from the manufacturer were followed (([MTS-Assay-Kit-Protocol-book-v4b-ab197010 (website).pdf (abcam.com)](MTS-Assay-Kit-Protocol-book-v4b-ab197010))). In parallel with the MTS assay, the MTT procedure was repeated. The MTS

assay did not require DMSO solubilisation and absorbance values were measured at 490 nm. As MTT and MTS assays are based on the same principle that higher metabolic reduction of MTT/MTS reagents corresponds to higher rate of cell proliferation, it can be assumed that results from these two assays would be comparable. Then, accordingly, in BT-549 cells, ART IC_{50} value of MTS assay would be similar to that supposedly obtained in MTT assay. MTT assay was also used to check how a simultaneous and a sequential treatment of TP-0903 plus ART influenced cell viability. In pursuit of this, cells were treated with 1) TP-0903; 2) ART; 3) simultaneous treatment with TP-0903 plus ART; 4) pre-treatment with TP-0903 for 24 h, before a further treatment with TP-0903 plus ART for 2 days or 3 days. After subtracting blank absorbance, the growth inhibition rate was determined by dividing (1 - absorbance of samples treated with drugs) by absorbance of control. Then, each value was used as input in the CompuSyn software (Chou, 2005) to calculate the combination index (CI) that determines the type of the interaction between drugs; in particular, with CI = 1, drugs had an additive effect, with CI > 1, drugs shown antagonism while with CI < 1, drugs shown synergism.

3.2.4. Muse Oxidative stress assay/CM-DCFH DA assay

Muse Oxidative stress assay. In order to check superoxide levels induced by ART in TNBC, the Muse Oxidative stress kit was used (no. MCH100111) and instructions of manufacturer were followed (untitled (cytekbio.com)). This assay uses the reagent dihydroethidium that, after oxidation by cellular superoxide, intercalates the DNA and emits a red light. Then, two populations of cells can be distinguished: blue (superoxide negative) and red (superoxide positive). In brief, $2,5 \times 10^5$ cells were seeded before conducting the test. First, an intermediate solution was prepared by diluting 1:100 the Muse oxidative stress reagent with Assay buffer 1X. Then, the solution was further diluted 1:80 in the Assay buffer 1X before taking 190 µl and mixed to 10 µl of cells to have an optimal concentration of 10^6 cells/ml. Then, cells were incubated for 30 min at 37°C before analysis with the Muse cell analyzer.

CM-DCFH DA assay. In order to check hydrogen peroxide levels in MDA-MB-231/sh ZEB1 cells and MDA-MB-231 cells treated with ART, TP-0903 and a combination of two, the 5-(and-6)-chloromethyl-2′,7′-dichlorodihydrofluorescein diacetate, acetyl ester (CM-H2DCF-DA) probe was used (no. C6827, Thermo Fischer) and instructions of the manufacturer were followed (Reactive Oxygen Species (ROS) Detection Reagents (thermofisher.com)). This assay uses the H2DCF-DA reagent that is firstly converted to dichlorofluorescin (DCF) by cellular esterases. Then, DCF is oxidized by hydrogen peroxide

and emits a green light. In brief, $2,5 \times 10^5$ cells were seeded in a 6 well plates containing coverslips and cells at confluence of 70%-80% were treated according to treatment type and schedule requested. Then, after treatment cells were washed one time by medium, two times with PBS before applying the DCFH DA solution at 8 µM. Then, cells were incubated for 30 min at 37°C. Then, cells were washed two times with PBS and coverslips were placed to the slide to make the mounting medium to distribute. Then, slides were observed by a fluorescent microscopy and DCFH DA signal was detected by using the green fluorescent protein (GFP) wavelenght.

3.2.5. PCR and qPCR

PCR. In order to check and quantify gene expresion of antioxidant enzymes, a polymerase chain reaction (PCR) and quantitative (q) PCR were performed. There are three steps required: 1) RNA extraction; 2) cDNA synthesis: 3) PCR and qPCR.

1) To extract and purify total RNA from cancer cells the RNeasy Mini Kit (no. 74104, Qiagen) was used and instructions from the manufacturer were followed. After that cell pellet was displaced by flicking the eppendorf, 350 µl of buffer RLT was added to disrupt cells. Then, 70% ethanol was added to the lysate, and mix well by pipetting. Then, cells were homogenised by vortex for 2 min. Then, 700 µl of sample was transferred to a RNeasy spin column and centrifugated for 15 s at 8000 g. The flow-through was discarded. Then, 700 µl of buffer RW1 was added again to the RNeasy spin column, centrifugated for 15 s at 8000 g and the flow-through was discarded. Then, 500 µl of buffer RPE was added to the RNeasy spin column, centrifugated for 15 s at 8000 g and the flow-through was discarded. Then, 500 µl of buffer RPE was inserted in the RNeasy spin column, centrifugated for 2 min at ≥8000 g and the RNeasy spin column was placed in a new 2 ml collection tube before adding 30–50 µl of RNase free water directly to the spin column membrane; then, centrifugation for 1 min at ≥8000 g waas conducted to elute the RNA and the total RNA amount was lower than 30 µg. The RNA was quantified by using a Nanodrop spectrophotometer.

2) The iScript Select cDNA synthesis kit (no.170-8897, Qiagen) was used to make the cDNA synthesis from RNA samples and instructions from the manufacturer were followed. First, all components of the kit, except iScript reverse transcriptase, were thawed, mixed thoroughly and briefly centrifuged to collect contents at the bottom of tube and placed on ice. Then, 7 µl of nuclease free water, 4 µl 5x iScript select reaction mix, 2 µl Oligo(dT)20 primer or random primer, 6 µl of RNA sample (1 µg total RNA) and 1 µl variable iScript reverse transcriptase were inserted in a PCR tube and placed on ice. After mixing gently, the tubes

were incubated for 60–90 min at 42°C and incubated at 85°C for 5 min to inactivate the reverse transcriptase. The cDNA was placed at –20°C. Then, to check quality of cDNA, samples were amplified for glyceraldheyde 3 phosphate deydrogenases (*GAPDH*) by PCR. The *GAPDH* primers were bought from OriGene (no.HP205798). In brief, a reaction mix of 40 µL in a PCR tube was prepared by adding the following reagents: Taq PCR reaction master mix (Sigma, no 4600), nuclease free water, primers (0.5 µM) and template (44 ng/µl). Each eppendorf contained water (12 µl), primers for catalase or glyceraldheyde 3 phosphate deydrogenases (*GAPDH*) (4µl for forward and 4 µl for reverse primers), template (8 µl) and 12 µl of PCR reaction master mix. Then, after mixing and centrifugation, a negative control was prepared without template cDNA. A PCR reaction was performed as follows: initial denaturation (94°C, 5 min), denaturation (94°C, 30 sec), primer annealing (60°C, 30 sec), extension (72°C, 60 sec) and final extension (72°C, 5 min). These steps were repeated for 30 cycles. The PCR products for GAPDH were separated by running in the agarose gel electrophoresis in TBE buffer and visualised by UV transilluminator of the ChemiDoc machine.

3) PCR. To check *CAT* and *GAPDH* gene expression a PCR was performed. All steps as in 2) were repeated (only temperature of annealing for *CAT* was changed).

qPCR. To calculate gene expression of *SOD1, SOD2, GPX4 and GPX8* a qPCR was performed. To do this, the following reagents were used: template cDNA at 44 ng/µl, nuclease free water, *GAPDH* and antioxidant enzymes primers (0.5 µM) and SYBRS green supermix from Biorad (no. 172-4270) that contains polymerase, dNTPs, buffers and the dye. The final volume was 40 µl. The primers sequences were validated by BLAST primer. In sum, for each sample were prepared two eppendorf. The first eppendorf contained water (12 µl), primers for antioxidant enzymes (4µl for forward and 4 µl for reverse primers), template (8 µl) and 12 µl of SYBRS super mix. The second eppendorf contained the same reagents but GAPDH primers in place of those for antioxidant enzymes. Then, each tube was briefly centrifugated and placed in the appropriate well of a MicroAmp optical 96 well reaction plate bought from ThermoFischer (no. 8010560) that was centrifugatd at 1000 rpm for 2 min before analysis with a qPCR machine that run for almost 2 h. Also a negative control for both GAPDH and each antioxidant enzymes was prepared. The relative gene expression was calculated by the ΔΔCt method. The Ct parameter is the cycle number at which the fluorescence generated crosses the threshold when sufficient amplicons accumulate. The Ct values of *GAPDH* are compared to those of the genes of interest. This method does not

require standards and reducing reagents assuming that amplification efficiency in each well is equal. The primers sequences for amplification of antioxidant enzymes are in Table I.

Table 1. Primers sequences for amplification of *SOD2, GPX8, CAT, GPX4* and *GAPDH*.

Target gene	Forward sequence	Reverse sequence	T annealing (°C)
SOD2	AGCACCAGCACTAGCAAGCATG	CCGTAGTCGTAGGGCAGGTCG	56,4
GPX8	GCCTCTTGCAGCTTACCCGC	GTTGGCAGTCACTGGCCAGC	58,5
CAT	AGCCTTCGACCCAAGCAACA	AGCCTTCGACCCAAGCAACA	56,6
GPX4	ACAAGAACGGCTGCGTGGTGA	GGTGCACGCTGGATTTTCGG	56,9
GAPDH	GTCTCCTCTGACTTCAACAGCG	ACCACCCTGTTGCTGTAGCCAA	60

3.2.6. siRNA transfection

In pursuit of verifying whether AXL or ZEB1 depleted cells were more sensitive to ART than those AXL/ZEB1 expressing, cells were transfected with siRNA that prevented AXL and ZEB1 protein expression. Briefly, cells were grown until they were 70% confluent in a six well plates. Then, a first dilution of 10μl Lipofectamine LTX in 150μl of Opti-MEM medium and a second dilution of 1μl of two different siRNA targeting AXL/ZEB1 or siRNA negative control with 1μl of Plus reagent in 150μl of Opti-MEM medium were made. After incubation for 5 min, 150μl of diluted LTX were inserted in the diluted siRNA AXL/ZEB1 or siRNA negative control, incubated for 20 min before taking 250μl from that mixture and inserted in the siRNA AXL/ZEB1 and control containing wells. After 6 hr post-transfection medium was replaced while after thirty-six hours cells were untreated (control) or treated with ART at 40 μM before analysis.

3.2.7. Heat Map and Hierarchical Clustering

In order to check the relative gene expression of *AXL* and antioxidant enzymes in breast cancer and in some additional cancer types, a Heat Map/Hierarchical analysis was performed. The datasets were downloaded from an in-silico experiment performed in Expession Atlas – EMBL-EBI database. Original downloaded data was edited to facilitate downstream analyses.

All analyses were performed in R v.4.2.3 in the RStudio v2023.03.0 Build 386 environment. Used packages were pheatmap and corrplot.

3.2.8. Statistical analysis

The unpaired t-test and one sample t-test were used to compare two groups while in presence of more than two groups the Dunnett's test and the Tukey's test were adopted. The Dunnett's test and the Tukey's test were within the ANOVA statistical analysis function proposed by the statistical software used. The p-value is indicated as a number and only comparison with p-value less than or equal to 0.05 are displayed. The statistical tests were conducted after that all assumptions required were satisfied (normal distribution, homogeneity of variance, independence of measurements). Statistical analysis was conducted by GraphPad Prism 9.0 program.

CHAPTER 4: RESULTS

4.1. TNBC cell lines presented EMT markers

TNBC cell lines were checked for expression of EMT markers. First, the heat map and hyerarchical clustering analysis of the relative gene expression of AXL, CDH2 (N-cadherin), VIM (mesenchymal markers) and CDH1, junction plakoglobin (JUP) (epithelial markers) in a panel of breast cancer cell lines shown that AXL co-clustered with CDH2 and VIM (Fig. 7A). The same cluster was also found in different cancer types (Supplementary Figure S7A). The protein expression of EMT markers was checked in the TNBC cell lines MDA-MB-231, MDA-MB-436, BT-549 and the non TNBC cell lines ZR-75-1, T-47D, SK-BR-3 and MCF-7.In Fig. 7B, Western Blot shows that in TNBC cell lines mesenchymal markers AXL and VIM were present while the epithelial marker E-cadherin was absent. The non TNBC cell lines only expressed E-cadherin. In Fig. 7C, phase contrast images show that mesenchymal breat cancer cell lines MDA-MB-436 and BT-549 had a mesenchymal phenotype while the non TNBC cell lines T-47D and MCF-7 had an epithelial phenotype.
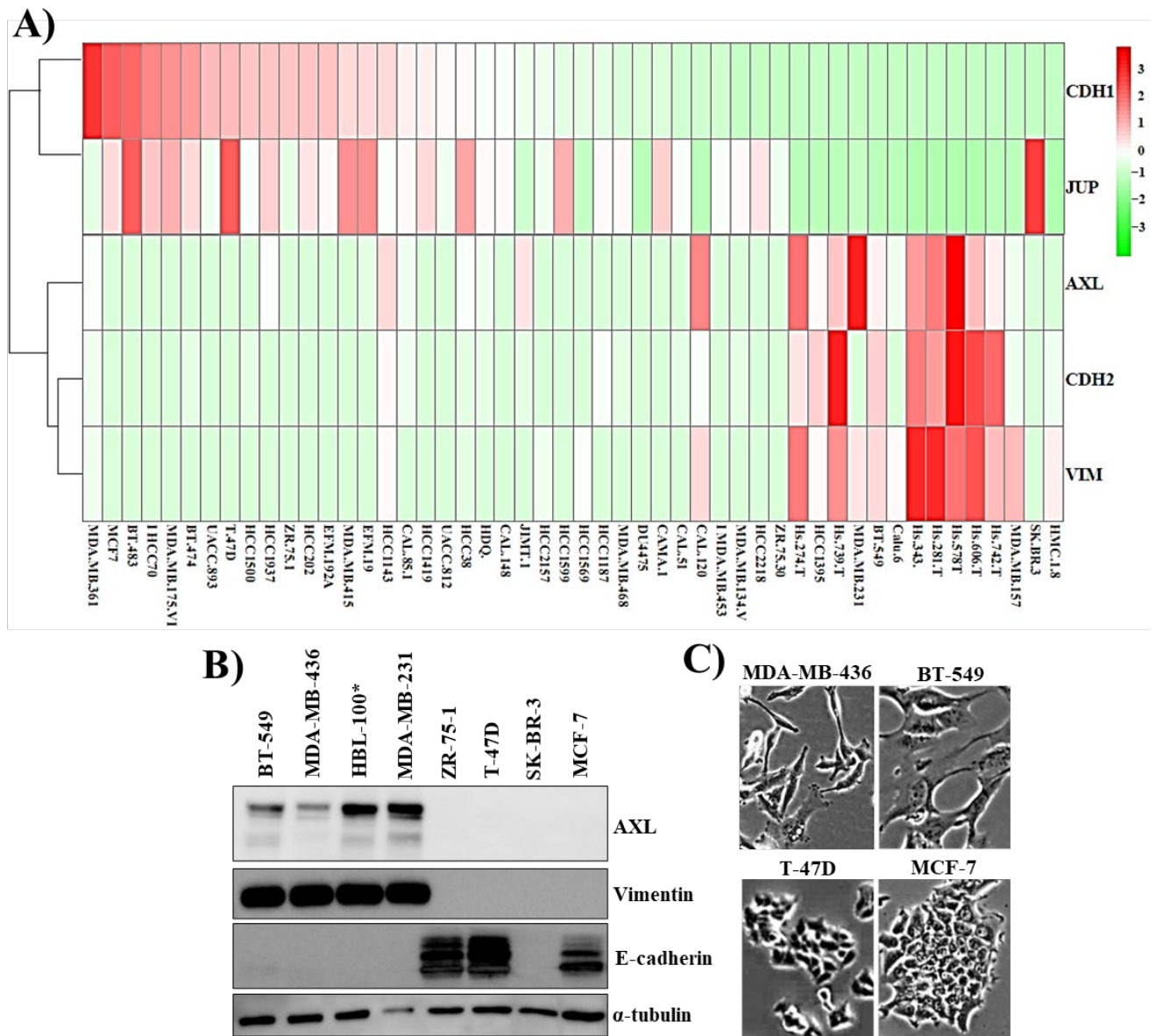
Figure 7. TNBC cell lines had mesenchymal markers. **A)** Heat Map analysis in a panel of breast cancer cell lines. The relative expression of AXL, CDH1, CDH2, VIM and JUP in breast cancer cell lines is shown. AXL co-clustered with mesenchymal markers. Genes are hierarchical clustered using Euclidean distances. Data was downloaded from in silico experiments conducted in EMBL-EBI database. Data are z-scored. **B)** Western Blot. Characterization of breast cancer cell lines shows that mesenchymal proteins VIM and AXL were in TNBC-derived cell lines. Non-TNBC-derived cells expressed epithelial marker E-cadherin. * = non tumorigenic triple negative breast cell line; **C)** TNBC cell lines had a mesenchymal phenotype while non TNBC cell lines had an epithelial phenotype.

4.2. TNBC cell lines were more resistant to ART

To check ART cytotoxicity in breast cancer, non TNBC and TNBC cell lines were treated with ART at different concentrations (20 μM – 320 μM) for 72 h before analysis with MTT assay. ART cytotoxicity in BT-549 cells was checked by MTS after treatment with

ART at different concentrations (16 μM – 256 μM) for 72 h. Fig. 8 shows that TNBC cells were more resistant to ART with IC_{50} values ranging 37 μM-74 μM. ART IC_{50} of non TNBC cells ranged 27 μM - 25 μM, These findings suggested that AXL/EMT could render TNBC cell lines resistant to ART cytotoxicity.
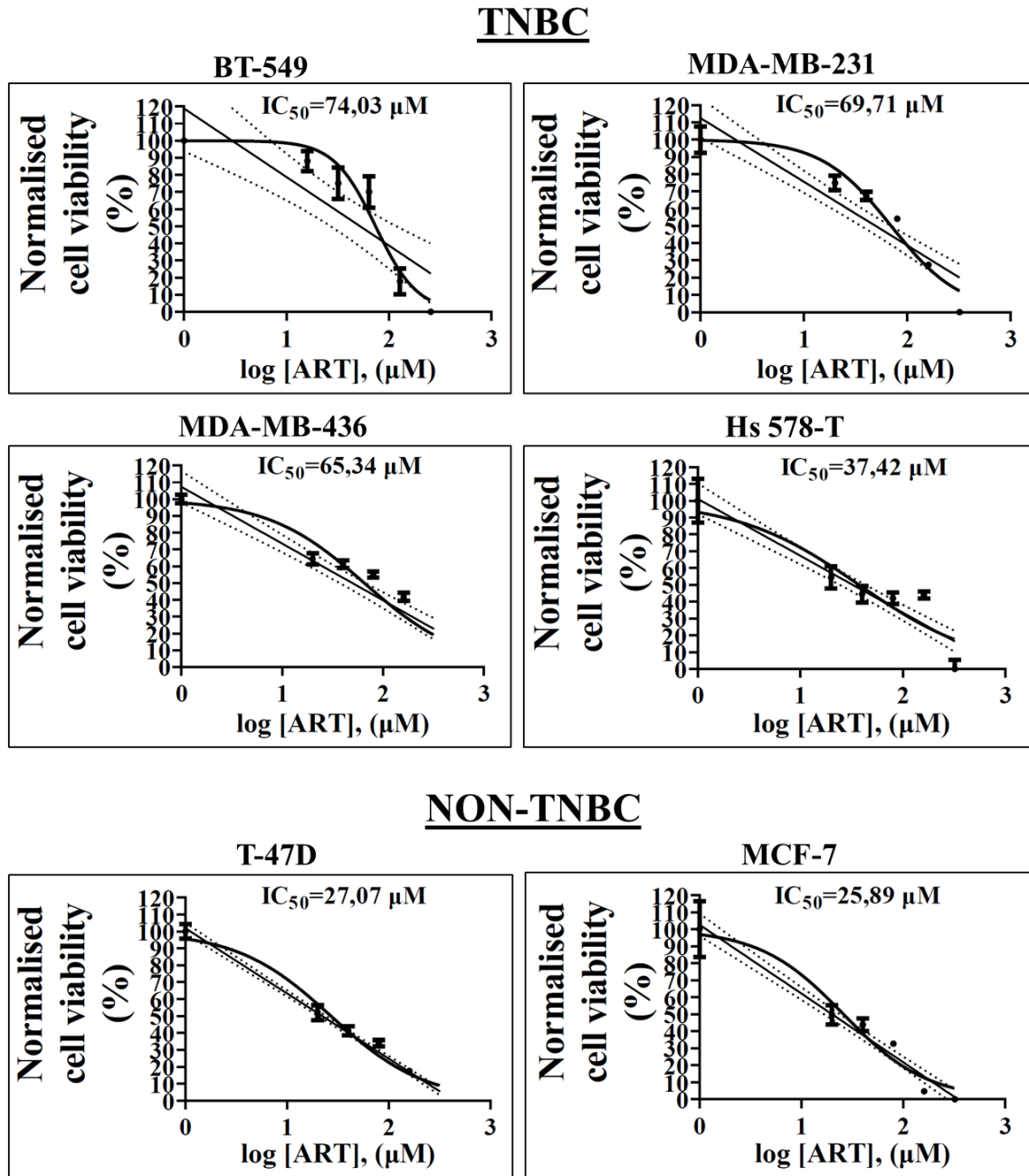
Figure 8. TNBC cell lines were more resistant to ART. MTT/MTS assay. ART IC_{50} were higher in TNBC cells than in non-TNBC cells. ART IC_{50} for MCF-7 and MDA-MB-231 was extrapolated from MCF-7/ZEB1 (-) Dox and MDA-MB-231 siRNA cntrl of Fig. 9A. Results are expressed as mean ± SEM of six technical replicates. The figure includes the 95% Confidence Bands of the best-fit line after a linear regression analysis. In some figures, the SEM values are too small and not visible.

4.3. ZEB1 activation induced EMT and decreased ART cytotoxicity

In order to check how ZEB1 influenced cell viability after treatment with ART, MCF-7/ZEB1 cells were treated with doxicycline (Dox) to induce ZEB1 while MDA-MB-231 cells were treated with siRNA ZEB1 before ART treatment. In Fig. 9A, phase contrast images show that MCF-7/ZEB1 (-) and (+) Dox cells had an epithelial and mesenchymal phenotype, respectively. Western Blot shows that activation of ZEB1 in MCF-7/ZEB1 (+) Dox cells suppressed E-cadherin while depletion of ZEB1 in MDA-MB-231 increased E-cadherin (Fig. 9B). In Fig. 9C, MTT results show that ART IC_{50} of MCF-7/ZEB1 (+) Dox cells was higher than that of MCF-7/ZEB1 (-) Dox (49.02 μM and 25.89 μM, respectively) In the reverse experiment, ART IC_{50} of MDA-MB-231 siRNA ZEB1 cells was lower than that of MDA-MB-231 siRNA cntrl (48.9 μM and 69.71 μM, respectively).
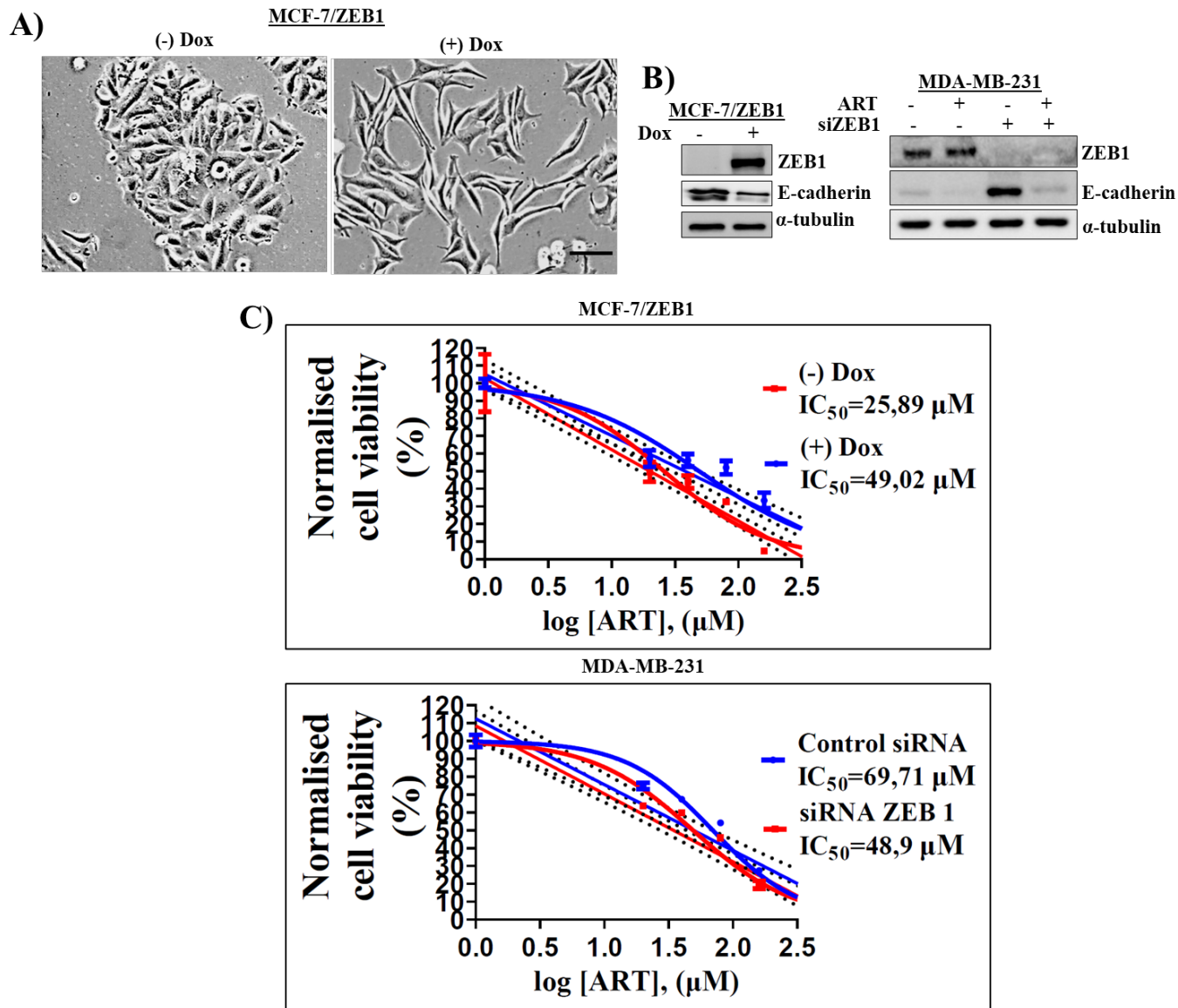
Figure 9. ZEB1 decreased ART cytotoxicity. **A)** Phase contrast images. ZEB1 activation in MCF/ZEB1 (+) Dox cells induced a mesenchymal phenotype. **B)** Western Blot. EMT was induced by ectopic expression of ZEB1 in MCF-7 cells (left panel) or reverted by ZEB1 depletion in MDA-MB-231 cells (right panel). EMT increased viability of ART-treated MCF-7 cells while activating partial epitelisation in MDA-MB-231 cells sensitized cells to ART. **C)** MTT assay. ZEB1 activation decreased ART cytotoxicity in MCF-7/ZEB1 (+) Dox compared to (-) Dox cells. In contrast, ZEB1 knockdown in MDA-MB-231 cells increased sensitivity to ART. Results are expressed as mean ± SEM of six technical replicates. The figure also includes the 95% Confidence Bands of the best-fit line after a linear regression analysis. In some data points, the SEM values are too small to be visualised.

4.4. ZEB1 knockdown sensitised TNBC to ART mediated apoptosis

ZEB1 could sensitise TNBC cells to ART induced apoptosis. In Fig. 10A, MDA-MB-231 cells were treated with ART 40 μM, siRNA AXL, siRNA ZEB1 #1 #2 and #3 and a combination of siRNA and ART for 72 h. Western Blot results shows that ZEB1 knockdown and not AXL knockdown increased E-cadherin, P-cadherin and ART induced cleaved caspase 3 in MDA-MB-231 cells (Fig. 10A). AXL knockdown decreased pAKT 473 in MDA-MB-231 and BT-549 cells (Supplementary Figure 10A/1). Then, MDA-MB-231 and MDA-MB-231 cells stably depleted for ZEB1 (shZEB1) were treated with ART. In Fig. 10B, shZEB1 cells presented P-cadherin that was absent in MDA-MB-231/cntrl. Annexin V assay results shown that ART 160 μM induced a significant higher late/early apoptotic cells rate in shZEB1 cells compared to MDA-MB-231/cntrl cells after 48 h. Phase contrast images show that ART for 72 h was more cytotoxic, in terms of cell viability, in MDA-MB-231/shZEB1 cells compared to MDA-MB-231/cntrl cells (Supplementary Figure S10B/2). Then, MDA-MB-436 cells were treated with ART at 40 μM, siRNA ZEB1 #2 and #3 and a combination of siRNA ZEB1 and ART for 72 h. In Fig. 10C, Western Blot results shows that ZEB1 knockdown increased E-cadherin and sensitised cells to ART induced cleaved caspase in MDA-MB-436 cell line. In the Supplementary Figure S10C, results of an additional experiment in MDA-MB-436 cells confirmed activation of apoptosis induced by siRNA ZEB1 plus ART. Then, in Fig. 10D, Western Blot shows that Hs 578-T/shZEB1 cells had higher ART induced cleaved caspase 3 compared to Hs 578-T/cntrl cells. In the Supplementary Figure S10D/1, ZEB1 expression in shZEB1 cells is much lower tha Hs 578-T/cntrl. In the Supplementary Figure S10D/2, phase contrast images show that ART for 72 h was more cytotoxic, in terms of cell viability, in shZEB1 cells compared to Hs 578-T/cntrl cells. In the Supplementary Figure S10D/3 results of an additional experiment in Hs 578/cntrl and Hs 578/ZEB1 cells confirm activation of higher extent of apoptosis in shZEB1 cells compared control cells.
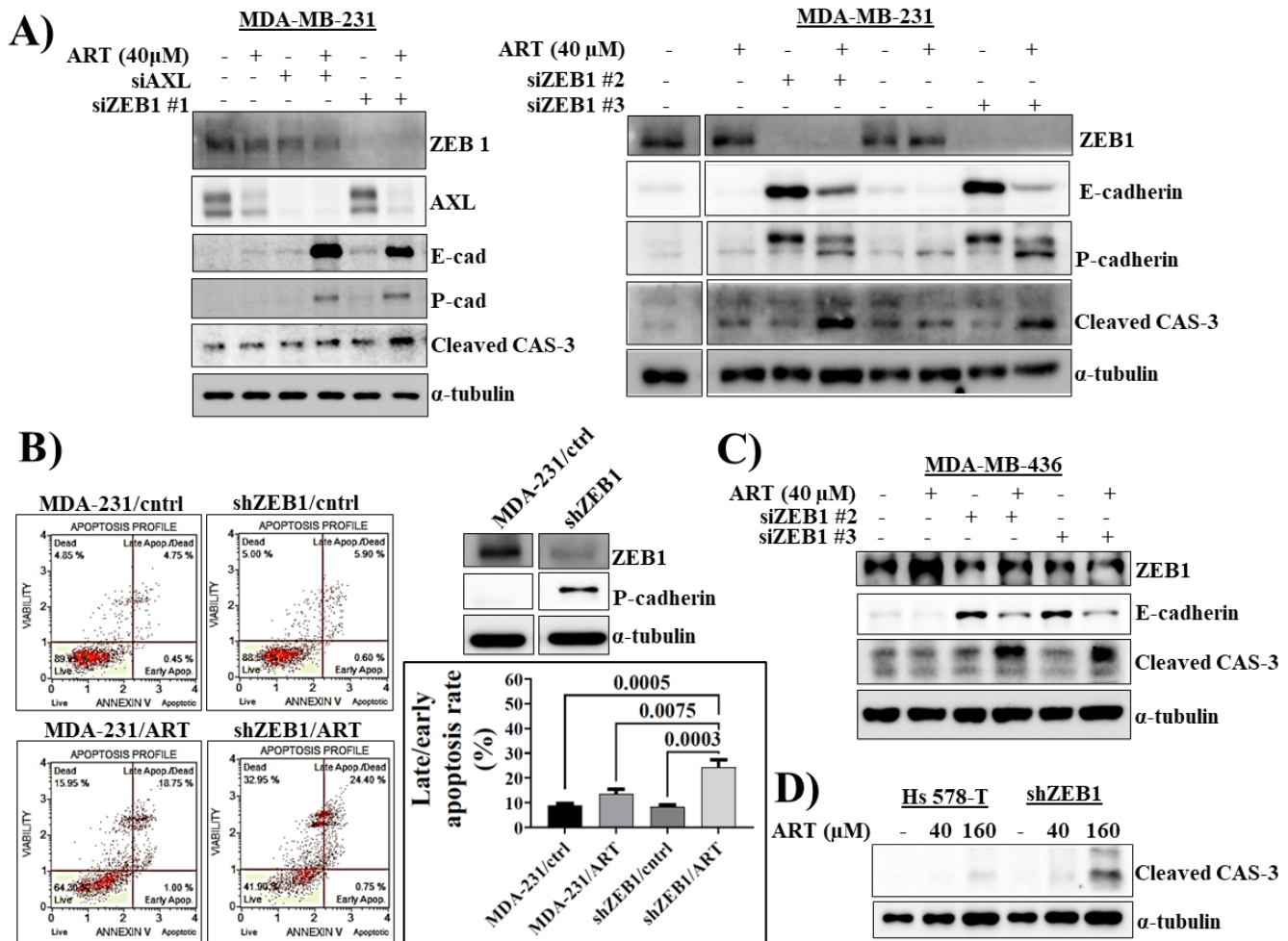
Fig. 10. ZEB1 knckdown sensitised TNBC cells to ART induced apoptosis. **A)** Western Blot. MDA-MB-231 cells were treated with siRNA AXL, ZEB1 #1, #2 and #3, ART 40 μM and their combination for 72 h. ZEB1 knockdown and not AXL knockdown increased cleaved caspase 3 expression induced by ART. **B)** MDA-MB-231 cells presented ZEB1 while P-cadherin was absent; shZEB1 cells had low ZEB1 expression and presented P-cadherin. Muse Annexin V assay. ART 160 μM induced significant higher apoptosis in shZEB1 compared to MDA-MB-231 cells. Results are expressed as mean ± SEM of four independent measurements (two independent experiments were run at different days and each experiment was repeated two times the same day by using two different flasks as source of cell seeding). The Tukey's test was used to check significance among groups; significant p-value lower than or equal to 0.05; **C)** Western Blot. MDA-MB-436 were treated with siRNA ZEB1 #1 or #2, ART 40 μM and their combination for 72 h. **D)** Hs 578-T cntrl/shZEB1 cells were treated with ART for 72. The cleaved caspase 3 expression induced by ART was higher in sh cells compsred to control ZEB1 expressing cells.. The blots related to siRNA AXL/ZEB1 #1 and siRNA ZEB1#1/#2 in **A)** are a part of the entire blots reported in the Supplementary Figure S10A/2 and S10A/3, respectively. The blot related to P-cadherin expression in **B)** is a part of the entire blot reported in the Supplementary Figure S10B/1.

4.5. TP-0903 inhibited AXL and EMT

To check whether AXL inhibtors R428 and TP-0903 inhibited AXL, MDA-MB-231 cells were treated for 24 h with TP-0903 at 0.06 μM - 1 μM. In Fig. 11A, Western Blot results show that MDA-MB-231 control cells had consitutive phosphorylation of AXL at Y779; TP-0903 and not R428 at 24 h linearly decreased pAXL 779 at increasing concentrations. Phase contrast images show that R428 did not change cell phenotype, increased Snail, Slug and induced high intracellular vesiculation after 24 h in MDA-MB-231 cells (Supplementary Figure S11A/1). TP-0903 induced clustering and reversed mesenchymal phenotype (Supplementary Figure S11A/2). Fig. 11B and C show that in MDA-MB-231 cells TP-0903 at 0.25 μM significantly decreased ZEB1 while increasing E-cadherin protein expression, respectively.
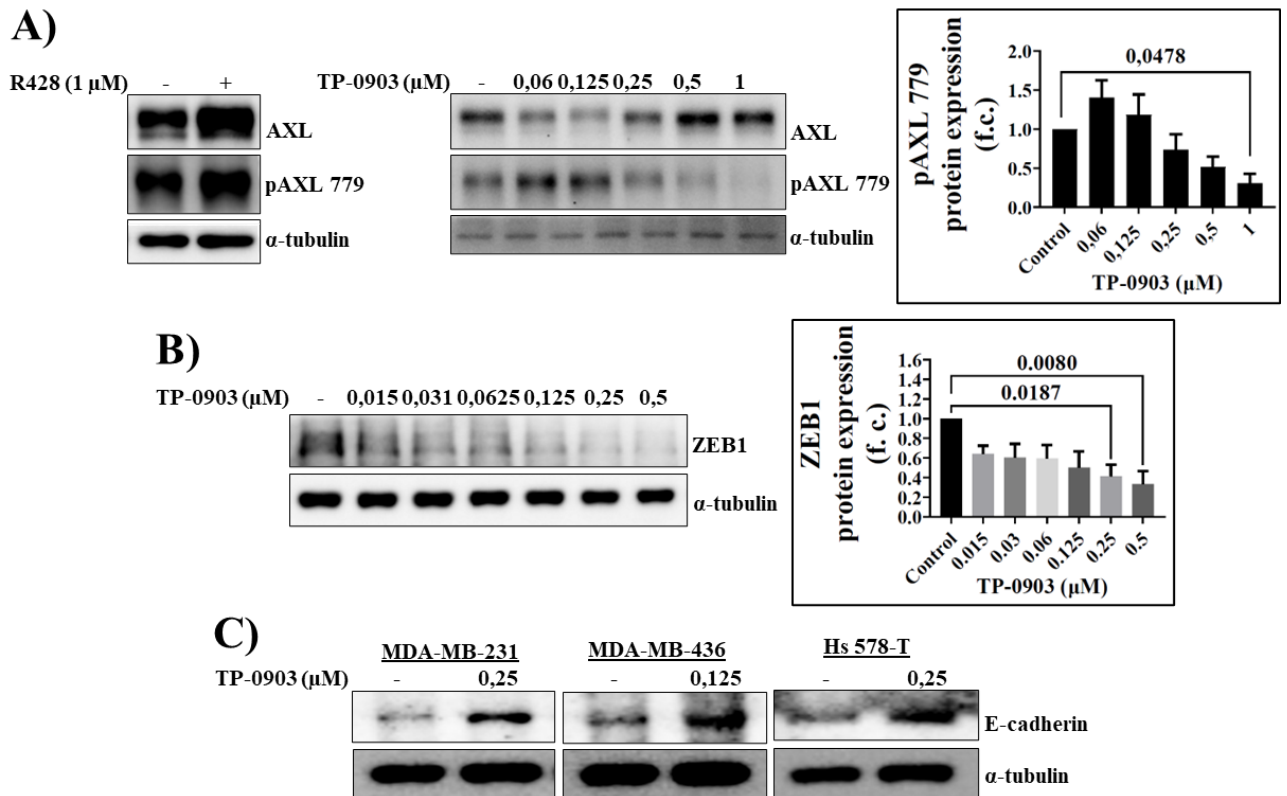
Figure 11. TP-0903 repressed pAXL 779 and ZEB1. **A)** Western Blot. TP-0903 and not R428 linearly inhibited pAXL 779 by increasing TP-0903 concentration after 24 h. **B)** Western Blot. TP-0903 linearly reduced ZEB1 expression by increasing its concentration after 24 h. Results are expressed as mean ± SEM of four (for pAXL779) and three (for ZEB1) independent measurements. The Dunnett's test was used to check significance between control and treatment groups; significant p-value lower than or equal to 0.05. **C)** Western blot. TP-0903 at 48 h increased E-cadherin in TNBC cell lines.

4.6. TP-0903 synergised with ART more in a sequential treatment

In order to check whether TP-0903 and ART synergised to decrease cell viability, MDA-MB-231 cells were treated for 96 h with a simultaneous or a sequential treatment of TP-0903 plus ART. In a sequential treatment, cells were pre-treated with TP-0903 for 24 h before treatment with TP-0903 plus ART for futher 72 h. Fig. 12A shows Combination Index (CI) values after combination of TP-0903 at different concentrations plus ART 40 μM. A sequential combination had a higher number of CIs showing synergism (CI lower than 1) compared to a simultaneous treatment. Interestingly, in a sequential treatment, TP-0903 at 0.03, 0.06, 0.25 and 0.5 μM synergised with ART at concentrations lower than 40 μM (2.5, 5, 10 and 20 μM); in contrast, in a simultaneous treatment, only TP-0903 at 0.25 μM synergised with ART at 2.5, 5, 10 and 20 μM suggesting that in a sequential treatment a synergism between TP-0903 and ART could be obtained by using relatively lower concentrations of both compounds (Supplementary Figure S12A). As TP-0903 reverted EMT in breast cancer cells at 0.25 μM (Fig. 11 A, B and C), this concentration was chosen for further experiments

Simultaneous treatment

CI Data for Non-Constant Combo: AT40 (A+T)			
Dose A	Dose T	Effect	CI
40.0	0.015	0.46919	1.36316
40.0	0.03	0.50099	1.56532
40.0	0.06	0.59841	1.39338
40.0	0.125	0.65341	1.71287
40.0	0.25	0.84449	0.68855
40.0	0.5	0.91297	0.49516
40.0	1.0	0.89530	1.25436
40.0	2.0	0.93219	1.22885

Sequential treatment

CI Data for Non-Constant Combo: AT40 (A+T)			
Dose A	Dose T	Effect	CI
40.0	0.015	0.48098	0.87522
40.0	0.03	0.53649	0.93747
40.0	0.06	0.64883	0.79601
40.0	0.125	0.67205	1.27059
40.0	0.25	0.89673	0.31792
40.0	0.5	0.90668	0.52709
40.0	1.0	0.93963	0.53764
40.0	2.0	0.91707	1.71881

Fig. 12. TP-0903 plus ART synergism in a simultaneous and sequential treatment. A representative Compusyn report after simultaneous/sequential treatment of MDA-MB-231 cells with TP-0903 at different concentrations plus ART 40 μM for 72 h. The cells were pre-treated with TP-0903 for 24 h. The number of CIs values showing synergism was higher in the sequential treatment. Dose A= ART; Dose T= TP-0903; Effect= growth inhibition; CI= Combination Index. CI<1 indicates synergism. Effect and CI were calculated after performing the MTT assay on four technical replicates.

4.7. TP-0903 sensitised TNBC cell lines to apoptosis induced by ART

In Fig. 13A, Muse Annexin V results show that TP-0903 and ART significantly increased late apoptotic cells compared to drugs alone and control in MDA-MB-23 cells. In Fig. 13B, Western Blot results show that after pre-treatment of MDA-MB-231 cells with TP-0903 at 0,25 μM for 24 h, treatment with TP-0903 plus ART for further two days completely

suppressed ZEB1 and increased cleaved caspase 3 compared to control and drugs alone. Also, after treatment of MDA-MB-231 cells with TP-0903 1 μM, ART 1 μM, 4 μM and 16 μM and a combination of TP-0903 plus ART for 24 h, TP-0903 plus ART induced higher cleaved caspase 3 expression compared to control and drugs alone (Supplemenatry Figure S13/1). TP-0903 plus ART in Hs 578-T cells induced a significant higher cleaved caspase 3 expression compared to control and drugs alone (Fig. 13C). Phase contrast images show that in MDA-MB-231 cells, TP-0903 plus ART treated cells had broken protrusions compared to TP-0903 while TP-0903 plus ART induced apoptotic bodies at higher extent than TP-0903 in both Hs 578-T and MDA-MB-436 cells (Supplementary Figure S13/2).
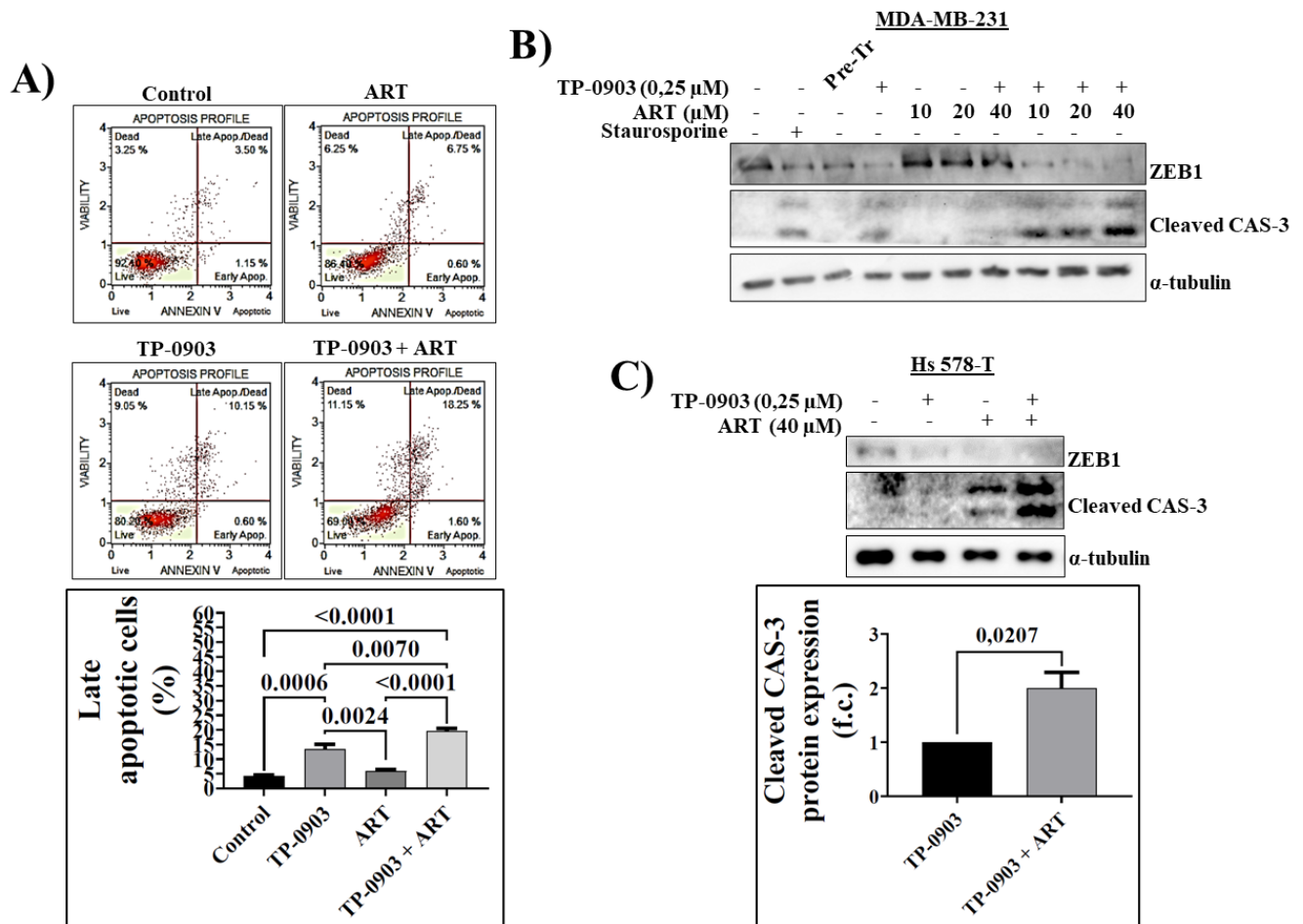
Figure 13. TP-0903 sensitised TNBC cell lines to ART induced apoptosis. **A)** Muse Annexin V assay. TP-0903 plus ART significantly increased late apoptotic cells compared to drugs alone and control. The Tukey's test was used to check significance among groups; significant p-value lower than or equal to 0.05. Results are expressed as mean ± SEM of three independent measurements (two independent experiments were run at different days and one experiment was repeated two times the same day by using two different flasks as source of cell seeding). **B)** Western Blot. MDA-MB-231 cells were pre-treated with TP-0903 at 0.25 μM for 24 h before TP-0903 plus ART treatment for further 2 days. TP-0903 plus ART increased cleaved caspase 3 compared to TP-0903. **C)** Western Blot. In Hs 578-T cells, TP-0903 plus ART induced higher extent of cleaved caspase 3 compared to control and drugs alone. A one sample t-test was conducted to check significance; significant p-value lower than or equal to 0.05. Results are expressed as mean ± SEM of three independent measurements.

4.8. ZEB1 expression influenced superoxide levels

In order to check whether ZEB1/EMT could decrease levels of superoxide induced by ART, MCF-7/ZEB1 cells, in presence or absence of Dox, and MDA-MB-231 cells were treated with ART 80 μM for 48 h before analysis with Muse Oxidative assay. In Fig. 14A, ART increased significantly percentage of superoxide positive cells in MCF-7/ZEB 1 (-) Dox compared to MCF-7/ZEB 1 (+) Dox. In order to check whether ZEB1 knockdown induced

higher levels of superoxide, MDA-MB-231/cntrol cells and shZEB1 cells were treated with ART 160 μM for 48 h before analysis with Muse Oxidative assay. Fig. 14B shows that ART induced a higher increase of superoxide in MDA-MB-231/shZEB1 cells compared to MDA-MB-231/cntrl cells and superoxide levels were significantly higher in shZEB1/ART compared to shZEB1/cntrl cells.
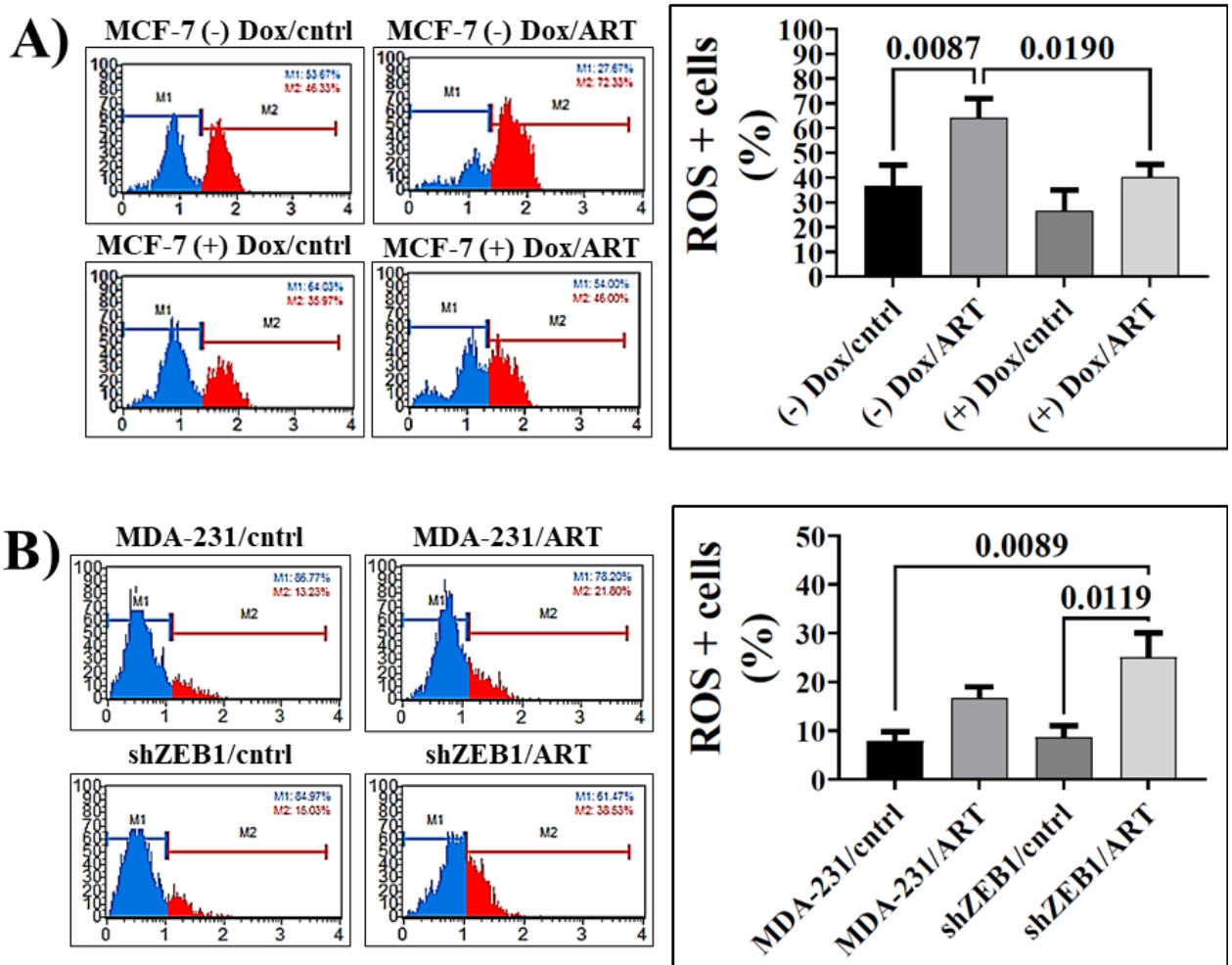
Figure 14. ZEB1 expression impact on ART-generated superoxide levels. **A)** Muse Oxidative stress assay. MCF-7/ZEB1 cells, in presence or absence of Dox, and MDA-MB-231 cells were treated with ART 80 μM for 48 h. ART increased significantly ROS only in MCF-7/ZEB 1 (-) Dox cells. Results are expressed as mean ± SEM of three independent measurements (two independent experiments were run at different days and one experiment was repeated two times the same day by using two different flasks as source of cell seeding). **B)** Muse Oxidative stress assay. MDA-MB-231/cntrl and MDA-MB-231/shZEB1 cells were treated with ART 160 μM for 48 h. ART induced higher ROS in shZEB1 cells. Results are expressed as mean ± SEM of four independent measurements (two independent experiments were run at different days and each experiment was repeated two times the same day by using two different flasks as source of cell seeding). The Tukey's test was used to check significance among groups; significant p-value lower than or equal to 0.05.

4.9. ZEB1 knockdown increased total ROS and DNA damage

In order to check total ROS levels, MDA-MB-231/cntrl and shZEB1 cells were treated with ART before doing the CM-DCFH DA test. Fig. 15A shows that total ROS were higher in shZEB1/cntrl compared to MDA-MB-231/cntrl cells and in shZEB1/ART treated cells compared to MDA-MB-231/ART treated cells. The images of cells with green signal are shown in the Supplementary Figure S15A/1. These results were also found in an additional field of cells (Supplementary Figure S15A/2). In Fig. 15B, Western Blot shows that in MDA-MB-231 and Hs 578-T cells, a transient and stable knockdown of ZEB1, respectively, increased ART induced pH2AX.
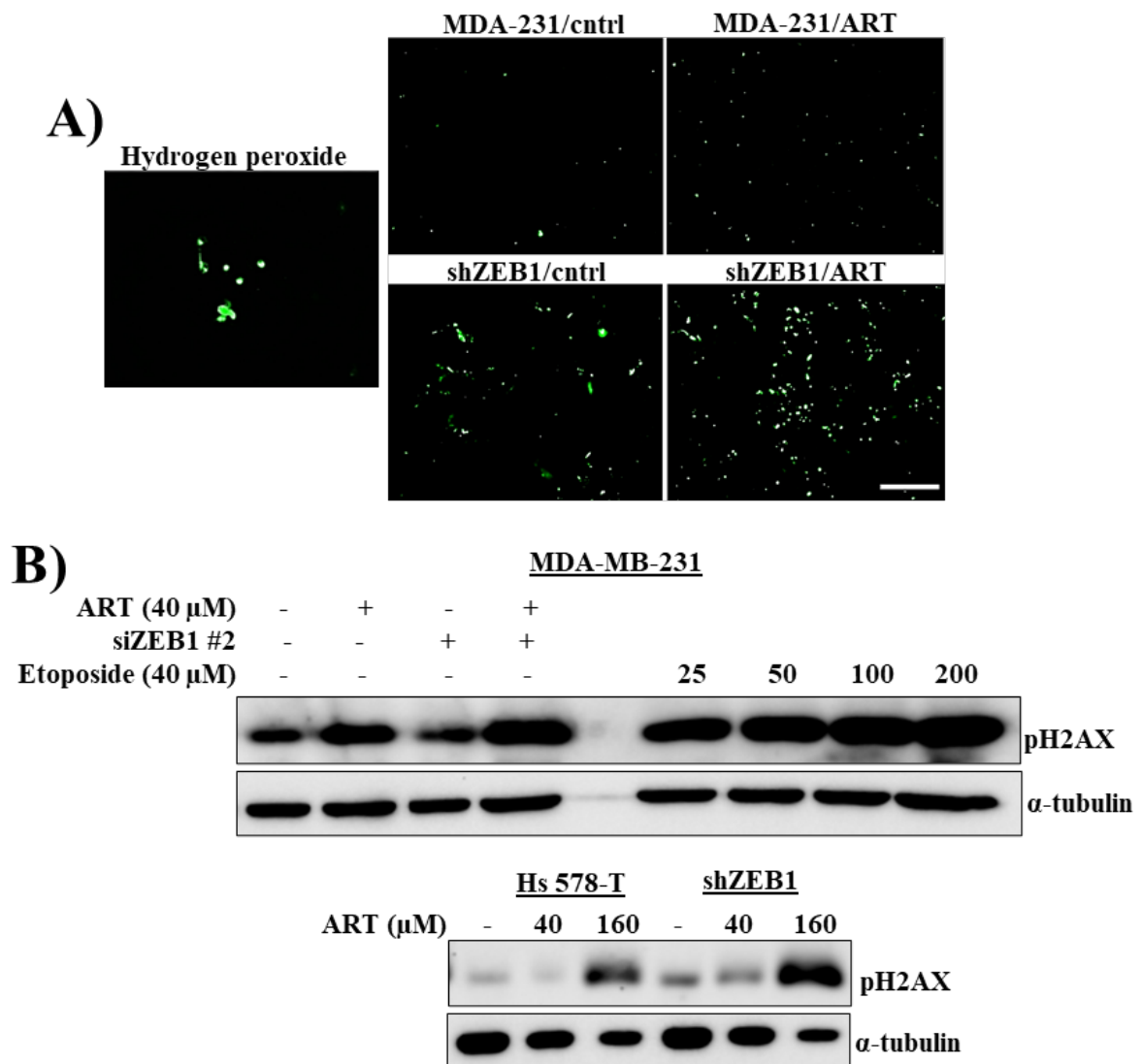
Fig. 15. ZEB1 knockdown increased total ROS and DNA damage. **A)** Fluorescence intensity of DCFH-DA staining as a measure of total ROS. Total ROS of shZEB1/cntrl and shZEB1/ART treated cells were higher compared to MDA-MB-231/cntrl and MDA-MB-231/ART treated cells, respectively. The pictures were taken at magnification of 10x; scale bar 100 μm. **B)** Western blot. A transient and stable genetic depletion of ZEB1 in MDA-MB-231 and Hs 578-T cells, respectively, enhanced DNA damage induced by ART after 72 h.

4.10. TP-0903 and ART synergised to increase total ROS and DNA damage

In order to check total ROS levels, MDA-MB-231 cells were pre-treated with TP-0903 at 0.25 μM for 24 h before treatment with TP-0903 at 0.25 μM and ART at 160 μM for further 24 h. The CM-DCFH DA probe was used to detect total ROS. Figure 16A shows that TP-0903 plus ART induced significant higher total ROS levels compared to control and drugs alone after normalization to total protein concentration. The phase contrast images of cells merged with the green signal are reported in the Supplementary Figure S16A/1. Of note, a statistical comparison between control and TP-0903 only showed that TP-0903 had significantly higher total ROS (Supplementary Figure S16A/2). In Fig. 16B, Western Blot shows that addition of ART to TP-0903 further increased pH2AX compared to TP-0903 in TNBC cell lines.
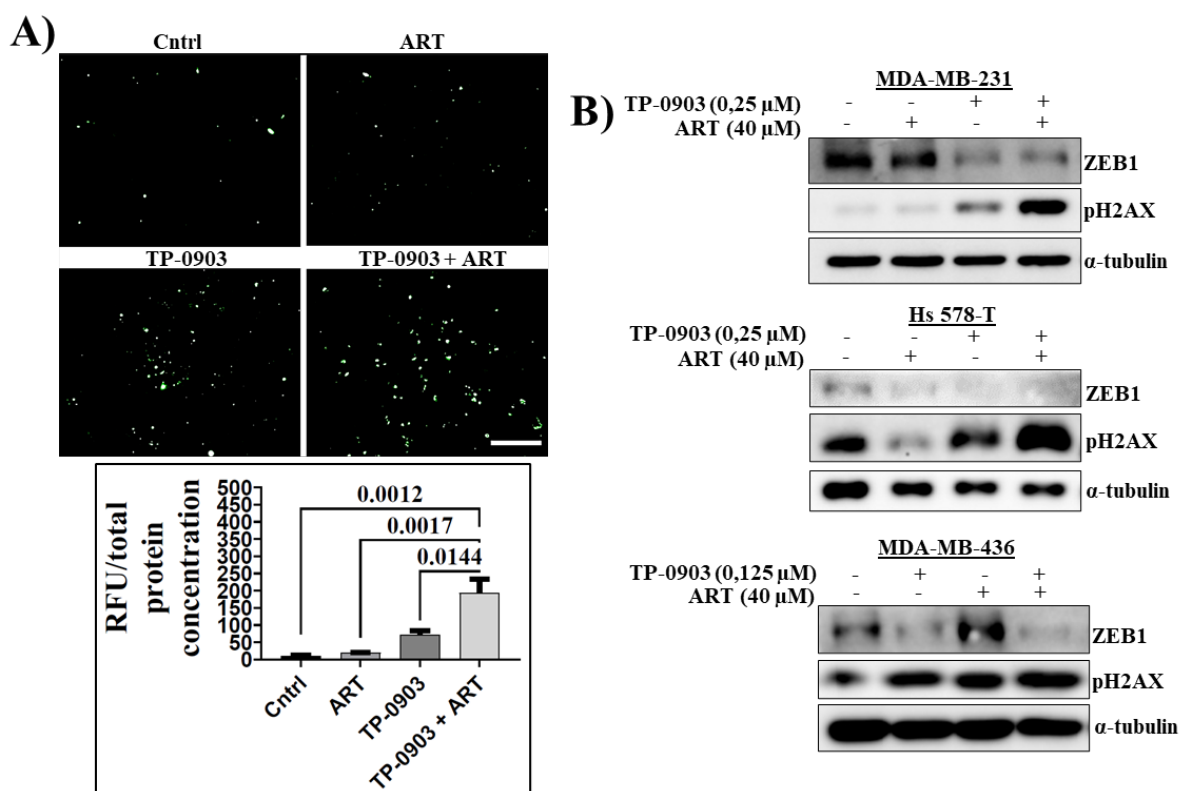
Figure 16. TP-0903/ART combination induced ROS and DNA damage in TNBC cells. **A)** Fluorescence intensity of DCFH-DA staining as a measure of total ROS after treatment of MDA-MB-231 cells with TP-0903, ART and a combination of the two. TP-0903 plus ART induced a significant higher levels of total ROS compared to TP-0903 after normalization to total protein concentration. The Tukey's test was used to check significance between control and treatment groups; significant p-value lower than or equal to 0.05. Results are expressed as mean ± SEM of three different fields taken from the same coverslip. The pictures were taken at magnification of 10x; scale bar 100 μm. **B)** Western Blot. Combined treatment of TNBC cells with TP-0903 and ART enhanced the extent of damaged DNA in TNBC cell lines as shown by pH2AX antibody.

4.11. *SOD2, GPX8* and *CAT* genes correlated with mesenchymal markers

In order to check the correlation between mesenchymal markers, epithelial markers and antioxidant enzymes, the relative gene expression of antioxidant enzymes (*SOD2, CAT, GPX8*), epithelial markers (*CDH1, JUP, mir 200c*) and mesenchymal markers (*VIM, ZEB1, SNAI2*) was checked by a heat map and hierarchical clustering analysis in a panel of breast cancer cell lines. Figure 17 shows that antioxidant enzymes co-clustered with mesenchymal markers *ZEB1, VIM* and *SNAI2*. The same cluster was also found in different cancer types (Supplementary Figure S17).
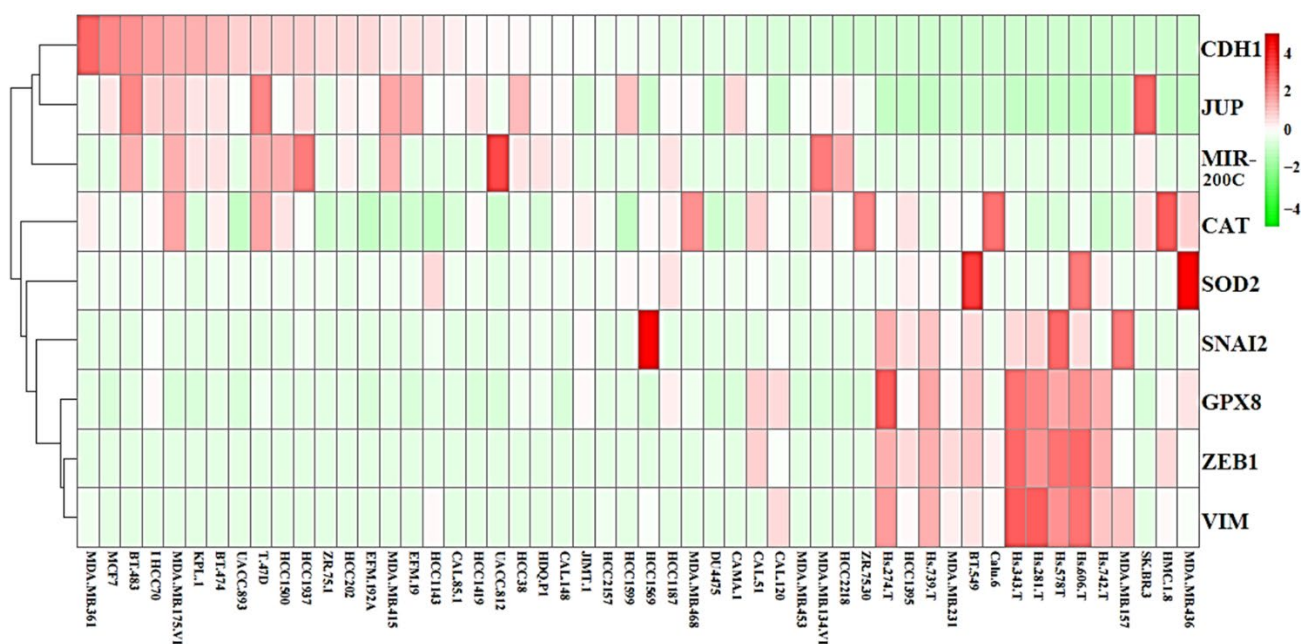
Figure 17. *SOD2, GPX8* and *CAT* expression in breast cancer. Heat Map analysis. The relative expression of *SOD2, CAT, GPX8, CDH1, JUP, mir 200c, VIM, ZEB1* and *SNAI2* is shown. The antioxidant enzymes were in cluster with mesenchymal markers. Genes are hierarchical clustered using Euclidean distances. Data was downloaded from in silico experiments conducted in EMBL-EBI database. Data are z-scored.

4.12. ZEB1 was not upstream of SOD2, GPX8 and CAT in TNBC cell lines

In order to check whether ZEB1 was upstream of *SOD2, GPX8* and *CAT*, different breast cancer cell lines, expressing or not ZEB1, were analysed. In Fig. 18A, qPCR analysis shows that MCF-7/ZEB1 (+) Dox cells had a significant lower expression of *SOD1* and significantly higher expression of *SOD2* and *GPX8* compared to MCF-7/ZEB1 (-) Dox. However, in Fig. 18B, Western Blot shows that stable knockdown of ZEB1 in MDA-MB-231

and Hs-578 cells did not decrease SOD2 and GPX8 expression compared to control cells. Of note, MDA-MB-231/shZEB1 cells had a significant increase of SOD2 compared to MDA-MB-231/cntrl cells. As for *CAT* gene expression, Dox treatment did not affect *CAT* gene expression in MCF-7/ZEB1 cells while siRNA ZEB1 increased *CAT* gene expression in MDA-MB-231 cells (Supplementary Figure S18).
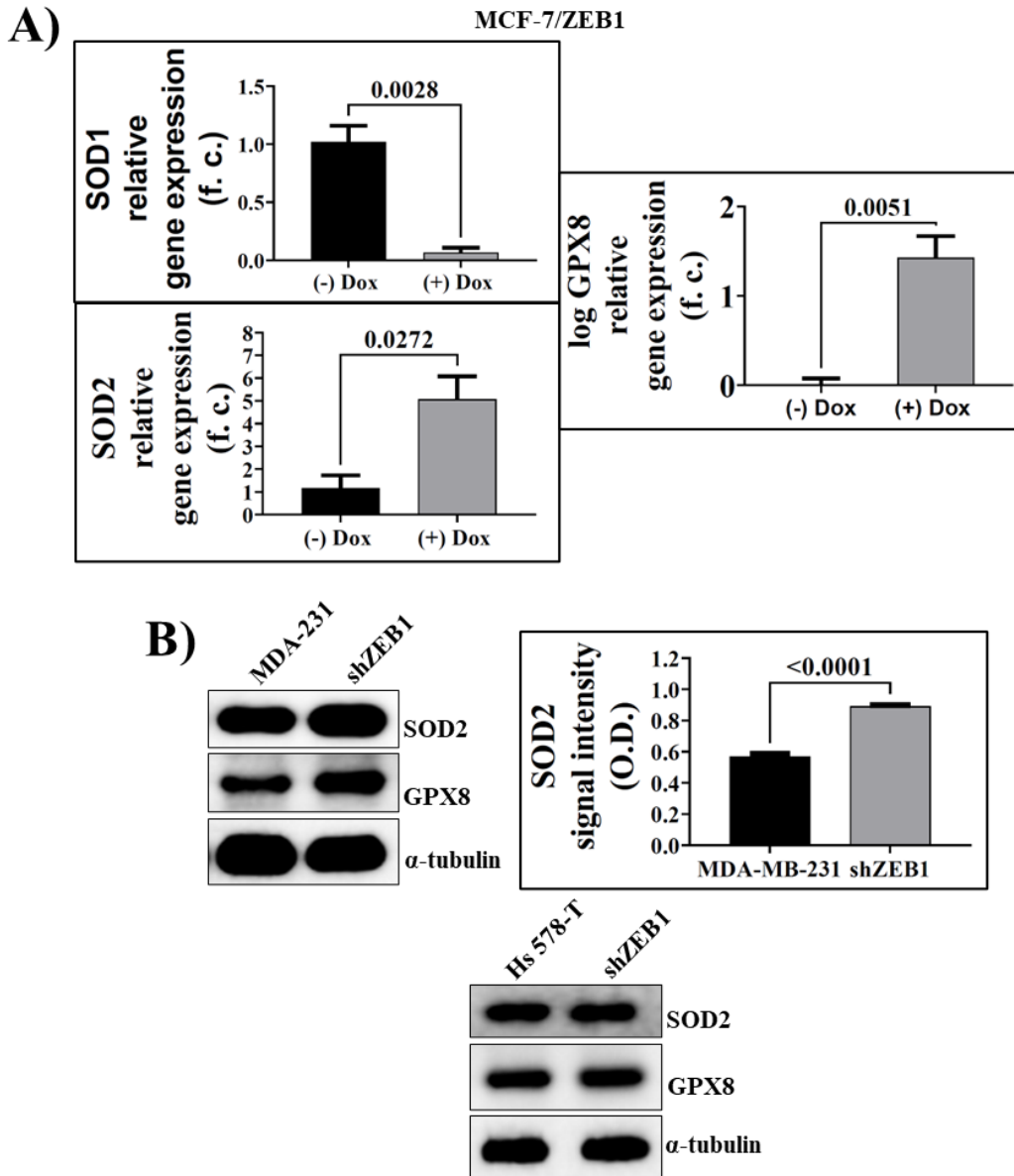
Fig. 18. ZEB1 and modulation of antioxidant enzymes genes. **A)** qPCR analysis. MCF-7/ZEB1 (+) Dox had a significant decrease of *SOD1* and a significant increase of *SOD2* and *GPX8* expression compared to MCF-7/ZEB1 (-) Dox. **B)** Western Blot. A stable knockdown of ZEB1 did not reduce SOD2 and GPX8 expression in MDA-MB-231 and Hs 578-T cells. The unpaired t-test was performed; significant p-value lower than or equal to 0.05. Results are expressed as mean ± SEM of a technical triplicate.

4.13. TP-0903 significantly suppressed GPX8 and CAT

In Fig. 19A, PCR analysis shows that TP-0903 abrogated CAT expression. In Fig. 19B, Western Blot shows that in MDA-MB-231 cells, TP-0903 significantly decreased GPX8 expression while ART significantly increased SOD2 expression. TP-0903 plus ART significantly decreased SOD2 and GPX8 expression. In Hs 578-T and MDA-MB-436 cells, TP-0903 decreased GPX8 expression though the effect was higher on GPX8. TP-0903 plus ART highly decreased both SOD2 and GPX8 expression compared to control though the effect was higher in Hs 578-T cells.
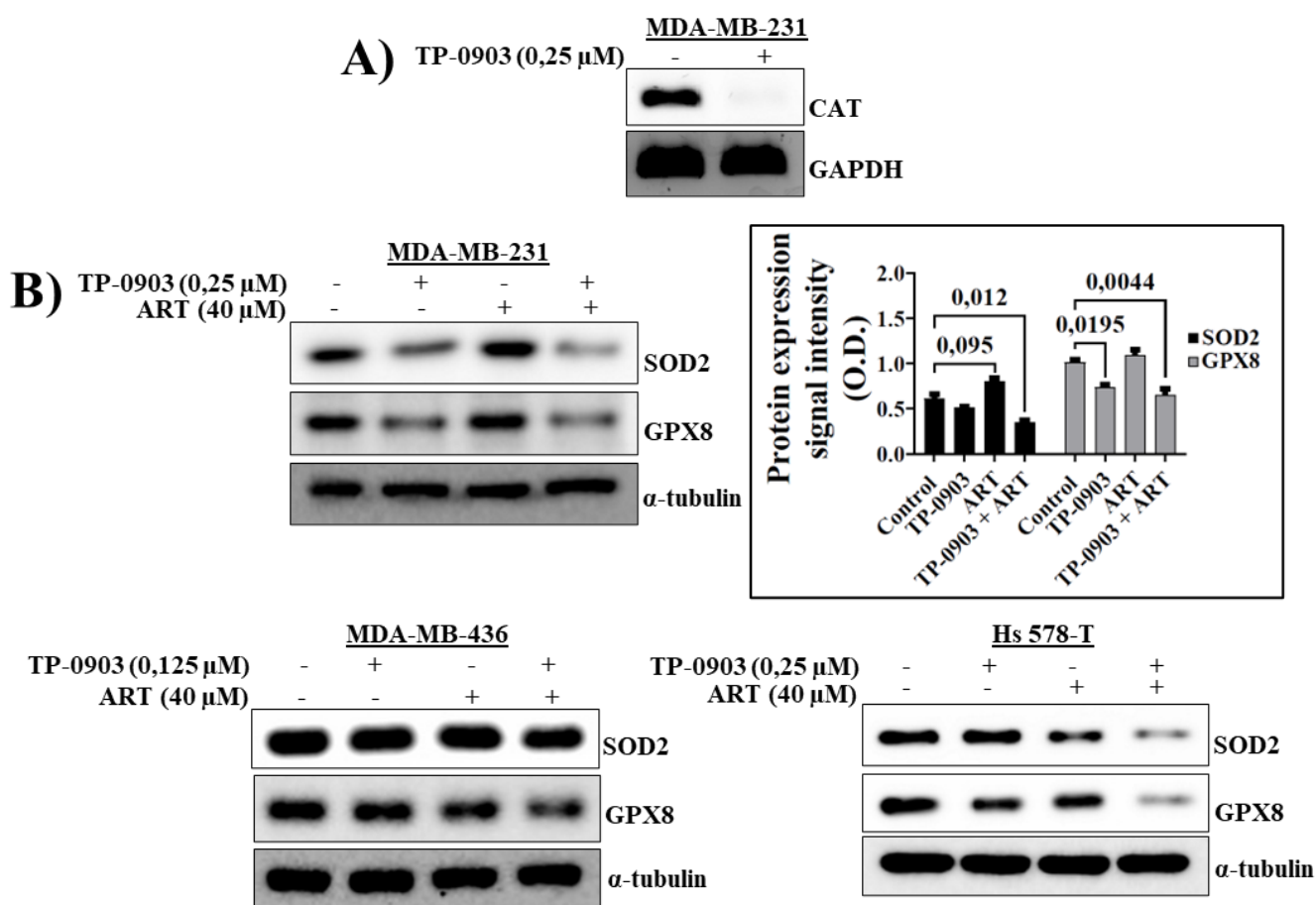
Fig. 19. Effect of TP-0903 and TP-0903 plus ART on antioxidant enzymes. **A)** PCR analysis. In MDA-MB-231 cells, TP-0903 suppressed CAT; **B)** Western Blot. In MDA-MB-231 cells, TP-0903 significantly suppressed GPX8 and ART significantly increased SOD2. TP-0903 plus ART significantly decreased SOD2 and GPX8. The Tukey's test was used to check significance between control and treatment groups; significant p-value lower than or equal to 0,05. Results are expressed as mean ± SEM of three independent measurements. In Hs 578-T and MDA-MB-436 cells, TP-0903 plus ART decreased both SOD2 and GPX8 expression compared to control. The picture in **A)** is a part of the Supplementary Figure S18.

4.14. TP-0903 suppressed Snail, Slug and Rad51 in TNBC cell lines

In Fig. 19A, MDA-MB-231 cells were treated with TP-0903 at 1 μM for 1 h, 4 h and 24 h before checking by Western Blot expression of the two EMT TFs Snail and Slug. TP-0903 highly reduced Snail and Slug expression after 24 h. In Fig. 19B, MDA-MB-231 and Hs 578-T cells were treted with TP-0903 at 0.25 μM for three days before checking by Western Blot expression of Rad51. TP-0903 suppressed Rad51 in MDA-MB-231 and Hs 578-T cells while siRNA ZEB1 did not have any effect on Rad51 in MDA-MB-231 and MDA-MB-436 cells (Supplementary Figure S20B).
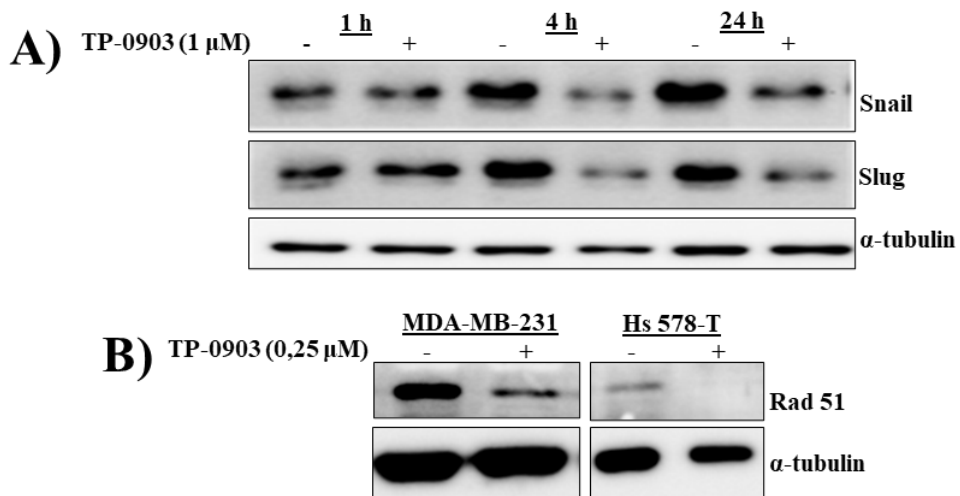
Fig. 20. TP-0903 effect on Snail, Slug and Rad51. **A)** Western Blot. MDA-MB-231 cells were treated with TP-0903 at 1 μM at 1 h, 4 h and 24 h. TP-0903 highly suppressed Snail and Slug after 24 h. **B)** Western Blot. MDA-MB-231 and Hs 578-T cells were treated with TP-0903 at 0.25 μM for three days. TP-0903 suppressed Rad51 in MDA-MB-231 and Hs 578-T cells.

CHAPTER 5: DISCUSSION

TNBC is charaterised by EMT, a cellular program that confers chemoresistance, survival and metastasis (Gjerdrum et al., 2010). In TNBC, the RTK AXL is overexpressed and is a crucial regulator of EMT to promote invasiveness, metastasis and chemoresistance (Bottai et al., 2016). AXL activation can be prevented by using tyrosine kinase inhibitors (TKIs) that target the kinase domain of AXL to block its phosphorylation (Holland et al., 2010). In cancer, TKIs are generally used as chemosensitizers in a drug combination therapy (Rosenzweig, 2018). In addition to AXL, ZEB1 is also overexpressed in TNBC (Karihtala et al., 2013). ZEB1 regulates EMT and promotes cancer progression, metastasis and chemoresistance in breast cancer (Zhang, Sun et al., 2015; Zhang et al., 2018). In the fight to cancer, many natural compounds have been repurposed for cancer treatment. Artemisinin, a natural compound of the medical herb Artemisia annua, is specifically cytotoxic to many cancer cell lines by inducing accumulation of ROS (Michaelis et al., 2010). The artemisinin derivative artesunate (ART) caused ROS mediated mitochondrial apoptosis in TNBC (Hamacher-Brady et al., 2010). However, the EMT presenting MDA-MB-231 cells developed resistance after prolonged treatment with ART (Bachmeier et al., 2011). Of note, ART cytotoxicity inversely correlated with intracellular antioxidant capacity (Roh et al., 2017; Efferth et al., 2003). In breast cancer, increased gene expression of *AXL* inversely correlated with ART cytotoxicity (Anfosso et al., 2006) and ZEB1 overexpression has been shown to induce chemoresistance (Zhang, Sun et al., 2015; Zhang et al., 2018).

In this research project, it was hypothesized that reversal of EMT could sensitise TNBC cell lines to ART cytotoxicity. To address this, I used several breast cancer cell lines exhibiting mesenchymal properties and reverted their phenotype to the more epithelial state by two means, knockdown of AXL/ZEB1 or by applying AXL inhibitors TP-0903/R428. Then, I tested whether EMT reversal potentiated cytotoxic effects of ART.

5.1. TNBC cell lines presented EMT markers

First, TNBC cell lines were checked for the presence of the EMT markers. The heat map and hyerarchical clustering analysis of the relative gene expression of mesenchymal markers *AXL, CDH2* (N-cadherin), *VIM* (mesenchymal markers) and epithelial markers *CDH1,* junction plakoglobin *(JUP)* in a panel of breast cancer cell lines shown that *AXL* co-clustered with mesenchymal markers (Fig. 7A). The same cluster was also found in different cancer types (Supplementary Figure S7A). In Fig. 7B, Western Blot results shown that AXL

and VIM were present in TNBC cell lines while the epithelial marker E-cadherin was absent. In contrast, non TNBC cell lines did not express AXL and VIM while E-cadherin was present (Fig. 7B). In addition, TNBC cells had a fibroblastic phenotype while non TNBC cells were more epithelial and grown in clusters (Fig. 7C). In the analysis conducted by D'Alfonso et al., (2014), AXL was upregulated in TNBC basal B cells compared to luminal or TNBC basal A cells. AXL and EMT correlate in breast cancer. VIM induced expression of Slug and AXL in non tumorigenic breast epithelial cells (Vuoriluoto et al., 2011) and in the non cancerous epithelial MCF10a cell line the EMT transcription factors Snail, Slug, Twist or ZEB2 induced AXL (Gjerdrum et al., 2010). In addition, Asiedu et al., (2014) found that AXL was overexpressed in breast cancer stem cells and induced EMT by regulating expression of E-cadherin, N-cadherin, Snail and Slug. In relation to clinical parameters, AXL expression has been found to correlate with poorly differentiated breast tumor tissues (Jin et al., 2016). Gjerdrum et al., (2010) showed that AXL expression in breast cancer was higher in metastatic lesions and correlated with poorer overall patient survival. In addition, Truong et al. (2015) found an association between AXL and lymphovascular invasion (LVI), supporting the role of AXL in mediating invasion, and metastasis.

The mesenchymal marker VIM was only present in TNBC cells (Fig. 7B). In line with this, Bindels et al., (2006) found that the TNBC cell lines MDA-MB-231, BT-549 and Hs 578-T expressed VIM protein that was absent in the non TNBC cell lines MCF-7 and T-47D. VIM is a type III intermediate filament protein crucial in the formation of the cytoskeletal network in mesenchymal cells (Bermejo et al., 2022). Thompson et al., (1992) demonstrated that "ESR+/VIM- (MCF-7, T47D, ZR-75-1) and ESR-/VIM- (MDAMB-468, SK-Br-3) cell lines" did not have any invasion capacity, while the "ESR-/VIM+ (BT549, MDA-MB-231, MDA-MB-435, MDA-MB-436, Hs 578-T) cell lines" were highly invasive. Yamashita et al., (2013) found that VIM was an independent prognostic factor of overall survival in basal-like breast cancer.

E-cadherin is a crucial epithelial protein that maintains the homophilic cell–cell adhesion in the epithelium. These junctions are calcium-regulated (Eger et al. 2005). E-cadherin was absent in MDA-MB-231, MDA-MB-436, Hs 578-T, BT-549 cells while MCF-7 cells had E-cadherin expression (Nieman et al., 1999). E-cadherin is a canonical epithelial marker and its reduced expression in breast tumours significantly correlated with shorter survival (Charpin et al., 1998). Thus, TNBC cell lines analysed in the study can be categorised into two groups, that epithelial, expressing E-cadherin and negative for VIM and AXL and that mesenchymal, E-cadherin-negative and AXL and VIM-positive.

5.2. TNBC cell lines were more resistant to ART cytotoxicity

In this project, the sensitivity of TNBC and non TNBC cell lines to ART was checked. In Fig. 8A, MTT assay results show that after treatment with ART for 72 h, TNBC cells lines were more resistant to ART with IC_{50} values ranging 37 µM - 74 µM compared to non TNBC cell lines whose ART IC_{50} ranged 25 µM - 27 µM. The ART IC_{50} was calculated in a log dose response and accordingly MDA-MB-231 and BT-549 cells were the most resistant cell lines to ART. Importantly, the difference of sensitivity to ART between epithelial and mesenchymal breast cancer cell lines is more evident in a linear scale (Supplementary Figure S8). In a linear scale, non TNBC cell viability was reduced by approximately 70% at ART 80 µM while that of TNBC was decreased by approximately 30% - 40% at this ART concentration. These results are in line with Greenshields et al., (2019); they found that after 72 h, MDA-MB-231 cells were the most resistant cells while ESR positive cell lines the most responsive; interestingly, in a linear scale, they shown that the ART inhibitory effect on the growth of MDA-MB-231 cells was approximately 50% while cell viability of ESR positive cell lines was inhibited by approximately 80%. Jamalzadeh et al., (2017) found that ART IC_{50} of MCF-7 cells was approximately 20 µM after 72 h. In line with my findings, 1) the cell counting kit 8 (CCK-8) assay shown that the DHA IC_{50} in MDA-MB-231 cells was higher than 50 µM after 96 h (Feng et al., 2015); 2) in T-47D cells, ART IC_{50} of DHA was of 17.18 µM after 72 h (Mao et al., 2013). However, different results concerning ART sensitivity in breast cancer have been found. Bachmeier et al., (2019) found that ART could already reduce by 40% cell viability of MDA-MB-231 cells after 24 h. However, MDA.MB-231 cells developed an extent of resistance after continuous ART treatment while MDA-MB-468 cells continued to be sensitive to ART. This confirmed that TNBC cells classified as basal A and with lower metastatic capacity, such as MDA-MB-468, were more sensitive to ART compared to MDA-MB-231 cells, classified as basal B and with higher metastatic capacity (Riehl et al., 2020). In addition, though Kumari et al., (2017) found different ART IC_{50} values in breast cancer compared to those found in this project, the authors still shown that the epithelial breast cancer cell lines were more responsive to ART treatment compared to MDA-MB-231 cells after 24 h.

MTT assay represents a valid and effective approach to calculate cell viability, expressed as the concentration at which drug eliminates 50% of cells (IC_{50}) generally after 3-4 days in comparison to a control dissolved in the drug vehicle (DMSO) (Ghasemi et al., 2021). However, MTT results can be influenced by some parameters. Kobayashi et al., (1992) found that an increase of cell density decreased the cytotoxicity of some drugs, such as vincristine

and doxorubicin and this phenomenon is named inoculum effect. In case of high cell density, the acidity of the medium could increase (Kobayashi et al., 1992) and this could inactivate cytotoxicity of some chemotherapeutics (Trebinska-Stryjewska et al., 2020). ART stability in acqueous solution is low at neutral and acidic environment (WHO, 2006). This could destabilise ART and its citotoxicity could be reduced. In addition, Hafner et al., (2017) introduced the growth rate (GR) value to calculate drug response (in terms of magnitude) according to a division basis. They found that high cell density caused a low division rate and this affected response to drugs. In addition, time at which optical density (OD) is taken can influence MTT results (Ghasemi et al., 2021); each cell line has a specific matabolism and then require different incubation time with MTT. However, though some differences in ART IC$_{50}$ values, it is possible to conclude that ART is less cytotoxic in TNBC compared to non TNBC cell lines.

These results may suggest that ART could be more clinically beneficial to patients with more differentiated breast tumors. Bachmeier et al., (2011) found that MDA-MB-231 cells treated with repeated doses of ART developed resistance while ART sensitivity of MDA-MB-468 cells remained unchanged. The molecular and functional profiles in MDA-MB-231 cells resistant to ART revealed an upregulation of the transcription factors NF-κB and AP-1 that in turn activated the anti-apoptotic bcl-2 while suppressing the pro-apoptotic bax genes. In addition, the expression and activity of MMP-1 was enhanced. All together, my project and Bachmeier et al., (2011) suggest that ART could treat more efficiently less aggressive and more differentiated breast tumours.

5.3. EMT activation decreased ART cytotoxicity

After checking that TNBC cell lines were more resistant to ART, it was verified whether activation of EMT in breast cancer cell lines could induce resistance to ART. Fig. 9A shows that MCF-7/ZEB1 cells in presence of Dox had a mesenchymal phenotype compared to (-) Dox cells that had an epithelial phenotype. Western Blotting results show that MCF-7/ZEB1 (+) Dox cells had activation of ZEB1 while downregulation of E-cadherin; in contrast, MDA-MB-231 cells depleted for ZEB1 by siRNA had an increase of E-cadherin (Fig. 9B). MTT results shown that ART IC$_{50}$ of MCF-7/ZEB1 (+) Dox cells was higher than that of MCF-7/ZEB1 (-) Dox (25.89 μM and 49.02 μM, respectively). In a reverse experiment, ART IC$_{50}$ of MDA-MB-231 siRNA ZEB1 cells was lower than that of MDA-MB-231 siRNA cntrl (48.9 μM and 69.71 μM, respectively) (Fig. 9C). Of note, MTT absorbance values of Dox-treated MCF-7/ZEB1 control cells were 32% lower than those of (-

) Dox control cells (Supplementary Figure S9C) suggesting that ZEB1/EMT could mediate ART resistance by regulating proliferation or metabolism. In MDA-MB-231 cells, ZEB1 knockdown induced MYB, a positive regulator of proliferation (Hugo et al., 2013). In HeLa cells, ZEB1 enhanced number of cells in the G1 phase of cell cycle while decreasing those in the S and G2/M phases (Netsvetai et al., 2021). Then, according to my results, EMT activation reduced ART effect on cell viability of breast cancer cells probably via altering cell cycle control mechanisms.

5.4. AXL was not a mediator of ART resistance

As activation and inhibition of EMT induced resistance and sensitisation to ART, respectively (Fig. 9C), I tested whether the EMT marker AXL could be involved in ART response. AXL downregulation by siRNA did not sensitise MDA-MB-231 cells to apoptosis induced by ART (Fig. 10A). In spite of these results, AXL has been shown as a determinant of chemoresistance in cancer (Asiedu et al., 2014). In NSCLC, AXL overexpression induced acquired resistance to the EGFR inhibitor cetuximab and the AXL inhibitor R428 significantly inhibited cell proliferation but without inducing apoptosis (Brand et al., 2014). Wilson et al., (2014) showed that AXL inhibition synergised with docetaxel to decrease cell proliferation of HeLa cells. In MDA-MB-231 cells, AXL induced resistance to EGFR TKIs by diversifying the EGFR signaling (Meyer et al., 2016). Then, according to these results, AXL caused chemoresistance by eliciting proliferation, migration and invasion rather than survival and protection from apoptosis. This could justify my results that AXL knockdown in MDA-MB-231 cells did not increase apoptosis induced by ART (Fig. 10A). It is important to note that Brand et al. (2014) and Wilson et al. (2014) used some proliferation assays to show that AXL depleted cells had lower cell viability compared to those which expressed AXL. However, a change in the cell viability could be caused by the reduction in the metabolic activity and not by increase in cell death. To exclude this, additional assays are required (cell toxicity assays or analysis of apoptotic and survival markers downstream of AXL).

In other studies, AXL has been shown to protect from apoptosis both in tumorigenic and non tumorigenic cells via AKT signaling. In oligodendrocytes, AXL activated PI3k/AKT to protect cells from tumor necrosis factor alpha (TNFα)-mediated caspase 3 activation (Shankar et al., 2006); and in endothelial cells and cutaneous squamous cell carcinoma AXL inhibited caspase 3 by activating AKT (Hasanbasic et al., 2004; Papadakis et al., 2011). In breast cancer, AXL depletion decreased pAKT levels and sensitised MCF-7/ADR cells to doxorubicin by increasing protein expression of Bim and Bad (Wang et al., 2016). Results of

my project also showed that AXL induced phosphorylation of AKT in both MDA-MB-231 and BT-549 cell lines (Supplementary Figure S10A/1). However, though MDA-MB-231 cells depleted for AXL shown a reduction of pAKT, they were still resistant to apoptosis induced by ART (Fig. 10A). This suggested that the AXL/AKT pathway mediated regulation of apoptosis is specific to cell lines and tumors of a particular origin.

Though TP-0903 suppressed AXL activation (Fig. 11A) and sensitised TNBC cells to ART mediated reduced cell viability (Fig. 12) and apoptosis (Fig. 13), this was independent of AXL. Indeed, MDA-MB-231 cells depleted for AXL were not sensitised to ART mediated apoptosis (Fig. 10A). In addition, as ART induced apoptosis by ROS in breast cancer (Hamacher-Brady et al., 2011), AXL is presumably not involved in the regulation of ROS/antioxidant enzymes in MDA-MB-231 cells. There is no data in the literature to show that AXL is able to activate ROS production. In contrast, AXL signaling was reported downstream of ROS (Huang et al., 2013; Oien et al. 2018). In conclusion, AXL mediated regulation of apoptosis could be tumor and cancer cell line specific. This is in line with my results that knockdown of AXL did not increase apoptosis induce by ART in MDA-MB-231 cells.

5.5. ZEB1 was a mediator of ART resistance

After exclusion of AXL as mediator of resistance to ART induced apoptosis, the EMT transcription factor ZEB1 was assumed as a regulator of cell sensitivity to ART. In Fig. 10 A, MDA-MB-231 cells depleted for ZEB1 by siRNA had increased E-cadherin and P-cadherin and were more sensitive to ART induced cleaved caspase 3 (Fig. 10A). In Fig. 10B, MDA-MB-231/shZEB1 cells (cells with stable knockdown of ZEB1) presented P-cadherin expression that was absent in MDA-MB-231/cntrl cells. In addition, Annexin V assay results shown that ART induced a significant higher late/early apoptotic cells rate in shZEB1 cells compared to cntrl cells (Fig. 10B). In Fig. 10C, MDA-MB-436 depleted for ZEB1 by siRNA plus ART had higher cleaved caspase 3 compared to ART; Hs 578-T/shZEB1 cells had higher ART induced cleaved caspase 3 compared to Hs 578-T/cntrl cells (Fig. 10C). Of note, phase contrast images show that ART was more cytotoxic, in terms of cell viability, in MDA-MB-231 shZEB1 and Hs 578-T/shZEB1 cells compared to respective control cells (Supplementary Figure S10B/2 and S10D/2, respectively). Then, ZEB1 knockdown blocked EMT and increased apoptosis induced by ART.

5.6. TP-0903 blocked EMT and synergysed with ART to induce apoptosis

The two AXL inhibitors R428 and TP-0903 have been shown to block AXL signaling and reverse EMT. R428 is a potent and specific AXL inhibitor *in vitro* with IC_{50} of 14 nM. In MDA-MB-231 cells, R428 reduced AXL phosphorylation (Holland et al., 2010) and vimentin expression levels (Bottai et al., 2016). In MDA-MB-231 cells, R428 did not prevent AXL phosphorylation at Tyr 779 (Fig.11A), increased expression of Snail, Slug and caused intracellullar vesiculation (Supplementary Figure S11A/1). It is known that cancer cells use vesiculation, in terms of extracellular vesicles (EVs), to load and pump out drugs (Shedden et al., 2003; Federici et al. 2014; Ifergan et al., 2005; Ciravolo et al., 2012, Battke et al., 2011). In line with this, MDA-MB-231 cells could internalise R428 in vesicles to decrease efficacy of R428 to block AXL/EMT (Supplementary Figure S11A/1).

In contrast to R428, TP-0903 significantly inhibited reduced AXL phosphorylation at Y779 (Fig. 11A), expression levels of ZEB1 (Fig. 11B), Snail and Slug (Fig. 18A), while increasing E-cadherin (Fig. 11C). According to CI values, TP-0903 and ART synergised to decrease cell viability more in a sequential than in a simultaneous treatment in MDA-MB-231 cells (Fig. 12). In relation to apoptosis, TP-0903 0.25 μM plus ART 40 μM synergised to induce late apoptotic cells (Fig.13A), and Western Blot results show that 40 μM ART further increased extent of cleaved caspase 3 induced by TP-0903 (Fig. 13B). Likewise, in Hs 578-T cells, TP-0903 plus ART potently stimulated caspase 3 cleavage (Fig. 13C).

In conclusion, though TP-0903 reduced AXL phosphorylation at Y779 (Fig 11A) and sensitised TNBC cells to ART-mediated apoptosis (Fig. 13, A, B and C), AXL knockdown did not increase sensitivity to apoptosis induced by ART in MDA-MB-231 cells (Fig. 10A). This suggested that TP-0903 could sensitise TNBC cells to ART independently of AXL. In place of AXL, the EMT transcription factor ZEB1 could mediate ART resistance in TNBC cells. TP-0903 suppressed ZEB1 in TNBC cells (Fig. 13 B and C). Also, knockdown of ZEB1 significantly increased sensitivity to ART in TNBC cell lines (Fig. 10A, B, C and D) and likewise, in the reverse experiments, ectopic expression of ZEB1 in epithelial MCF-7 cells resulted in ART resistance (Fig. 9C) concomitant with the induction of EMT (Fig. 9 A and B). Accordingly, it can be assumed that TP-0903 sensitised TNBC cells to ART mediated apoptosis through suppression of ZEB1.

5.6.1. TP-0903 inhibits EMT and is a chemosensitiser in cancer

In cancer, TP-0903 is a powerful EMT inhibitor and chemosensitiser. Artigues et al., (2022) found that in acquired trastuzumab-resistant cell lines, TP-0903 decreased "VIM,

fibronectin and N-cadherin". In CRC, TP-0903 had an IC_{50} value ranging 4.5 nM-123 nM and in the HCT-116 xenograft model, TP-0903 inhibited by 69% tumor growth at 40 mg/kg while in a KRAS-mutant PDX model TP-0903 inhibited tumor growth by 44%. (Mangelson, Peterson et al., 2019). TP-0903 also shown high inhibitory effect on growth of ovarian cancer cell lines with IC_{50} values ranging 33 nM-840 nM. TP-0903 reversed EMT in ovarian cancer by decreasing expression of Snail and Slug. TP-0903 reduced metastatic capacity in xenograft models (Tomimatsu et al., 2006). Treatment with TP-0903 of KPfC, a genetically engineered mouse models (GEMMs) of pancreatic ductal adenocarcinoma (PDA), increased survival to 78 days and significantly reduced tumor weight. TP-0903 plus gemcitabine increased survival to 92.5 days and significantly decreased tumor size (Zhang et al., 2022). Also, hystological analysis from the orthotopic C57BL/6 mice with PDA tumors shown that TP-0903 induced tumor differentiation as E-cadherin expression increased while that of VIM decreased (Zhang et al., 2022). The efficacy of TP-0903 and gilteritinib, a fms-like tyrosine kinase 3 (FLT3) inhibitor, was checked in AML xenograft models resistant to FLT3 inhibitors (Jeon et al., 2020). TP-0903 at 60mg/kg or gilteritinib at 30 mg/kg, "administered once daily for 5 days/week for 3 weeks" significantly increased survival to 31 days compared to vehicle (22 days). TP-0903 caused differentiation as indicated by the presence of multilobulated nuclei (Jeon et al., 2020). In small cell lung cancer, TP-0903 (50 mg/kg) plus the mitosis inhibitor protein kinase 1 (WEE1) inhibitor AZD1775 (60 mg/kg) significantly decreased tumor growth compared to drugs alone and control after 36 days *in vivo*. Of note, TP-0903 plus AZD1775 permitted to all mice to survive after 80 days (Sen et al., 2017). TP-0903 synergised with inhibitors of PD-L1 agent in a syngeneic TNBC mouse model (Soh et al., 2016). These data suggest that TP-0903 is an efficient chemosensitiser in cancer treatment; also, AXL inhibition negatively affects features generally associated with EMT, such as invasion and metastasis.

5.7. ART cytotoxicity in cancer

In cancer, Artemisinins cytoxocity associates with effects on cell viability, EMT, migration, invasion, metabolism and apoptosis (Efferth, Sauerbrey et al., 2003). ART inhibited significantly migration of A549 and H1975 cells at 65 μM - 130 μM at 24 h, increased protein expression of E-cadherin while that of N-cadherin, VIM and fibronectin was inhibited (Wang et al., 2020). In hepatoma cell lines, ART and DHA at 25 μM and 50 μM blocked cell cycle at G1 phase and decreased expression of "cyclin D1, E, cyclin-dependent kinase 2 (CDK2), cyclin-dependent kinase 4 (CDK4) and E2 transcription factor 1 (E2F1)"

while cyclin dependent kinase inhibitor 1 (p21) and cyclin dependent kinase inhibitor 1B (p27) were increased. ART and DHA activated caspase 3, increased the Bax/Bcl-2 ratio and cleaved Parp. In xenograft mice, ART and DHA inhibited tumor growth and synergised with gemcitabine (Hou et al., 2008). ART and DHA at 100 mg/Kg significantly decreased tumor size and incidence of metastasis and extended survival in the 4T1 breast cancer model (Yao et al., 2018). DHA (100 mg/kg) treatment of the MDA-MB-231 mouse xenograft model for 28 days significantly reduced tumor volume (232.05 ± 46.08 mm3) compared to vehicle (355.98 ± 44.22 mm3) (Feng et al., 2016). ART could also modulate metabolism in cancer. In NSCLC, DHA decreased glucose uptake by suppressing expression of glucose transprter 1 (GLUT1); DHA and 2-Deoxy-D-glucose (2DG, a glycolysis inhibitor) synergised to inhibit cell viability while inducing apoptosis by activation of caspase 8, 9 and 3 (Mi et al., 2015). As for ZEB1, DHA has been shown to suppress ZEB1 in the canine mammary tumors (CMTs) (Dong et al., 2019). However, there were not additional findings showing the impact of ART on ZEB1. Results from my project showed that ART reduced ZEB1 protein expression in the TNBC cell line Hs 578-T (Fig. 13C) and TP-0903 and ART synergised to suppress ZEB1 (Fig. 13B and C).

5.7.1. ART induces apoptosis by ROS in cancer

In relation to this project, it is important to mention that in cancer, ART induces DNA damage and apoptosis through accumulation of ROS (Berdelle et al., 2023). In the doxorubicin-resistant leukemic T cells, ART at 10 µM and after 30 min induced high levels of hydrogen peroxide that induced intrinsic apoptosis. NAC prevented apoptosis by completely inhibiting ROS (Efferth et al., 2007). In LN-229 glioblastoma cells, ART at 1 µM - 130 µM significantly induced apoptosis and addition of ferrosanol significantly increased apoptosis suggesting that ROS could be involved in apoptosis. ART at 40 µM for 24 h significantly increased ROS and 8-oxoG, a major DNA oxidation product. NAC suppressed ROS and significantly reduced cytotoxicity of ART (Berdelle et al., 2011). In MDA-MB-468 and SK-BR-3 cells, ART at 50 µM induced caspase activity and the pan-caspase inhibitor Z-VAD reduced the cytotoxic effect of ART. ART also increased the mitochondrial outer membrane permeability (MOMP) with a release of cytochrome c in the cytoplasm. ART significantly induced ROS and addition of glutathione inhibited accumulation of ROS, apoptosis and pH2AX. Of note, pre-treatment with holotransferrin (HT) significantly increased the ART mediated suppression of cell viability in MDA-MB-468 and SK-BR-3 cells suggesting that ART cytotoxicity was ROS and iron dependent (Greenshields et al., 2019). In embryonal

Rhabdomyosarcoma ART from 10 μM significantly induced cleaved caspase 3 and ROS while addition of NAC significantly decreased effect of ART on cell viability and cleavage of caspase 3. ART also induced pH2AX and NAC almost completely abrogated ART mediated DNA damage (Beccafico et al., 2015). In MCF-7 cells, ART at 25 μM - 50 μM significantly increased cell death at 24 h and 48 h. H2DCF-DA assay shown that ART significantly increased ROS and the iron chelator deferoxamine mesylate (DFO) that targets lysosomal iron decreased significantly ROS, prevented disruption of endolysosomal trafficking and activation of mitochondrial outer membrane permeability (MOMP) induced by ART at 50 μM (Hamacher-Brady et al., 2011). In T-47D and MDA-MB-231 cells, ART at 25 μM -50 μM induced fragmentation of the mitochondrial network by activation of lysosomal iron. (Hamacher-Brady et al., 2011). In T-47D cells, ART and DHA induced apoptosis by activating caspase 8 and caspase 9; however, it was not checked whether apoptosis could be induced by ROS (Mao et al., 2013). Then, ART has been generally shown to induce apoptosis by accumulation of ROS in different cancer cell lines.

5.7.2. ART cytotoxicity correlates with antioxidant activity in cancer

Artesunate cytotoxicity has been found to correlate with the intracellular antioxidant capacity (Efferth et al., 2003). In head and neck cancer ART induced ferroptosis by increasing lipid ROS and ART cytotoxicity was decreased after silencing of kelch-like ECH-associated protein 1 (Keap1), a negative regulator of Nrf2. In contrast, Nrf2 silencing restored ART cytotoxicity *in vitro* and *in vivo* suggesting that modulation of the Nrf2 pathway influenced ART induced ferroptosis (Roh et al., 2017). A correlation between the basal mRNA gene expression in 55 human tumor cell lines and ART IC_{50} indicated that *CAT* expression was inversely correlated with ART IC_{50} (Efferth et al., 2003). In MDA-MB-231 cells, the artemisinin derivative C-16 carba-dimer (AG-1) at 50 μM significantly induced a more oxidized environment compared to control; NAC significantly suppressed AG-1-induced toxicity. Then, transfection of cells with cDNA of *SOD2* and *CAT* genes significantly suppressed by 70% the AG-1 induced cytotoxicity (Kalen et al., 2020). The transfection with cDNA of glutathione cysteine synthetase, the rate limiting enzyme in the biosynthesis of glutathione, increased by 2.5x ART resistance of MSV-HL13 cells compared to control (Efferth and Wolm, 2005). Then, in Ramos cells *CAT* gene expression inversely correlated with ART cytotoxicity; ART could bind the surface of chain D of CAT (Sertel et al., 2010). In relation to ER stress, ART has been shown to mainly locate in the ER (Liu et al., 2010). In cancer, ART at 4 μM and for 72 h increased significantly unfolded protein response (UPR) to

cause apoptosis (Huang et al., 2022, Wang et al., 2019). Then, in cancer, ART cytotoxicity decreases in presence of high expression of antioxidant enzymes.

5.8. ZEB1 correlation with ROS and antioxidant enzymes

As ART exerts its cytotoxicity by ROS to induce apoptosis, an excessive antioxidant activity could block ART. To support the fact that ZEB1 could be upstream of ROS, different breast cancer models were used to evaluate expression of antioxidant enzymes and levels of ROS in presence or absence of ZEB1.

5.8.1. ZEB1 decreased ART induced ROS

After ART treatment, MCF-7/ZEB1 (-) Dox cells contained a signifcant higher amount of superoxide compared to MCF-7/ZEB1 (+) Dox (Fig. 14A). In line with this observation, ART treated MDA-MB-231/shZEB1 cells had a significantly higher amount of superoxide compared to MDA-MB-231/sh control cells (Fig. 14B). Also, total ROS level was higher in MDA-MB-231/shZEB1 than that detected in MDA-MB-231/cntrl cells (Fig. 15A and Supplementary Figure S15A/2). These observations are compatible with the hypothesis that ZEB1 is involved in the regulation of antioxidant mechanisms.

5.8.2. ZEB1 activated *SOD2* and *GPX8*

The heat map and hyerarchical clustering analysis of the relative gene expression of mesenchymal markers (*VIM*, *SNAI2*, *ZEB1*), epithelial markers (*CDH1*, junction plakoglobin (*JUP*), *mir200c*) and antioxidant enzymes (*SOD2, CAT*, *GPX8*) in a panel of breast cancer cell lines showed that ZEB1 co-clustered with *SOD2, GPX8* and *CAT* and mesenchymal markers (Fig. 17). The same cluster was also found in different cancer types (Supplementary Figure S17). In relation to antioxidant enzymes expression, ZEB1 overexpression in MCF-7/ZEB1 cells significantly decreased expression of *SOD1* while significantly increased that of *SOD2* and *GPX8* (Fig. 18A). *CAT* expression was unchanged (Supplementary Figure S18). It has been shown that mesenchymal features are associated with reduced levels of ROS and increased antioxidant activity. Khanzode et al., (2003) found that SOD levels in the serum of breast cancer patients significantly increased from Stage I to Stage IV and the total level of glutathione in the lymph node metastases was 4x higher than that in normal breast tissue (Perry et al., 1993). In addition, glutathione expression was increased in tumors lacking estrogen receptors and GPX expression significantly correlated with shorter overall survival (Jardim et al., 2013). Of note, non TNBC had higher oxidative stress compared to TNBC

(Herrera et al., 2012). These findings indicate that TNBC has increased antioxidant activity and, therefore, EMT/ZEB1 could be involved in the regulation of antioxidant mechanisms.

ZEB1 overexpression in MCF-7/ZEB1 cells induced a significant increase in the gene expression of *SOD2* (Fig. 18A). In cancer, SOD2 and EMT correlated. Coelho et al., (2022) demonstrated that MCF-7 cells transfected with SOD2 had high expression of CD44, VIM, Slug and ZEB1 while CD24 and E-cadherin decreased; also, as shown by immunohistochemistry analyses, SOD2 expression level was significantly higher in the metastatic sites compared to primary tumor tissues. In addition, SOD2 was present at higher level in TNBC cell lines compared to non TNBC cell lines (Kattan et al., 2008) and its overexpression induced a mesenchymal phenotype in MCF-7 cells (Kumar et al., 2014). In addition, SOD2 correlated with drug sensitivity (Hur et al., 2003, Tomkova et al., 2019, Luanpitpong et al., 2018). The SOD2 capacity to induce EMT coud be associated with the modulation of the intracellular redox ratio of superoxide:hydrogen peroxide that was shown crucial in the regulation of cell fate decisions (Loo et al., 2016).

ZEB1 activation in MCF-7/ZEB1 cells significantly decreased expression of *SOD1*. SOD1 is overexpressed in breast cancer and induced resistance to doxorubicin in MCF-7 cells. (Kepinska et al., 2018). Of note, in breast cancer, a switch from SOD1 to SOD2 has been recently reported by Gomez et al., (2019). The authors proposed that high expression of SOD1 coincides with the early stage of transformation in which oncogenic activation would keep SOD2 at low levels to sustain high superoxide levels, proliferation and epithelial phenotype. In this situation, SOD1 could maintain superoxide at levels that would not damage mitochondria, Then, in presence of excessive superoxide levels, cells would increase SOD2 to convert superoxide to hydrogen peroxide and this would decrease proliferation while inducing EMT.

ZEB1 activation in MCF-7/ZEB1 cells significantly increased expression of *GPX8*. Khatib et al., (2020) showed that gene and protein expression of GPX8 was higher in the TNBC cell lines MDA-MB-231, MDA-MB-436 and Hs 578-T cells, compared to MCF-7 cells. GPX8 expression correlated with the EMT markers fibronectin, ZEB1, ZEB2 and cadherin 11 (CDH11). GPX8 is mainly located to the ER of the cells in which the regulation of the disulfide bond formation is crucial for a correct protein folding (Khatib et al. 2020). In TNBC, high GPX8 expression could contribute to maintain proper protein folding by regulating the glutathione-glutathione disulfide ratio (Khatib et al., 2020).

According to my results, the ZEB1 mediated upregulation of *SOD2* and *GPX8* and the ZEB1 mediated downregulation of *SOD1* could represent the mechanism of resistance to ART in EMT-presenting breast cancer cells,

5.8.3. ZEB1 knokdown did not inhibit SOD2, GPX8 and CAT

Though ZEB1 could induce *SOD2* and *GPX8* genes in MCF-7/ZEB1 (+) Dox cells (Fig. 18A), MDA-MB-231/shZEB1 cells and Hs 578-T/shZEB1 cells, did not have a lower expression of SOD2 and GPX8 protein levels compared to the respective control cells (Fig. 18B). Also, MDA-MB-231 siRNA ZEB1 cells did not have a decrease of *CAT* gene expression compared to control (Supplementary Figure S18). However, total ROS were higher in MDA-MB-231/shZEB1 cells compared to MDA-MB-231/cntrl cells (Fig. 15A and Supplementary Figure S15A/2). In MDA-MB-231 and Hs 578-T cells, a transient and stable knockdown of ZEB1, respectively, increased ART induced pH2AX (Fig. 15B) suggesting that ZEB1 or EMT could be involved in DDR or ROS regulation. TNBC is generally more resistant to DNA damage compared to epithelial breast cancer. In effect, it has been shown that ZEB1 and the methionine sulfoxide reductase (MSRB3) had a role in the protection from oncogene-induced DNA damage to support cancer progression of cancer stem cells (Morel et al., 2017). However, ZEB1 has been found to induce ROS or suppress antioxidant enzymes in TNBC cells. In MDA-MB-231 cells, ZEB1 knockdown inhibited transcription of the lactate monocarboxylate transporter 4 (MCT4) and this induced ROS in the tumor microenvironment. In contrast, SOD and GPX activites significantly increased in ZEB1 depleted cells. In addition, in the MDA-MB-231 xenograft mice, inhibition of the ZEB1/MCT4 pathways increased activity of GPx and SOD while reducing tumor growth (Han et al., 2022). In MDA-MB-231 cells, ZEB1 inhibited GPX4 transcription and supported breast cancer progression by inducing ROS. The ZEB1/GPX4 pathway had also an effect on breast cancer metabolism (Han et al., 2021). In this project, it was also found that MDA-MB.231 cells depleted for ZEB1 had a high increase of *GPX4* gene expression compared to control (Supplementary Figure S15A/3). These findings show that in MDA-MB-231 cells, ZEB1 was a repressor of antioxidant enzymes. In line with this, SOD2 expression in MDA-MB-231/shZEB1 cells was significantly higher compared to MDA-MB-231/cntrl cells; GPX8 also increased. (Fig. 18B). In addition, ZEB1 depletion by siRNA ZEB1 highly increased *CAT* gene expression in MDA-MB-231 cells (Supplementary Figure S18). The increase of SOD2 protein levels and *CAT* gene expression after ZEB1 knockdown could still represent a mechanism to sensitise TNBC cells to ART. In MDA-MB-231 cells, overexpression of SOD2

decreased growth and survival (Weydert et al., 2008). In breast cancer, ectopic expression of SOD2 or SOD1 decreased xenograft tumor growth compared to control (Weydert et al., 2006). In cancer, SOD2 overexpression inhibits growth by increasing hydrogen peroxide and the half-cell reduction potential (Ehc) (Buettner et al., 2006). CAT overexpression increased sensitivity of cancer cells to paclitaxel, etoposide and arsenic trioxide (Glorieux et al., 2011). These findings support the fact that the increase of SOD2 (Fig. 18B) and *CAT* expression (Supplementary Figure S18) in MDA-MB-231 cells depleted for ZEB1 could still represent a mechanism of sensitisation to ART. However, total ROS levels were higher in MDA-MB-231/shZEB1 cells compared to MDA-MB-231/cntrl cells (Fig. 15A) suggesting that ZEB1 could be still upstream of other antioxidant enzymes or that expression and activity of antioxidant enzymes do not linearly correlate.

5.9. ZEB1 correlation with DNA damage and DDR enzymes

As ART has been shown to induce apoptosis by ROS mediated DBSs (Berdelle et al., 2011), in this project was checked whether ZEB1 could modulate extent of DNA damage and expression of some DDR enzymes. In MDA-MB-231 and Hs 578-T cells, a transient and stable knockdown of ZEB1, respectively, increased ART induced pH2AX (Fig. 15B). This suggested that ZEB1 could modulate expression of some DDR enzymes. In particular, as ART cytotoxicity increased after Rad51 knockdown (Berdelle et al., 2011), in this project was checked whether ZEB1 knockdown could suppress expression of Rad51 in TNBC cells. ZEB1 knockdown did not reduce protein expression of Rad 51 (Supplementary Figure S20B).

5.10. TP-0903 AXL inhibition correlation with ROS and antioxidant enzymes

In MDA-MB-231 cells, TP-0903 induced higher total ROS compared to control and addition of ART significantly increased total ROS (Fig. 16A and Supplementary Figure S16A). Of note, TP-0903 significantly increased the levels of total ROS in comparison with control only (Supplementary Figure S16A/2). In relation to antioxidant enzymes, in MDA-MB-231 cells, TP-0903 abrogated *CAT* gene expression (Fig. 19A); TP-0903 significantly decreased GPX8 protein expression while only slightly SOD2 (Fig. 19B); ART significantly increased SOD2 expression (Fig. 19B); addition of ART to TP-0903 significantly decreased SOD2 and GPX8 (Fig. 19B). In Hs 578-T and MDA-MB-436 cells, TP-0903 highly decreased GPX8 protein expression while SOD2 was slightly reduced. In Hs 578-T and MDA-MB-436 cells, addition of ART further reduced SOD2 and GPX8 though the effect was higher in Hs 578-T cells (Fig. 19B).

It is important to note that TP-0903 plus ART significantly increased total ROS (Fig. 16 A) and this correlated with a significant decrease of SOD2 and GPX8 in MDA-MB-231 cells (Fig. 19B). The excess of ROS induces a defective antioxidant defense mechanism, a damage of membrane, DNA, proteins and disrupts the mitochondrial membrane to activate apoptosis (Aggarwall et al., 2019). Among the most relevant ROS inducing apotosis, hydrogen peroxide has a primary role (Giorgio et al., 2007). In conclusion, combination of TP-0903 and ART could induce an excessive oxidative stress that ultimately dysregulate the expression of antioxidant enzymes defense to cause apoptosis.

5.11. TP-0903 AXL inhibition correlation with DNA damage and DDR enzymes

In TNBC cell lines, TP-0903 induced pH2AX that was further increased by addition of ART (Fig. 16B). TP-0903 has been reported to suppress enzymes involved in DDR (Balaji et al., 2017). In relation to ART, it has been shown how ART cytotoxicity was higher in cancer cells depleted for Rad51 (Berdelle et al., 2011) suggesting how DDR was involved in protection from ART. In this project, TP-0903 inhibited protein expression of Rad51 (Fig. 20B). However, TP-0903 suppressed Rad51 independently of ZEB1 (Supplementary Figure S20B); also, it was not shown whether TNBC cells depleted for Rad51 could be more sensitive to ART.

5.12. TP-0903 suppressed Snail and Slug

TP-0903 suppressed Snail and Slug (Fig. 20A) and for this it cannot be excluded that Snail or Slug could be involved in SOD2, GPX8 and CAT regulation. In MCF-7 cells, ROS induced the distal-less homeobox-2 (Dlx-2) gene that in turn activated Snail and EMT (Lee et al., 2019). In CRC, ROS activated EMT by AKT and Snail (Jiao et al., 2016). In MCF-7 cells, treatment with hydrogen peroxide activated EMT by increasing Snail and Slug (Zhao et al., 2016). However, these findings shown that Snail and Slug were downtream of ROS.

5.13. ZEB1 mediated ART resistance independently of antioxidant pathways
5.13.1. Regulation of glycolisis

The metabolism and redox rate are associated in cancer cells. TNBC is characterised by high glycolysis and low oxidative phosphorylation to maintain low levels of superoxide/ROS (Marcucci et al., 2022). In breast cancer, inhibition of glycolysis increased sensitivity to drug cytotoxicity (Minamoto et al., 2002). In MDA-MB-231 cells ZEB1 regulated transcription of the glycolytic enzymes hesokinase 2 (HK2), Phosphofructokinase, Platelet (PFKP), pyruvate

kinase M2 (PKM2). ZEB1 activated glycolysis by the PI3K/AKT/HIF-1α pathway that also associated with migration and chemoresistance. Also, the immunohistochemistry analysis from breast cancer tissues indicated that ZEB1, lactate dehydrogenase A (LDHA) and monocarboxylate transporter 4 (MCT4) significantly associated (Jiang et al., 2022). In NSCLC, ZEB1 directly induced transcription of glucose transporter 3 (GLUT3) that associated with EMT and poor overall survival (Masin et al., 2014). Then, ZEB1 could induce resistance to ART in TNBC cells by regulation of glycolysis. However, this was not checked.

5.13.2. Regulation of radiosensitivity

ZEB1 has been shown to regulate radiosensitivity and DDR in breast cancer (Zhang, Wei et al., 2014). ATM was shown to phosphorylate and stabilize ZEB1 in response to DNA damage. ZEB1 in turn interacted with ubiquitin carboxyltrminal hydrolase 7 (USP7) to deubiquitylate and stabilize checkpoint kinase 1 (CHK1) to promote HR (Zhang, Wei et al., 2014). ZEB1 has been shown to regulate genes involved in DDR, such as USP17-like family member 2 (DUB3), chromodomain helicase DNA-binding protein 1-like (CHD1L) and double homeobox 4 (DUX4) (Wang, He et al., 2017). In addition, ZEB1 depleted cells were more sensitive to cisplatin and etoposide mediated apoptosis (Wang, He et al., 2017). In relation to ART, glioma cells depleted for Rad51 were more sensitive to ART mediated ROS, oxidative DNA lesions and apoptosis (Berdelle et al, 2011). According to my data, though TP-0903 suppressed Rad51 (Fig. 18B), this effect was independent of ZEB1 (Supplementary Figure S18B). However, it was not tested whether ZEB1 could regulate additional DDR enzymes in TNBC cells.

5.13.3. Regulation of apoptosis and survival factors

ZEB1 could mediate ART resistance by regulating proliferation, apoptosis, survival and drug transporters. In an analysis of human breast cancer subjects, ZEB1 associated positively with Bcl-xl, a predictor of chemoresistance and in MDA-MB-231 cells, ZEB1 directly regulated expression of the survival factors Baculoviral IAP repeat-containing protein 3 (BIRC3) and Pim-3 Proto-Oncogene, Serine/Threonine Kinase (PIM3) (Zhang et al., 2018). In mouse xenograft models of mantle cell lymphoma, ZEB1 induced myc, the anti-apoptotic factor bcl-2 and inhibited the pro-apoptotic factor bax. ZEB1 also induced expression of drug transporters, such as MDR1 (Tillò et al., 2014). Then, in cancer, ZEB1 modulates expression of apoptotic, survival factors and drug transporters. However, in this project this was not checked in TNBC cells.

5.13.4. Regulation of E-cadherin

ZEB1 depletion in TNBC cells increased expression of E-cadherin (Fig. 10A). Also, MDA-MB-231/shZEB1 cells had restoration of P-cadherin expression compared to control cells (Fig. 10B). Kashiwagi et al., (2010) found that in TNBC patients treated with adjuvant chemotherapy, low expression of E-cadherin correlated significantly with lower overall survival, higher tumor size and grade and distant metastasis. Also, E-cadherin independently predicted overall survival (Rakha et al., 2005). As TP-0903 suppressed ZEB1 (Fig. 11B) while increasing E-cadherin (Fig. 11C), sensitisation of TNBC cells to ART by TP-0903 is likely to involve the ZEB1/E-cadherin pathway.

5.14. TP-0903 plus ART molecular mechanism

In Fig. 21 is depicted a schematic representation of the molecular mechanism by which TP-0903 and ART could synergise to induce apoptosis in TNBC. ZEB1 induced resistance to ART mediated ROS, pH2AX and apoptosis in TNBC. ZEB1 also decreased E-cadherin. ZEB1 knockdown and TP-0903 enhanced E-cadherin and ART mediated ROS, pH2AX and apoptosis. This suggested that ZEB1 could induce resistance to ART by modulating some antioxidant mechanisms. However, while TP-0903 suppressed GPX8 and CAT, knockout of ZEB1 did not have the same effect. Then, TP-0903 sensitised TNBC to ART independently of the ZEB1-antioxidant pathway. However, ZEB1 depleted cells had higher total basal ROS levels compared to control. In addition, TP-0903 repressed Snail and Slug suggesting that a complete and not a partial EMT inhibition could be required to suppress CAT and GPX8. TP-0903 also inhibited Rad51 independently of ZEB1. Then, in concomitance with EMT inhibition, TP-0903, independently of ZEB1 could sensitise TNBC to ART by suppressing GPX8, CAT and Rad51.
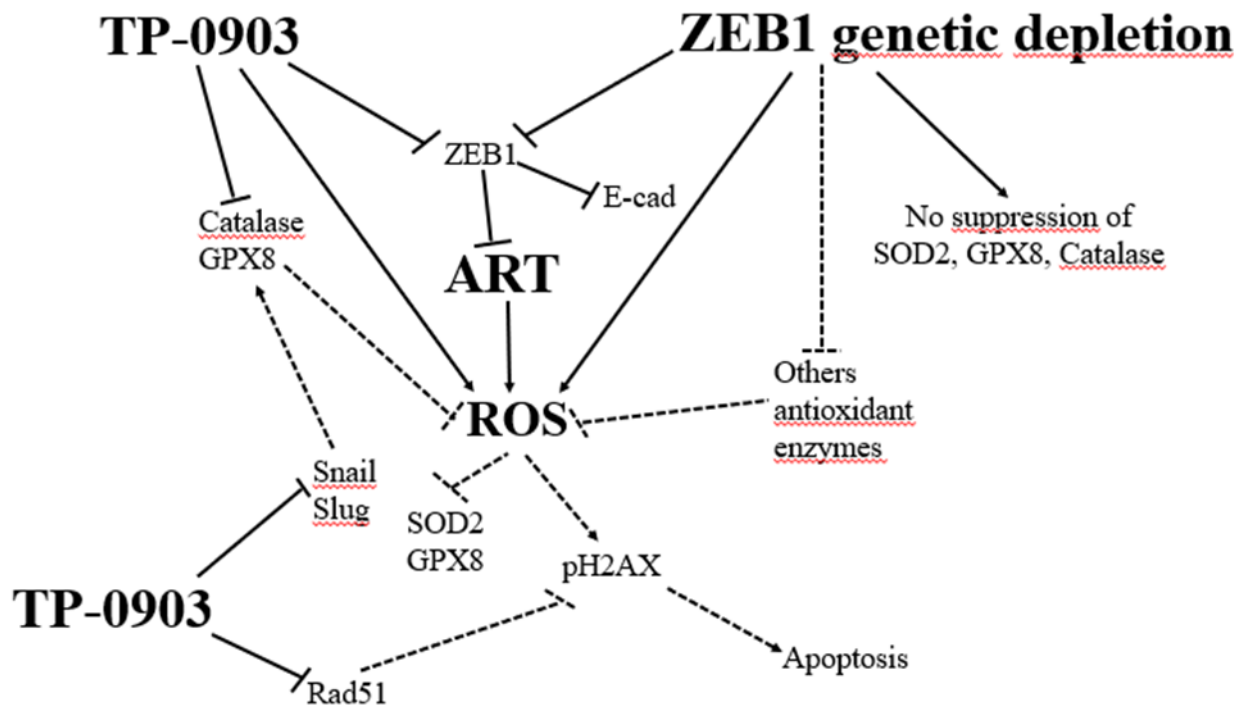
Fig. 21. TP-093 plus ART molecular mechanism. ZEB1 inhibition by TP-0903 and genetic knockout increased E-cadherin and ART induced ROS, pH2AX and apoptosis. ZEB1 could induce resistance to ART by regulating some antioxidant mechanisms. However, while TP-0903 suppressed GPX8 and CAT, a stable and transient knockout of ZEB1 did not have the same effect. However, shZEB1 cells had higher total ROS levels compared to control. TP-0903 plus ART synergised to decrease SOD2 and GPX8. In addition, TP-0903 suppressed Snail and Slug that could have a role in the modulation of GPX8 and CAT. TP-0903 also abrogated Rad51 but independently of ZEB1. Then, in concomitance with EMT inhibition, TP-0903, independently of ZEB1, could sensitise TNBC to ART by suppressing GPX8, CAT and Rad51.

CHAPTER 6: CONCLUSIONS

Triple-negative breast cancer (TNBC) is a lethal cancer. TNBC associates with the epithelial-mesenchymal transition (EMT), a cellular program that confers chemoresistance and metastasis. Therapy approaches could rely on the EMT reversal to sensitise mesenchymal tumours to compounds effective against epithelial cancers. In this project, the ROS inducer compound artesunate (ART) was more cytotoxic in epithelial compared to mesenchymal breast cancer cell lines. ZEB1 ectopic expression in epithelial or ZEB1 knockdown in mesenchymal cells, decreased and enhanced ROS, DNA damage and apoptosis induced by ART, respectively. ZEB1 activated gene expression of the antioxidant enzymes superoxide dismutase 2 (*SOD2*) and glutathione peroxidase 8 (*GPX8*) in epithelial cells. *CAT* gene expression was not changed. Although ZEB1 knockdown in mesenchymal cells did not decrease antioxidant enzymes protein expression, stable ZEB1 knockdown increased total ROS. The RTK AXL assscoiates with EMT and is highly expressed in TNBC. The AXL inhibitor TP-0903 inhibited EMT and synergised with ART to activate ROS, DNA damage and apoptosis in TNBC cells. TP-0903 decreased protein expression of GPX8 and SOD2 and gene expession of *CAT*. In addition, TP-0903 suppressed expression of the DDR enzyme Rad51 but independently of ZEB1. Thus, TP-0903 and ZEB1 knockdown sensitised TNBC cells to ART likely via different pathways. The synergistic interaction between TP-0903 and ART suggests that a combination of TP-0903 and ART could treat TNBC.

CHAPTER 7: FUTURE PERSPECTIVES

The results of this project showed a synergism between ART and MET-inducing compound TP-0903 suggesting that a combination with these two compounds could treat TNBC. However, as TP-0903 plus ART significantly activated ROS, this could damage highly proliferative tissues in the body. Therefore, further research with mouse models of TNBC will define the toxicity/efficacy of TP-0903/ART combination.

CHAPTER 8: REFERENCES

Aggarwal, V., Tuli, H., S., Varol, A., Thakral, F., Yerer, M., B., Sak, K., Varol, M., Jain, A., Khan, M., A. and Sethi, G. (2019). Role of Reactive Oxygen Species in Cancer Progression: Molecular Mechanisms and Recent Advancements. *Biomolecules, 9*(11): 735. doi:10.3390/biom9110735.

Andreopoulou, E., Schweber, S., J., Sparano, J., A. and McDaid H., M. (2015). Therapies for triple negative breast cancer. *Expert Opin. Pharmacother., 16*(7): 983–998.

Anfosso, L., Efferth, T., Albini, A. and Pfeffer, U. (2006). Microarray expression profiles of angiogenesis-related genes predict tumor cell response to artemisinins. *The Pharmacogenomics Journal, 6,* 269–278.

Artigues. A., A., Arenas, E., J., Sabadell, A., M. Maristany, F., B., Cervera, R., Tormo, E., Hernando C., Martinez, M., T., Asins., J., C. and Cejalvo, J., M. (2022). Targeting HER2-AXL heterodimerization to overcome resistance to HER2 blockade in breast cancer *Science Advances, 8*(20). doi: 10.1126/sciadv.abk2746.

Asiedu, M., K., Beauchamp-Perez, F., D., Ingle, J., N., Behrens, M., D., Radisky, D., C. and Knutson, K., L. (2014). AXL induces epithelial-to-mesenchymal transition and regulates the function of breast cancer stem cells. *Oncogene*, *33*(10): 1316–1324.

Avtanski, D., B., Nagalingam, A., Bonner, M., Y, Arbiser, J., L., Saxena, N., K. and Sharma, D. (2014). Honokiol inhibits epithelial-mesenchymal transition in breast cancer cells by targeting signal transducer and activator of transcription 3/Zeb1/E-cadherin axis. *Mol. Oncol.*, *8*:565–80.

Axelrod, H. and Pienta, K., J. (2014). Axl as a mediator of cellular growth and survival. *Oncotarget*, *5*(19).

Bachmeier, B., Fichtner, I., Killian, P., H., Kronski, E., Pfeffer, U. and Efferth, T. (2011). Development of resistance towards artesunate in MDA-MB-231 human breast cancer cells. *PLoS ONE, 6* (5).

Bai, W., D., Ye, X., M., Zhang, M., Y., Zhu, H., Y., Xi, W., J., Huang, X., Zhao, J., Gu, B., Zheng, G, X., Yang, A., G., Jia, L., T. (2014). MiR-200c suppresses TGF-beta signaling and counteracts trastuzumab resistance and metastasis by targeting ZNF217 and ZEB1 in breast cancer. *Int. J. Cancer.*, *135*: 1356–68.

Balaji, K., Vijayaraghavan, S., Diao, L., Tong, P., Fan, Y., Carey, J., P., W., Bui, T., N., Warner, S., Heymach, J., V., Hunt, K., K., Wang, J., Byers, L., A. and Keyomarsi, K. (2017). AXL inhibition suppresses the DNA damage response and sensitizes cells to

PARP inhibition in multiple cancers. *Mol. Cancer Res., 15*(1):45-58. doi: 10.1158/1541-7786.MCR-16-0157.

Battke, C., Ruiss, R., Welsch, U., Wimberger, P., Lang, S., Jochum, S. and Zeidler, R. (2011). Tumour exosomes inhibit binding of tumour-reactive antibodies to tumour cells and reduce ADCC. *Cancer Immunol. Immunother., 60*(5):639-48. doi: 10.1007/s00262-011-0979-5.

Batty, K., T., Davis, T., M., Thu, L., T., Binh, T., Q, Anh, T., K and Ilett, K., F. (1996), Selective high-performance liquid chromatographic determination of artesunate and alpha and beta-dihydroartemisinin in patients with falciparum malaria. *J Chromatogr B Biomed Appl, 677*: 345–350.

Beccafico, S., Morozzi G., Marchetti, M., C., Riccardi, C., Sidoni, A., Donato, R. and Sorci, G. (2015). Artesunate induces ROS- and p38 MAPK-mediated apoptosis and counteracts tumor growth in vivo in embryonal rhabdomyosarcoma cells. *Carcinogenesis, 36*(9): 1071–1083. doi:10.1093/carcin/bgv098.

Berdelle, N., Nikolova, T., Quiros, S., Efferth, T. and Kaina, B. (2011). Artesunate induces oxidative DNA damage, sustained DNA double-strand breaks, and the ATM/ATR damage response in cancer cells. *Mol. Cancer Ther., 10*(12), 2224-33.

Bermejo, I., L., Jiménez, P., G., Duarte, S., Pajares, M., A. and Sala, D. P. (2022). Vimentin Tail Segments Are Differentially Exposed at Distinct Cellular Locations and in Response to Stress. *Frontiers in Cell and Developmental Biology, 10*(908263). doi: 10.3389/fcell.2022.908263.

Bermudez, M., Aguilar-Medina, M., Lizarraga-Verdugo, E., Avendano-Felix, M., Silva-Benitez, E., Lopez-Camarillo, C., et al. (2019). LncRNAs as regulators of autophagy and drug resistance in colorectal cancer. *Front. Oncol. 9*: 1008. doi: 10.3389/fonc.2019.01008

Bindels, S., Mestdagt, M., Vandewalle, C., Jacobs, N., Volders, L., Noël, A., van Roy, F., Berx, G., Foidart, J., M. and Gilles, C. (2006). Regulation of vimentin by SIP1 in human epithelial breast tumor cells. *Oncogene, 25*: 4975–4985.

Bottai, G., Raschioni, C., Székely, B., Di Tommaso, L., Szász, A. M., Losurdo, A., Győrffy, B., Ács, B.,Torrisi, R., Karachaliou, N., Tőkés, T., Caruso, M., Kulka, J., Roncalli, M., Santoro, A., Mantovani, A., Rosell, R., Reis-Filho, J., S. and Santarpia, L. (2016). AXL-associated tumor inflammation as a poor prognostic signature in chemotherapy-treated triple-negative breast cancer patients. *Breast Cancer, 2*(2):16033. doi: 10.1038/npjbcancer.2016.33.

Brand, T., M., Iida, M., Stein, A., P., Corrigan, K., L., Braverman, C., Luthar, N., Toulany, M., Gill, P., S., Salgia, R., Kimple, R., J. and Wheeler, D., L. (2014). AXL mediates resistance to cetuximab therapy. *Cancer Res.,74*(18): 5152–5164. doi: 10.1158/0008-5472.CAN-14-0294.

Breckenridge, D., G., Germain, M., Mathai, J., P., Nguyen, M. and Shore, G., C. (2003). Regulation of apoptosis by endoplasmic reticulum pathways. *Oncogene*, *22:* 8608-8618

Brunet, A., Bonni, A., Zigmond, M., J., Lin, M., Z., Juo, P., Hu, L., S., Anderson, M., J., Arden, K., C., Blenis, J. and Greenberget, M., E. (1999). Akt promotes cell survival by phosphorylating and inhibiting a Forkhead transcription factor. *Cell., 96*(6): 857–68.

Buettner, G., R, Ng, C., F., Wang, M., Rodgers, V., G. and Schafer, F., Q. (2006). A new paradigm: manganese superoxide dismutase influences the production of H2O2 in cells and thereby their biological state. *Free Radic. Biol Med., 41*:1338–50.

Buommino, E., Baroni, A., Canozo, N., Petrazzuolo, M, Nicoletti, R., Vozza, A. and Tufano, M., A. (2008). Artemisinin reduces human melanoma cell migration by downregulating αvβ3 integrin and reducing metalloproteinase 2 production. *Investigational New Drugs, 27*(5): 412–418.

Burdick, A., D., Davis, J., W., Liu, K., J., Hudson, L., J., Shi, H., Monske, M., L. and Burchiel, S. W. (2003). Benzo(a)pyrene quinones increase cell proliferation, generate reactive oxygen species, and transactivate the epidermal growth factor receptor in breast epithelial cells. *Cancer Res., 63*(22):7825–33.

Burk, U., Schubert, J., Wellner, U., Schmalhofer, O., Vincan, E., Spaderna, S and Brabletz, T., A. (2008). Reciprocal repression between ZEB1 and members of the miR-200 family promotes EMT and invasion in cancer cells. *EMBO Rep.*, *9*:582–9.

Chabot, T., Defontaine, A., Marquis, D., Renodon-Corniere, A., Courtois, E., Fleury, F. and Cheraud, Y. (2019). New phosphorylation sites of Rad51 by c-Met modulates presynaptic filament stability. *Cancers, 11*: 413.

Charpin, C., Garcia, S., Bonnier, P., Martini, F., Andrac, L., Choux, R., Lavaut, M., N. and Allasia, C. (1998) Reduced E-cadherin immunohistochemical expression in node-negative breast carcinomas correlates with 10-year survival. *Am J Clin Pathol*, *109:* 431–438.

Chen, H., H., Zhou, H., J., Wang, W., Q. and Wu, G., D. (2004). Anti-malarial dihydroartemisinin also inhibits angiogenesis. *Cancer Chemotherapy and Pharmacology*, *53*(5): 423–432.

Chen, X., Zhang, X., L., Zhang, G., H. and Gao, Y., F. (2019). Artesunate promotes Th1 differentiation from CD4+ T cells to enhance cell apoptosis in ovarian cancer via miR-142. *Braz J Med Biol Res., 52*(5): e7992. doi: 10.1590/1414-431X20197992.

Chi, F., Liu, J., Brady, S., W., Cosgrove, P., A., Nath, A., McQuerry, J., A., Majumdar, S., Moos, P., J., Chang, J., T., Kahn, M. and Bild, A., H. (2021). A 'one-two punch' therapy strategy to target chemoresistance in estrogen receptor positive breast cancer. *Translational Oncology, 14*(1) https://doi.org/10.1016/j.tranon.2020.100946.

Chua, H., L., Bhat-Nakshatri, P., Clare, S., E., Morimiya, A., Badve, S. and Nakshatri, H. (2007). NF-kappaB represses E-cadherin expression and enhances epithelial to mesenchymal transition of mammary epithelial cells: potential involvement of ZEB-1 and ZEB-2. *Oncogene*, *26*(5): 711-24. doi: 10.1038/sj.onc.1209808.

Ciravolo, V., Huber, V., Ghedini, G., C., Venturelli, E., Bianchi, F., Campiglio, M., Morelli, D., Villa, A., Della Mina, P., Menard, S., Filipazzi, P., Rivoltini, L., Tagliabue, E. and Pupa, S., M. (2012). Potential role of HER2-overexpressing exosomes in countering trastuzumab-based therapy. *J. Cell. Physiol., 227*(2):658-67. doi: 10.1002/jcp.22773.

Circu, M. L. (2010). Reactive oxygen species, cellular redox systems, and apoptosis. *Free Radic. Biol. Med., 48*: 749-762

Circu, M., L., Aw., T., Y. (2012). Glutathione and modulation of cell apoptosis. *Biochim. Biophys. Acta*, *1823*: 1767-1777

Cochrane, D. R., Spoelstra, N. S., Howe, E. N., Nordeen, S. K., and Richer, J. K. (2009). MicroRNA-200c mitigates invasiveness and restores sensitivity to microtubule-targeting chemotherapeutic agents. *Mol. Cancer Ther. 8*: 1055–1066. doi: 10.1158/1535-7163.MCT-08-1046

Coelho, D., R., Palmaa, F., R., Paviania, V., Hec, C., Danesa, J., M., Huanga, Y., Caladoa, J., C., P., Hartd, P., C., Furduie, C., M., Poolef, L., B., Schipmab, M., J. and Boninia, M., G. (2022). Nuclear-localized, iron-bound superoxide dismutase-2 antagonizes epithelial lineage programs to promote stemness of breast cancer cells via a histone demethylase activity. *PNAS*, *119*(29): e2110348119. doi:10.1073/pnas.2110348119.

Colavito, S., A. (2020). AXL as a Target in Breast Cancer Therapy. *J. Oncol., 2020*: 5291952. doi: 10.1155/2020/5291952;

Corallo, D., Porcù, E., Pantilea, M., Bosob, D., Zanona, C., Viola, G., Sidarovich, V., Mariotto, E., Quattrone, A., Basso, G. and Tonini, G., P. (2018). TP-0903 inhibits neuroblastoma cell growth and enhances the sensitivity to conventional chemotherapy. *Molecular and cellular pharmacology*, *818*(5): 435-448.

Cortes, J., Rugo, H., S., Cescon, D. W., Im, S., A., Yusof, M., M., Gallardo, C., Lipatov, O., Barrios, C., H., Perez-Garcia, J., Iwata, H., Masuda, N., Otero, M., T., Gokmen, E., Loi, S., Guo, Z., Zhou, X., Karantza, V., Pan, W. and Schmid, P. (2022). Pembrolizumab plus Chemotherapy in Advanced Triple-Negative Breast Cancer. *N. Engl. J. Med., 387*(3): 217-226; doi: 10.1056/NEJMoa2202809.

Crespo-Ortiz, M., P. and Wei, M. Q. (2012). Antitumor Activity of Artemisinin and Its Derivatives: From a Well-Known Antimalarial Agent to a Potential Anticancer Drug. *Journal of Biomedicine and Biotechnology, 2012*: 2012:247597. doi: 10.1155/2012/247597.

Cui, Y., Qin, L., Tian, D., Wang, T., Fan, L., Zhang, P., et al. (2018). ZEB1 promotes chemoresistance to cisplatin in ovarian cancer cells by suppressing SLC3A2. *Chemotherapy*, *63*: 262–271. doi: 10.1159/000493864

D'Alfonso, T., M., Hannah, J., Chen, Z., Liu, Y., Zhou, P. and Shin, S., J. (2014). Axl receptor tyrosine kinase expression in breast cancer. *J. Clin. Pathol., 67*(8):690-6. doi: 10.1136/jclinpath-2013-202161.

De Cock J., M., Shibue, T., Dongre, A., Keckesova, Z., Reinhardt, F. and Weinberg, R., A. (2016). Inflammation triggers Zeb1-Dependent escape from tumor latency. *Cancer Res., 76,* 6778–6784. 10.1158/0008-5472.CAN-16-0608;

De Ruijter, T., C., Veeck, J., De Hoon, J., P., J., Van Engeland, M. and Tjan-Heijnen, V., C. (2011). Characteristics of triple-negative breast cancer. *J. Cancer Res.*, *137*: 183–192.

Dong, J., Yang, W., Han, J., Cheng, R., Guo, X. and Li, L. (2019). Effect of dihydroartemisinin on epithelial-to-mesenchymal transition in canine mammary tumour cells. *Res Vet Sci.*, *124:* 240-247. doi: 10.1016/j.rvsc.2019.03.020.

Efferth, T. and Volm, M. (2005). Glutathione-related Enzymes Contribute to Resistance of Tumor Cells and Low Toxicity in Normal Organs to Artesunate. *In vivo*, *19*: 225-232

Efferth, T., Giaisi, M., Merling, A., Krammer, P., H. and Weber, M., L. (2007). Artesunate induces ROS-mediated apoptosis in doxorubicin-resistant T leukemia cells. *PLoS One*, *2*(8): 693

Efferth, T., Margaret, M., Margaret, B. and Tome, E. (2003). Role of antioxidant genes for the activity of artesunate against tumor cells. *Int J Oncol*, *23*(4): 1231-5. doi: 10.3892/ijo.23.4.1231.

Efferth, T., Sauerbrey, A., Olbrich, A., Gebhart, E., Rauch, P., Weber, H., O., Hengstler, J., G., Halatsch, M., E., Volm, M., Tew, K., D., Ross, D., D., and Funk, J., O. (2003).

Molecular modes of action of artesunate in tumor cell lines. *Mol. Pharmacol, 64*, 382–394.

Efferth, T.and Kaina, B. (2010). Toxicity of the antimalarial artemisinin and its derivatives. *Critical Reviews in Toxicology*, *40*(5): 405–421.

Eger, A., Aigner, K., Sonderegger, S., Dampier, B., Oehler, S., Schreiber, M., Berx, G., Cano, A., Beug, H. and Foisner, R. (2005). DeltaEF1 is a transcriptional repressor of E-cadherin and regulates epithelial plasticity in breast cancer cells. *Oncogene*, *24*: 2375–85.

El Bezawy, R., Cominetti, D., Fenderico, N., Zuco, V., Beretta, G., L., Dugo, M. Arrighetti, N, Stucchi, C., Rancati, T., Valdagni, R., Zaffaroni, N. and Gandellini, P. (2017). MiR-875-5p counteracts epithelial-to-mesenchymal transition and enhances radiation response in prostate cancer through repression of the EGFR-ZEB1 axis. *Cancer Lett.*, *395*: 53–62. doi:10.1016/j.canlet.2017.02.033

Federici C., Petrucci F., Caimi S., Cesolini A., Logozzi M., Borghi M., D'Ilio S., Lugini L., Violante N., Azzarito T., Majorani, C., Brambilla, D. and Fais, S. (2014). Exosome release and low pH belong to a framework of resistance of human melanoma cells to cisplatin. *PLoS ONE, 9*(2). doi: 10.1371/journal.pone.0088193.

Felip, E., Brunsvig, P., Vinolas, N., Aix, P., S., Costa, E., C., Gomez, M., D., Perez, J., M., T., Arriola, E., Campelo, R., G., Spicer J., F., Thompson, J., R., Granados, A., L., O., Holt, R., J., Lorens, K., Lorens, J., B., Shoaib, M., Siddiqui, A., Schmidt, E., V., Chisamore, M., J. and Krebs, M. (2019). A phase II study of bemcentinib (BGB324), a first-in-class highly selective AXL inhibitor, with pembrolizumab in pts with advanced NSCLC: OS for stage I and preliminary stage II efficacy. *Journal of Clinical Oncology*, *37*: 9098.

Felty, Q, Singh, K., P. and Roy, D. (2005). Estrogen-induced G1/S transition of G0-arrested estrogen-dependent breast cancer cells is regulated by mitochondrial oxidant signaling. *Oncogene, 24*(31): 4883–93.

Felty, Q., Xiong, W., C., Sun, D., Sarkar, S., Singh, K., P., Parkash, J. and Roy, D. (2005). Estrogen-induced mitochondrial reactive oxygen species as signal-transducing messengers. *Biochemistry. 44*(18):6900–9.

Feng, M., X., Hong, J., X., Wang, Q., Fan, Y., Y., Yuan, C., T., Lei, X., H., Zhu, M., Qin, A., Chen, H., X. and Hong, D. (2016). Dihydroartemisinin prevents breast cancer-induced osteolysis via inhibiting both breast cancer cells and osteoclasts. *Sci. Rep.,* 6: 19074.

Firestone, G., L. and Sundar S. N., "Anticancer activities of artemisinin and its bioactive derivatives. *Expert Reviews in Molecular Medicine*, *11*: 32.

Galal, A., M., Ross, S., A., ElSohly, M., A, et al. (2002). Deoxyartemisinin derivatives from photooxygenation of anhydrodeoxydihydroartemisinin and their cytotoxic evaluation. *Journal of Natural Products*, *65*(2): 184–188.

Geng, B., Zhu, Y., Yuan, Y., Bai, J., Dou, Z., Sui, A. and Luo, W. (2021). Artesunate Suppresses Choroidal Melanoma Vasculogenic Mimicry Formation and Angiogenesis via the Wnt/CaMKII Signaling Axis. *Frontiers in Oncology*, *11*(714646). doi.org/10.3389/fonc.2021.714646

Ghasemi, M., Turnbull, T., Sebastian, S. and Kempson, I. (2021). The MTT Assay: Utility, Limitations, Pitfalls, and Interpretation in Bulk and Single-Cell Analysis. *Int. J. Mol. Sci., 22*(23), 12827. doi.org/10.3390/ijms222312827

Gheldof, A., Hulpiau, P., van Roy, F. , De Craene, B. , & Berx, G. (2012). Evolutionary functional analysis and molecular regulation of the ZEB transcription factors. *Cellular and Molecular Life Sciences*, 69, 2527–2541.

Ghosh, A., K., Secreto, C., Boysen, J., Sassoon, T., Shanafelt, T., D., Mukhopadhyay, D. et al. (2011). The novel receptor tyrosine kinase Axl is constitutively active in B-cell chronic lymphocytic leukemia and acts as a docking site of nonreceptor kinases: implications for therapy. *Blood., 117*: 1928–37.

Giorgio, M., Trinei, M., Migliaccio, E. and Pelicci, P., G. (2007). Hydrogen peroxide: a metabolic by-product or a common mediator of ageing signals? *Nat. Rev. Mol. Cell. Biol., 8*(9): 722-8. doi: 10.1038/nrm2240.

Gjerdrum, C., Tiron, C., Stefansson, T., I., Haugen, H., Sandal, T., Collett, K., Li, S., McCormack, E., Gjertsen, B., T., Micklem, D., R., Akslen L., A. Glackin, C. and Lorens, J., B. (2010). Axl is an essential epithelial-to-mesenchymal transition-induced regulator of breast cancer metastasis and patient survival. *PNAS, 107*(3), 1124-1129.

Glorieux, C., Dejeans, N., Sid, B., Beck, R., Calderon, P., B. and Verrax, J. (2011). Catalase overexpression in mammary cancer cells leads to a less aggressive phenotype and an altered response to chemotherapy. *Biochem. Pharmacol., 82*(10):1384-90. doi: 10.1016/j.bcp.2011.06.007.

Gomez, M., L., Shah, N., Kenny, T., C., Jenkins, E., C. and Germain, D. (2019). SOD1 is essential for oncogene-driven mammary tumor formation but dispensable for normal development and proliferation. *Oncogene, 38*: 5751–5765.

Goyette, M. A., Duhamel, S., Aubert, L., Pelletier, A., Savage, P., Thibault, M., P., Johnson, R., M., Carmeliet, P., Basik, M., Gaboury, L., Muller, W., J., Park, M., Roux, P., P., Gratton, J., P. and Côté, J., F. (2018). The receptor tyrosine kinase AXL is required at

multiple steps of the metastatic cascade during HER2-positive breast cancer progression. *Cell Rep., 23*(5), 1476-1490. https://doi:10.1016/j.celrep.2018.04.019.

Greenshields, A., L., Fernando, W. and Hoskinabc, D., W. (2019). The anti-malarial drug artesunate causes cell cycle arrest and apoptosis of triple-negative MDA-MB-468 and HER2-enriched SK-BR-3 breast cancer cells. *Experimental and Molecular Pathology*, 107: 10-22

Gregory, P., A., Bert, A., G., Paterson, E., L., Barry, S., C., Tsykin, A., Farshid, G., Vadas, M., A., and Goodall, G., J. (2008). The miR-200 family and miR-205 regulate epithelial to mesenchymal transition by targeting ZEB1 and SIP1. *Nat. Cell Biol., 10*:593–601.

Grimm, S. (2012). The ER-mitochondria interface: the social network of cell death. *Biochim. Biophys. Acta, 1823*: 327-334.

Grundy, M., K., Buckanovich, R., J. and Bernstein, K., A. (2020). Regulation and pharmacological targeting of RAD51 in cancer. *Cancer, 2*(31). doi: 10.1093/narcan/zcaa024.

Ha, D., Williams, E. and Cadenas, E. (2001). Mitochondrial respiratory chain-dependent generation of superoxide anion and its release into the intermembrane space. *Biochem J., 353*: 411–6.

Habashy, H., O., Powe, D., G., Staka, C., M, Rakha, E., A., Ball, G., Green, A., R, Aleskandarany, M., Paish, E., C., Douglas, M., R, Nicholson, R., I, Ellis, I., O and Gee, J., M. (2010). Transferrin receptor (CD71) is a marker of poor prognosis in breast cancer and can predict response to tamoxifen. *Breast Cancer Res Treat, 119*:283–293.

Hafner, M., Heiser, L., M., Williams, E., H., Niepel, M., Wang, N., J., Korkola, J., E., Gray, J., W. and Sorger, P., K. (2017). Quantification of sensitivity and resistance of breast cancer cell lines to anti-cancer drugs using GR metrics. *Scientific Data, 4*(170166).

Halestrap, A., P. (2009). What is the mitochondrial permeability transition pore? *J. Mol. Cell. Cardiol., 46* (2009): 821-831.

Hamacher-Brady, A., H., B., Stein, H., A., Turschner, S., Toegel, I., Mora, R., Jennewein, N., Efferth, T., Eils, R. and Brady, N., R. (2011). Artesunate activates mitochondrial apoptosis in breast cancer cells via iron-catalyzed lysosomal reactive oxygen species production. *J. Biol. Chem., 25*(8), 6587-601.

Han, X., Duan, X., Liu, Z., Long, Y., Liu, C. Zhou, J., Li, N., Qin, J. and Wang, Y. (2021). ZEB1 directly inhibits GPX4 transcription contributing to ROS accumulation in breast cancer cells. *Breast Cancer Res. Treat., 188*(2):329-342. doi: 10.1007/s10549-021-06301-9.

Han, X., Longa, Y., Duan, X., Liu, Z., Hu, X. Zhou, J., Li, N., Wang, Y. and Qin, J. (2022). ZEB1 induces ROS generation through directly promoting MCT4 transcription to facilitate breast cancer. *Experimental Cell Research, 412*(2). doi.org/10.1016/j.yexcr.2022.113044.

Han, Y., Luo, Y., Wang, Y., Chen, Y., Li, M., and Jiang, Y. (2016). Hepatocyte growth factor increases the invasive potential of PC-3 human prostate cancer cells via an ERK/MAPK and Zeb-1 signaling pathway. *Oncol. Lett.* 11, 753–759. doi: 10.3892/ol.2015.3943

Harris, J., L., Rabellino, A. and Khanna, K., K. (2018). RAD51 paralogs promote genomic integrity and chemoresistance in cancer by facilitating homologous recombination. *Ann. Transl. Med.*, 6:S122.

Hasanbasic, I., Cuerquis, J., Varnum, B. and Blostein, M., D. (2004). Intracellular signaling pathways involved in Gas6-Axl-mediated survival of endothelial cells. *Am. J. Physiol. Heart Circ. Physiol, 287*(3), 1207–1213. https://doi:10.1152/ajpheart.00020.2004. https://doi: 10.1007/s13277-015-4665-7.

Hine, C., M., Li, H., Xie, L., Mao, Z., Seluanov, A. and Gorbunova, V. (2014). Regulation of Rad51 promoter. *Cell Cycle*, *13*: 2038–2045.

Holland, S., J., Pan, A., Franci, C., Hu, Y., Chang, B., Li, W., Duan, M., Torneros, A., Yu, J., Heckrodt, T., Zhang, J., J., Ding, P., Apatira, A., Chua, J., Brandt, R., Pine, P., Goff, D., Singh, R., Payan, D., G. and Hitoshi, Y. (2010). R428, a selective small molecule inhibitor of Axl kinase, blocks tumor spread and prolongs survival in models of metastatic breast cancer. *Cancer Res, 70*(4).

Hou, J., Wang, D., Zhang, R. and Wang, H. (2008). Experimental Therapy of Hepatoma with Artemisinin and its Derivatives: *In Vitro* and *In Vivo* Activity, Chemosensitization, and Mechanisms of Action. *Clin. Cancer Res.*, *14* (17): 5519–5530. doi:10.1158/1078-0432.CCR-08-0197

Huang, J., S., Cho, C., H., Hong, C., C., Yan, M., D., Hsieh, M., C., Lay, J., D., Lai, G., M., Cheng, A., L. and Chuang, S., E. (2013). Oxidative stress enhances Axl-mediated cell migration through an Akt1/Rac1-dependent mechanism. *Free Radic. Biol. Med., 65*:1246-1256. doi: 10.1016/j.freeradbiomed.2013.09.011.

Huang, X., J., Li, L., Jiang, H., Jiang, K., Jin, Y. and Zheng, J. (2008). Dihydroartemisinin potentiates the cytotoxic effect of temozolomide in rat C6 glioma cells. *Pharmacology*, *82*(1): 1–9.

Huang, Z., Gan, S., Zhuang, X., Chen, Y., Lu, Y., Wang, Y., Qi, X., Feng, Q., Huang, Q. et al., (2022). Artesunate Inhibits the Cell Growth in Colorectal Cancer by Promoting

ROS-Dependent Cell Senescence and Autophagy. *Cells*, *11*: 2472. doi:10.3390/cells11162472.

Hugo, H., J., Pereira, L., Suryadinata, R., Drabsch, Y., Gonda, T., J., Gunasinghe, D., Pinto, C., Soo, E., T., L., van Denderen, B., J., W., Hill, P., Ramsay, R., G., Sarcevic, B., Newgreen, D., F. and Thompson, E., W. (2013). Direct repression of MYB by ZEB1 suppresses proliferation and epithelial gene expression during epithelial-to-mesenchymal transition of breast cancer cells. *Breast Cancer Research, 15*(R113)

Hur, G., C., Cho, S., J., Kim, C., H., Kim, M., K., Bae, S., I., Nam, S., Y., Park, J., W., Kim, W., H. and Lee, B., L. (2003). Manganese superoxide dismutase expression correlates with chemosensitivity in human gastric cancer cell lines. *Clin. Cancer Res., 9*(15): 5768-75.

Ifergan, I., Scheffer, G., L., Assaraf, Y., G. Novel extracellular vesicles mediate an ABCG2-dependent anticancer drug sequestration and resistance. *Cancer Res., 65*(23):10952-8. doi: 10.1158/0008-5472.CAN-05-2021.

Jamalzadeh, L., Ghafoori, H., Aghamaali,, M. and Sariri, R. (2017). Induction of Apoptosis in Human Breast Cancer MCF-7 Cells by a Semi-Synthetic Derivative of Artemisinin: A Caspase-Related Mechanism. *J. Biotechnol., 15*(3): 157–165. doi: 10.15171/ijb.1567.

Janicke, R., U., Sprengart, M., L., Wati, M., R. and Porter, A., G. (1998). Caspase-3 is required for DNA fragmentation and morphological changes associated with apoptosis. *J. Biol. Chem. 273*: 9357-9360.

Jardim, B., V., Moschetta, M., G., Leonel, C., Gelaleti, G., B., Regiani, V., R., Ferreira, L., C., Lopes, J. R., Pires, D., A. and de Campos Z. (2013). Glutathione and glutathione peroxidase expression in breast cancer: an immunohistochemical and molecular study. *Oncol Rep., 30*(3): 1119-28. doi: 10.3892/or.2013.2540.

Jeddi, F., Soozangar, N., Sadeghi, M., R., et al. Nrf2 overexpression is associated with P-glycoprotein upregulation in gastric cancer. *Biomed Pharmacother*., *97*: 286- 292.

Jeon, J., Y., Buelow, D., R., Garrison, D., A., Niu, M., Eisenmann, E., D. et al. (2020). TP-0903 is active in models of drug-resistant acute myeloid leukemia. *JCI Insight., 5*(23). https://doi.org/10.1172/jci.insight.140169.

Jiang, H., Wei, H., Wang, H., Wang, Z., Li, J., Ou, Y., Xiao, X., Wang, W., Chang, W., Sun, W., Zhao, L. and Yang, S. (2022). Zeb1-induced metabolic reprogramming of glycolysis is essential for macrophage polarization in breast cancer. *Cell Death and Disease, 13*(206).

Jiao, L., Li, D., Yang, C., Peng, R., Guo, Y., Zhang, X. and Zhu, X. (2016). Reactive oxygen species mediate oxaliplatin-induced epithelial-mesenchymal transition and invasive potential in colon cancer. *Tumour Biol.*, *37*(6): 8413-23. doi: 10.1007/s13277-015-4736-9.

Jin, G., Wang, Z., Wang, J., Zhang, L., Chen, Y., Yuan, P., Liu, D. (2016). Expression of Axl and its prognostic significance in human breast cancer. *Oncology Letters, 13*(2): 621-628;

Kalen, A., L., Wagner, B., A., Sarsour, E., H., Kumar, M., G., Reedy, J., L., Buettner, G., R., Barua, N., C. and Goswami, P., C. (2020). Hydrogen Peroxide Mediates Artemisinin-Derived C-16 Carba-Dimer-Induced Toxicity of Human Cancer Cells. *Antioxidants, 9*(2): 108.

Kaplan, H., G, Malmgren, J., A. (2008). Impact of triple negative phenotype on breast cancer prognosis. *Breast J., 14*: 456–463. doi: 10.1111/j.1524-4741.2008.00622.x.

Karihtala, P, Auvinen, P, Kauppila, S, Haapasaari, K., M, Jukkola-Vuorinen, A. and Soini, Y. (2013). Vimentin, zeb1 and Sip1 are up-regulated in triple-negative and basal-like breast cancers: association with an aggressive tumour phenotype. *Breast Cancer Res. Treat.*, *138*:81–90.

Kashiwagi, S., Yashiro, M., Takashima, T., Aomatsu, N., Ikeda, K., Ogawa, Y. et al. (2011). Advantages of adjuvant chemotherapy for patients with triple-negative breast cancer at Stage II: usefulness of prognostic markers E-cadherin and Ki67. *Breast Cancer Res.*, *13*(6): R122.

Katsura, A., Tamura, Y., Hokari, S., Harada, M., Morikawa, M., Sakurai, T., Takahashi, K., Mizutani, A., Nishida, J., Yokoyama, Y. et al. (2017). ZEB1-regulated inflammatory phenotype in breast cancer cells. *Mol. Oncol., 11*: 1241–62.

Kattan, Z., Minig, V., Leroy, P., Dauça, M. and Becuwe, P. (2008). Role of manganese superoxide dismutase on growth and invasive properties of human estrogen-independent breast cancer cells. Breast Cancer Res. Treat., 108(2):203-15. doi: 10.1007/s10549-007-9597-5.

Kaufmann, T., Strasser, A. and Jost, P., J. (2012). Fas death receptor signalling: roles of bid and XIAP. *Cell Death Differ.*, *19*: 42-50

Kepinska, M., Kizek, R. and Milnerowicz, H. (2018). Metallothionein and Superoxide Dismutase—Antioxidative Protein Status in Fullerene-Doxorubicin Delivery to MCF-7 Human Breast Cancer Cells. *Int J Mol Sci.*, *19*(10): 3253. doi: 10.3390/ijms19103253.

Khanzode, S., S., Muddeshwar, M., G., Khanzode, S., D. and Dakhale, G., N. (2004). Antioxidant Enzymes and Lipid Peroxidation in Different Stages of Breast Cancer. *Free Radical Research, 38*(1): 81-85

Khatib, A., Solaimuthu, B., Yosef, M., B., Rmaileh, A., A., Tanna, M., Oren, G., Frisch, M., S., Axelrod, J., H., Lichtenstein, M. and Shaul, Y., D. (2020). The glutathione peroxidase 8 (GPX8)/IL-6/STAT3 axis is essential in maintaining an aggressive breast cancer phenotype, *PNAS, 117*(35): 21420–21431. doi:10.1073/pnas.2010275117.

.

Kim, A., C., J., Yu, D., Kwon, Y., Lee, K., S., Sim, S., H., Kong, S., Y., Lee, E., S., Park, I., H. and Park, C. (2020). Genomic characteristics of Triple-Negative Breast Cancer nominate molecular subtypes that predict chemotherapy response. *Mol. Cancer Res., 18*: 253–63.

Kim, J., H., Cho, E., J., Kim, S., T. and Youn, H., D. (2005). CtBP represses p300-mediated transcriptional activation by direct association with its bromodomain. *Nat. Struct. Mol. Biol., 12*:423–8.

Klein, H., L. (2008) The consequences of Rad51 overexpression for normal and tumor cells. *DNA Repair (Amst.)*, *7*: 686–693.

Kobayashi, H., Takemura, Y. and Ohnuma, T. (1992). Relationship between tumor cell density and drug concentration and the cytotoxic effects of doxorubicin or vincristine: mechanism of inoculum effects. *Cancer Chemotherapy and Pharmacology, 31*: 6–10. doi: 10.1007/BF00695987.

Kumagai, Y., Oishi, J., Nakamura, M., Foulks, J., M., Whatcott, C., J., Warner, S., L., David, J., Bearss, D., J. and Goto, M. (2019). TP-0903, a potent AXL receptor tyrosine kinase inhibitor, enhances the activity of anti-PD-1 therapy in a metastatic preclinical syngeneic model of breast cancer. *Immunology, 79*:13.

Kumar, A., P., Loo, S., H., Shin, S., W., Tan, T., Z., Eng, C., B., Singh, R., Putti, T., C., Ong, C., W., Tellez, M., S., Goh, B., C., Park, J., I., Thiery, J., P., Pervaiz, S. and Clement, M., V. (2014). Manganese Superoxide Dismutase Is a Promising Target for Enhancing Chemosensitivity of Basal-Like Breast Carcinoma. *Antioxid. Redox Signal., 20*(15): 2326–2346. doi: 10.1089/ars.2013.5295.

Kumari, K. Keshari, S., Sengupta, D., Sabat, S., C. and Mishra, S., K. (2017) Transcriptome analysis of genes associated with breast cancer cell motility in response to Artemisinin treatment. *BMC Cancer, 17*: 858. doi: 10.1186/s12885-017-3863-7

Kundu, N., Zhang, S. and Fulton, A., M. (1995). Sublethal oxidative stress inhibits tumor cell adhesion and enhances experimental metastasis of murine mammary carcinoma. *Clin Exp Metastasis., 13*(1): 16–22.

Lai, H and Singh, N., P. (1995) Selective cancer cell cytotoxicity from exposure to dihydroartemisinin and holotransferrin. *Cancer Letters., 91*(1): 41–46.

Lander, H., M., Hajjar, D., P., Hempstead, B., L., Mirza, U., A., Chait, B., T., Campbell, S. and Quilliam, L., A. (1997). A molecular redox switch on p21(ras). Structural basis for the nitric oxide-p21(ras) interaction. *J Biol Chem., 272*(7): 4323–6.

Lauter, M., Weber, A. and Torka, R. (2019). Targeting of the AXL receptor tyrosine kinase by small molecule inhibitor leads to AXL cell surface accumulation by impairing the ubiquitin-dependent receptor degradation. *Cell Communication and Signaling*, 17:59.

Leconet, W., Chentouf, M., Du Manoir, S., Chevalier, C, Sirvent, A., Ait-Arsa, I., Busson, M., Jarlier, M., Radosevic-Robin, N., Theillet, C., Chalbos, D., Pasquet, J., M., Pelegrin, A., Larbouret, C. and Robert, B. (2017). Therapeutic activity of anti-AXL antibody against triple-negative breast cancer patient-derived xenografts and metastasis, *Clinical Cancer Research*, *23*(11): 2806–2816.

Lee, S., Y., Ju, M., K., Jeon, H., M., Lee, Y., J., Kim, C., H., Park, H., G., Han, S., Y. and Kang, H., S. (2019). Reactive oxygen species induce epithelial-mesenchymal transition, glycolytic switch, and mitochondrial repression through the Dlx-2/Snail signaling pathways in MCF-7 cells. *Mol Med Rep., 20*(3): 2339-2346. doi: 10.3892/mmr.2019.10466.

Lee, W., P., Liao, Y., Robinson, D., Kung, H., J., Liu, E., T. and Hung, M., C. (1999). Axl-gas6 interaction counteracts E1A-mediated cell growth suppression and pro apoptotic activity. *Mol. Cell. Biol., 19*:8075–82.

Li, L., N., Zhang, H., D., Yuan, S., J., Yang, D., X., Wang, L. and Sun, Z., X. (2008). Differential sensitivity of colorectal cancer cell lines to artesunate is associated with expression of beta-catenin and E-cadherin. *European Journal of Pharmacology, 588*(1): 1–8.

Lijuan W. (2010). Effect of artesunate on human endometrial carcinoma. *Journal of Medical Colleges of PLA, 25*(3): 143–151.

Liou, G., Y. and Storz, P. (2010). Reactive oxygen species in cancer. *Free Radic. Res., 44*(5): 10.3109/10715761003667554.

Liu, X., Zou, H., Slaughter, C. and Wang. (1997). DFF, a heterodimeric protein that functions downstream of caspase-3 to trigger DNA fragmentation during apoptosis. *Cell, 89*: 175-184

Liu, Y., Lok, C., N., Ko, B., C., Shum, T., Y., Wong, M., K. and Che, C., M. (2010). Subcellular localization of a fluorescent artemisinin derivative to endoplasmic reticulum. *Organic Letters,* 12(7): 1420–1423

Llorens, M., C., Lorenzatti, G., Cavallo, N., L., Vaglienti, M., V., Perrone, A., P., Carenbauer, A., L., Darling, D., S. and Cabanillas, A., M. (2016). Phosphorylation regulates functions of ZEB1 transcription factor. *J. Cell Physiol., 231*: 2205–17.

Lo, Y., Y. and Cruz, T., F. (1995). Involvement of reactive oxygen species in cytokine and growth factor induction of c-fos expression in chondrocytes. *J Biol Chem., 270* (20):11727–30.

Loo, S., Y., Hirpara, J., L., Pandey, V., Tan, T., Z., Yap, C., T., Lobie, P., E., Thiery, J., P., Goh, B., C., Pervaiz, S., Clément, M., V. and Kumar, A., P. (2016). Manganese Superoxide Dismutase Expression Regulates the Switch Between an Epithelial and a Mesenchymal-Like Phenotype in Breast Carcinoma. *Antioxidants and Redox Signaling, 25*(6). doi:10.1089/ars.2015.6524.

Lu, M., Jolly, M., K., Levine, H., Onuchic, J., N. and Ben-Jacob, E. (2013). MicroRNA-based regulation of epithelial-hybrid-mesenchymal fate determination. *Proc. Natl. Acad. Sci., 110*: 18144–9.

Luanpitpong, S., Poohadsuan, J., Samart, P, Kiratipaiboon, C., Rojanasakul, Y. and Issaragrisil, S. (2018). Reactive oxygen species mediate cancer stem-like cells and determine bortezomib sensitivity via Mcl-1 and Zeb-1 in mantle cell lymphoma. *Molecular Basis of Disease, 1864*(11): 3739-3753. doi:10.1016/j.bbadis.2018.09.010.

Lucibello, M., Adanti, S., Antelmi, E., Dezi, D., Ciafrè, S., Carcangiu, M., L., Zonfrillo, M., Nicotera, G., Sica, L., De Braud, F. and Pierimarchi, P. (2015). Phospho-TCTP as a therapeutic target of dihydroartemisinin for aggressive breast cancer cells. *Oncotarget, 6*(7): 5275–5291. doi: 10.18632/oncotarget.2971

Ludwig, K., F., Du, W., Sorrelle, N., B., Wnuk-Lipinska, K., Topalovski, M., Toombs, J., E., Cruz, V., C., Yabuuchi, S., Rajeshkumar, N., V., Maitra, A., Lorens, J., B. and Brekken, R., A. (2018). Small-molecule inhibition of Axl targets tumor immune suppression and enhances chemotherapy in pancreatic cancer. *Cancer Res; 78*(1).

Luo, H., Zhou, Z., Huang, S., Ma, M., Zhao, M, Tang, L., Quan, Y., Zeng, Y., Su, L., Kim, J. and Zhang, P. (2021). CHFR regulates chemoresistance in triple-negative breast cancer through destabilizing ZEB1. *Cell Death and Disease*, *12*(820).

Ma, Z., Woon, C., Y., N., Liu, C., G., Cheng, J., T., You, M., Sethi, G., Wong, A., L., A., Ho, P., C., L., Zhang, D., Ong, P., Wang, L. and Goh, B., C. (2021). Repurposing Artemisinin and its Derivatives as Anticancer Drugs: A Chance or Challenge? *Front. Pharmacol., 12*. https://doi.org/10.3389/fphar.2021.828856

Maacke, H., Opitz, S., Jost, K., Hamdorf, W., Henning, W., Kruger, S., Feller, A., C., Lopens. A., Diedrich, K., Schwinger, E. and Sturzbecher, H., W. Over-expression of wild-type Rad51 correlates with histological grading of invasive ductal breast cancer. *Int J Cancer, 88*(6): 907–913.

Mahmood, Z. and Shukla, Y. (2010). Death receptors: targets for cancer therapy. *Exp. Cell Res., 316:* 887-899

Malhotra, J., D., Miao, H., Zhang, K., Wolfson, A., Pennathur, S., Pipe, S., W. and Kaufman, R., J. (2008). Antioxidants reduce endoplasmic reticulum stress and improve protein secretion. *Proc. Natl. Acad. Sci.*, *105*: 18525-18530

Mangelson, R., Peterson, P., Foulks J., M., Matsumura, Y., Mouritsen, L., Whatcott, C., J., Bearss, D., J. and Warner, L., S. (2019). The AXL kinase inhibitor, TP-0903, demonstrates efficacy in preclinical models of colorectal cancer independent of KRAS mutation status. *Experimental and Molecular Therapeutics*, *79*:13.

Mangelson, R., Tyagi, E., Peterson, P., Siddiqui-Jain, A., Whatcott, C., J., Bearss, D., J. and Warner, S., L. (2019). The potent AXL kinase inhibitor, TP-0903, is active in pre-clinical models of EGFR positive non-small cell lung cancer. *Experimental and Molecular Therapeutics*, *79*(13).

Mao, H., Gu, H., Qu, X., Sun, J., Song, B., Gao, W., Liu, J. and Shao, Q. (2013). Involvement of the mitochondrial pathway and Bim/Bcl-2 balance in dihydroartemisinin-induced apoptosis in human breast cancer in vitro. *International journal of molecular medicine, 31*: 213-218, 2013. doi: 10.3892/ijmm.2012.1176

Marchetti, M., Resnick, L., Gamliel, E., Kesaraju, S., Weissbach, H. and Binninger, D. (2009). Sulindac enhances the killing of cancer cells exposed to oxidative stress. *PLoS One.*, *4*(6):e5804.

Marcucci, F. and Rumio, C. (2022). Tumor Cell Glycolysis—At the Crossroad of Epithelial–Mesenchymal Transition and Autophagy. *Cells, 11*(6): 1041.2022. doi: 10.3390/cells11061041.

Marotti, J., D., De Abreu, F., B., Wells, W., A. and Tsongalis, G., J. Triple-Negative Breast Cancer: Next-Generation Sequencing for target identification. (2017). *The American Journal of Pathology, 187*(10): 2133-2138

Masin, M., Vazquez, J., Rossi, S., Groeneveld, S., Samson, N., Schwalie, P., C et al. (2014). GLUT3 is induced during epithelial-mesenchymal transition and promotes tumor cell proliferation in non-small cell lung cancer. *Cancer and Metabolism*, *2*(11).

Maturi, V., Enroth, S., Heldin, C., H. and Moustakas, A. (2018). Genome–wide binding of transcription factor ZEB1 in triple-negative breast cancer cells. *J. Cell. Physiol., 233*(10): 7113–7127.doi: 10.1002/jcp.26634

McCloskey, P., Fridell, Y., W., Attar, E., Villa, J., Jin, Y., Varnum, B. and Liu, E., T. (1997). GAS6 mediates adhesion of cells expressing the receptor tyrosine kinase Axl. *J. Biol. Chem.,272*:23285–91.11.

McCubrey, J., A., Steelman, L., S., Chappell, W., H., Abrams, S., L., Wong, E., W., T., Chang, F., Lehmann, B., Terrian, D., M., Milella, M., Tafuri, A., Stivala, F., Libra, M., Basecke, J., Evangelisti, C., Martelli, A., M. and Franklin, R., A. (2007). Roles of the Raf/MEK/ERK pathway in cell growth, malignant transformation and drug resistance. *Biochim Biophys Acta., 1773*(8): 1263–84.

McLean, L., Soto, U., Agama, K., Francis, J., Jimenez, R., Pommier, Y., Sowers, L. and Brantley, E. (2008). Aminoflavone induces oxidative DNA damage and reactive oxidative species-mediated apoptosis in breast cancer cells. *Int J Cancer., 122*(7): 1665–74.

Mercer, A., E., Copple, I., M., Maggs, J., L., O'Neill, P., M. and Park, B., K. (2011). The role of heme and the mitochondrion in the chemical and molecular mechanisms of mammalian cell death induced by the artemisinin antimalarials. *Journal of Biological Chemistry*, *283*(2): 987–996.

Meyer, A., S., Miller, M., A., Gertler, F., B. and Lauffenburger, D., A. (2013). The receptor AXL diversifies EGFR signaling and limits the response to EGFR-targeted inhibitors in triple-negative breast cancer cells. *Sci. Signal., 6*(287).

Mi, Y., Geng, G., Zou, Z., Gao, J., Luo, X., Liu, Y., Li, N., Li, C., Chen, Y., Yu, X. and Jiang, J. (2015). Dihydroartemisinin inhibits glucose uptake and cooperates with glycolysis inhibitor to induce apoptosis in non-small cell lung carcinoma cells. *PLoS One*, *10*(3):e0120426. doi: 10.1371/journal.pone.0120426.

Michaelis, M., Kleinschmidt, M. C., Barth, S., Rothweiler, F., Geiler, J., Breitling, R., Mayer, B., Deubzer, H., Witt, O., Kreuter, J., et al. (2010). Anti-cancer effects of artesunate in a

panel of chemoresistant neuroblastoma cell lines. *Biochemical Pharmacology*, *79*(2): 130–136.

Minamoto, T., Mai, M. and Ronai, Z. (2000). K-ras mutation: early detection in molecular diagnosis and risk assessment of colorectal, pancreas, and lung cancers--a review. *Cancer Detect Prev., 24*(1): 1–12.

Mokhtari, R., B., Homayouni, T., S., Baluch, N., Morgatskaya, E., Kumar, S., Das, B. and Yeger, H. Combination therapy in combating cancer. (2017). *Oncotarget, 8*(23), 38022–38043. *Mol. Cancer Res.; 15*(1), 45–58.

Morel, A., Ginestier, C., Pommier, R., Cabaud, O., Ruiz, E., Wicinski, J., Devouassoux-Shisheboran, M., Combaret, M, Finetti, P., Chassot, C., Pinatel, C., Fauvet, F. et al. (2017). A stemness-related ZEB1-MSRB3 axis governs cellular pliancy and breast cancer genome stability. *Nat Med.*, *23*(5): 568-578. doi: 10.1038/nm.4323.

Mu, D., Chen, W., Yu, B., Zhang, C., Zhang, Y. and Qi, H. (2007). Calcium and survivin are involved in the induction of apoptosis by dihydroartemisinin in human lung cancer SPC-A-1 cells. *Methods and Findings in Experimental and Clinical Pharmacology*, *29*(1): 33–38.

Mudduluru, G, Ceppi, P., Kumarswamy, R., Scagliotti, G., V., Papotti, M. and Allgayer, H. (2011). Regulation of Axl receptor tyrosine kinase expression by miR-34a and miR-199a/b in solid cancer. *Oncogene*, *30:* 2888–99.

Netsvetai, S., Parfenyev, O., Fedorova, O., Shuvalov, A., Daks, N. and Barlev, N. (2021). The influence of ZEB1 transcription factor on the resistance to genotoxic

drugs during the epithelialmesenchymal transition *P08.272 S.*

Nieman, M., T., Prudoff, R., S., Johnson, K., R. and Wheelock, M., J. (1999) N-Cadherin Promotes Motility in Human Breast Cancer Cells Regardless of their E-Cadherin Expression. *The Journal of Cell Biology, 147*(3): 631–643.

Oien, D., B., Garay, T., Eckstein, S. and Chien, J. (2018). Chemotherapy drug-induced AXL activation and cell survival signaling via reactive oxygen species that can be inhibited to enhance drug efficacy in mesothelioma. *Cancer Res., 78* (13): 2448. doi:10.1158/1538-7445.AM2018-2448.

Orrenius, S., Gogvadze, V. and Zhivotovsky, B. (2015). Calcium and mitochondria in the regulation of cell death. Biochem. *Biophys. Res. Commun., 460*: 72-81.

Osada, S., Osada, S., Sakashita, F., Hosono, Y., Nonaka, K., Tokuyama, Y., Tanaka, H., Sasaki, Y., Tomita, H., Komori, S., Matsui, S. and Takahashi, T. (2008). Extracellular signal-regulated kinase phosphorylation due to menadione-induced arylation mediates

growth inhibition of pancreas cancer cells. *Cancer Chemother. Pharmacol., 62*(2): 315–20.

Ostrakhovitch, E., A and Cherian, M., G. (2005). Inhibition of extracellular signal regulated kinase (ERK) leads to apoptosis inducing factor (AIF) mediated apoptosis in epithelial breast cancer cells: the lack of effect of ERK in p53 mediated copper induced apoptosis. *J. Cell. Biochem., 95*(6): 1120–34.

Paccez, J., D., Vogelsang, M., Parker, M., I. and Zerbini, L., F. (2014). The receptor tyrosine kinase Axl in cancer: Biological functions and therapeutic implications. *Int. J. Cancer, 134:* 1024–1033.

Palisoul, M., L., Quinn, J., M., Schepers, E., Hagemann, I., S., Guo, L., Reger, K., Hagemann, A., R., McCourt, C., K., Thaker, P., H., Powell, M., A., Mutch, D., G. and Fuh, K., C. (2017). Inhibition of the receptor tyrosine kinase AXL restores paclitaxel chemosensitivity in uterine serous cancer. *Mol. Cancer Ther., 16*(12): 2881-2891. doi: 10.1158/1535-7163.

Pallepati, P. and Averill-Bates, D., A. (2011). Activation of ER stress and apoptosis by hydrogen peroxide in HeLa cells: protective role of mild heat preconditioning at 40 degrees C. *Biochim. Biophys. Acta, 1813*: 1987-1999

Panossian, L. A., Garga, N., I. and Pelletier, D. (2005). Toxic brain-stem encephalopathy after artemisinin treatment for breast cancer. *Annals of Neurology*, *58*(5): 812–813.

Park, I,. K., Mundy-Bosse, B., Whitman, S., P., Zhang, X., Warner, S., L., Bearss, D., J., Blum, W., Marcucci, G. and Caligiuri, M., A. (2015). Receptor tyrosine kinase Axl is required for resistance of leukemic cells to FLT3-targeted therapy in acute myeloid leukemia. *Leukemia*, *29*(12), 2382–2389

Parkash, J., Felty, Q. and Roy, D. (2006). Estrogen exerts a spatial and temporal influence on reactive oxygen species generation that precedes calcium uptake in high-capacity mitochondria: implications for rapid nongenomic signaling of cell growth. *Biochemistry, 45*(9): 2872–81.

Perry, R., R., Mazetta, B., S., J., Levin B., S., M. and Barranco, S., C. (1993). Glutathione levels and variability in breast tumors and normal tissue. *Cancer, 72*(3). doi:10.1002/1097-0142(19930801)72:3.

Pinilla, R., S., M., Sarrio, D., Honrado, E., Bueno, M., G., Hardisson, D., Calero, F., Benítez, J. and Palacios, J. (2007). Vimentin and laminin expression is associated with basal-like phenotype in both sporadic and BRCA1-associated breast carcinomas. *J Clin Pathol., 60*: 1006–1012. doi: 10.1136/jcp.2006.042143.

Porter, A., G. and Ja, R., U. (1999). Emerging roles of caspase-3 in apoptosis. *Cell Death and Differentiation, 6*, 99-104.

Postigo, A. A., Depp, J. L., Taylor, J. J., and Kroll, K. L. (2003). Regulation of smad signaling through a differential recruitment of coactivators and corepressors by ZEB proteins. *EMBO J.,22*:2453–2462. doi: 10.1093/emboj/cdg226.

Prakash, R., Zhang, Y., Feng, W. and Jasin, M. (2015). Homologous recombination and human health: the roles of BRCA1, BRCA2, and associated proteins. *Cold Spring Harb. Perspect. Biol.*, *7:*a016600.

Preca, B., T., Bajdak, K., Mock, K., Lehmann, W., Sundararajan, V., Bronsert, P., Matzge-Ogi, A., Orian-Rousseau, V., Brabletz, S., Brabletz, T., et al. (2017). A novel ZEB1/HAS2 positive feedback loop promotes EMT in breast cancer. *Oncotarget*, *8*: 11530–43.

Preca, B., T., Bajdak, K., Mock, K., Sundararajan, V., Pfannstiel, J., Maurer, J., Wellner, U., Hopt, U., T., Brummer, T., Brabletz, S., et al. (2015). A self-enforcing CD44s/ZEB1 feedback loop maintains EMT and stemness properties in cancer cells. *Int. J. Cancer*, *137*: 2566–77.

Prodhomme, M., K., Pommier, R., M., Franchet, C., Fauvet, F., Bergoglio, V., Brousset, P., Morel, A., P., Brunac, A., C., Shisheboran, M., D., Petrilli, V., Lalle, C., M., Hoffmann, J., S., Puisieux, A. and Tissier, A. (2021). EMT Transcription Factor ZEB1 Represses the Mutagenic POLθ-Mediated End-Joining Pathway in Breast Cancers. *Cancer Res., 81*(6): 1595–1606. doi:10.1158/0008-5472.CAN-20-2626

Radisky, D., C., Levy, D., D., Littlepage, L., E., Liu, H., Nelson, C., M., Fata, J., E., Leake, D., Godden, E., L., Albertson, D., G., Nieto, M., A, Werb, Z. and Bissell, M., J. (2005). Rac1b and reactive oxygen species mediate MMP-3-induced EMT and genomic instability. *Nature. 436*(7047):123–7.

Rakha, E., A., El Rehim, D., A. Pinder, S., E., Lewis, S., A. and Ellis, I., O. (2005). E-cadherin expression in invasive non-lobular carcinoma of the breast and its prognostic significance. *Histopathology*, *46*(6):685-93. doi: 10.1111/j.1365-2559.2005.02156.x.

Rasheed, S., A., K., Efferth, T., Asangani, I., A. and Allgayer, H. (2010). First evidence that the antimalarial drug artesunate inhibits invasion and *In vivo* metastasis in lung cancer by targeting essential extracellular proteases. *International Journal of Cancer, 127*(6):1475–1485.

Reddy, K., B. and Glaros, S. (2007). Inhibition of the MAP kinase activity suppresses estrogen-induced breast tumor growth both in vitro and in vivo. *Int. J. Oncol., 30*(4): 971–5.

Redza, M., Diana, D. and Bates, D. A., A. (2016). Activation of apoptosis signalling pathways by reactive oxygen species. *Biochimica et Biophysica Acta, 1863*(12): 2977-2992.

Reizenstein, P., 1991. Iron, free radicals and cancer. Med. Oncol. Tumor. Pharmacother. 8, 229–233

Reungpatthanaphong, P. and Mankhetkorn, S. (2002). Modulation of multidrug resistance by artemisinin, artesunate and dihydroartemisinin in K562/adr and GLC4/adr resistant cell lines. *Biological and Pharmaceutical Bulletin, 25*(12): 1555–1561.

Richard, G., Dalle, S., Monet, M., A., Ligier, M., Boespflug, A., Pommier, R., M. et al. (2016). ZEB1-mediated melanoma cell plasticity enhances resistance to MAPK inhibitors. *EMBO Mol. Med. 8,* 1143–1161. 10.15252/emmm.201505971;

Richardson, C. (2005). RAD51, genomic stability, and tumorigenesis. *Cancer Lett., 218*: 127–139.

Riehl, B., D., Kim, E., Lee, J., S., Duan, B., Yang, R., Donahue, H., J. and Lim, J., Y. (2020). The Role of Fluid Shear and Metastatic Potential in Breast Cancer Cell Migration. *J. Biomech. Eng. 142*(10): 101001; doi: 10.1115/1.4047076

Roh, J., L., Kim, E., H., Jang, H. and Shin, D. (2017). Nrf2 inhibition reverses the resistance of cisplatin-resistant head and neck cancer cells to artesunate-induced ferroptosis. *Redox Biology, 11*: 254-262

Rosenzweig, S., A. (2018). Acquired resistance to drugs targeting tyrosine kinases. *Adv. Cancer Res. 83*(8), 1041-8. https://doi:10.1016/bs.acr.2018.02.003

Rudel, T. and Bokoch, G., M. (1997). Membrane and morphological changes in apoptotic cells regulated by caspase-mediated activation of PAK2. *Science, 276*: 1571-1574

Russo, M., Mupo, A., Spagnuolo, C. and Russo, G., L. (2010). Exploring death receptor pathways as selective targets in cancer therapy. *Biochem. Pharmacol., 80*: 674-682

Sadahiro, H., Kang, K., D., Gibson, J., T., Minata, M., Yu, H., Shi, J., Chhipa, R., Chen, Z., Lu, S., Simoni, Y., Furuta, T., Sabit, H., Zhang, S., Bastola, S., Yamaguchi, S., Alsheikh, H., Komarova, S., Wang, J., Kim, S., H., Hambardzumyan, D., Lu, X., Newell, E., W., DasGupta, B., Nakada, M., Lee, L., J., Nabors, B., Norian, L., A. and Nakano, I. (2018). Activation of the receptor tyrosine kinase AXL regulates the immune microenvironment in glioblastoma. *Cancer Research, 78*(11): 3002–3013.

Sadeghi, M., R., Jeddi, F., Soozangar, N., et al. (2018). Nrf2/P-glycoprotein axis is associated with clinicopathological characteristics in colorectal cancer. *Biomed Pharmacother*., *104*: 458- 464.

Sakata, J., Utsumi, F., Suzuki, S., Niimi, K., Yamamoto, E., Shibata, K., et al. (2017). Inhibition of ZEB1 leads to inversion of metastatic characteristics and restoration of paclitaxel sensitivity of chronic chemoresistant ovarian carcinoma cells. *Oncotarget*, *8:* 99482–99494. doi: 10.18632/oncotarget.20107

Sakemura, R., Yang, N., Cox, M., Sinha, S., Hefazi, M., Hansen, M., Schick, K., Boysen, J., Mouritsen, L., Foulks, J., Warner, S., Parikh, S., Ding, W., Kay, N. and Kenderian, S. (2018). AXL-RTK inhibition directs the functional phenotype of chimeric antigen receptor T cells. *Blood*, *132*(1): 728.

Salomoni, P. and Khelifi, A., F. (2006) Daxx: death or survival protein? *Trends Cell Biol*., *16:* 97-104

Sanchez-Tillo, E., de Barrios O., Siles, L., Cuatrecasas, M., Castells, A. and Postigo, A. (2011). beta-catenin/TCF4 complex induces the epithelial-to-mesenchymal transition (EMT)-activator ZEB1 to regulate tumor invasiveness. *Proc. Natl. Acad. Sci., 108*: 19204–9.

Sano, R. and Reed, J., C. (2013). ER stress-induced cell death mechanisms. *Biochim. Biophys. Acta, 1833*: 3460-3470

Schmuck, G., Roehrdanz, E., Haynes, R., K. and Kahl, R. (2002). Neurotoxic mode of action of artemisinin. *Antimicrobial Agents and Chemotherapy, 46*(3): 821–827.

Segal, A., W. and Shatwell, K., P. (1997). The NADPH oxidase of phagocytic leukocytes. *Ann N Y Acad Sci., 832*: 215–22.

Sen, T., Tong, P., Diao, L., Li, L, Fan, Y., Hoff, J., Heymach, J., V., Wang, J. and Byers. L., A. (2017). Targeting AXL and mTOR Pathway Overcomes Primary and Acquired Resistance to WEE1 Inhibition in Small-Cell Lung Cancer. *Clin. Cancer Res., 23*(20): 6239–6253.doi: 10.1158/1078-0432.CCR-17-1284.

Sertel, S., Eichhornb, T., Sieber, S., Sauer, A., Weiss, J., Plinkert, P., K. and Efferth, T. (2010). Factors determining sensitivity or resistance of tumor cell lines towards artesunate. *Chemico-Biological Interactions*, *185*: 42–52

Shankar, S., L., O'Guin, K., Kim, M., Varnum, B., Lemke, G., Brosnan, C., F. and Zagardo, B., S. (2006). Gas6/Axl signaling activates the phosphatidylinositol 3-kinase/Akt1 survival pathway to protect oligodendrocytes from tumor necrosis factorα-induced

apoptosis. *Journal of Neuroscience,* *26*(21), 5638-5648. https://doi:10.1523/JNEUROSCI.5063-05.2006

Shedden, K., Xie, X., T., Chandaroy, P., Chang, Y., T. and Rosania, G., R. (2003). Expulsion of small molecules in vesicles shed by cancer cells: Association with gene expression and chemosensitivity profiles. *Cancer Res., 63*: 4331–4337.

Singh, N., P. and Verma, K., B. (2002). Case report of a laryngeal squamous cell carcinoma treated with artesunate. *Archive of Oncology*, *10*(4): 279–280.

Sinha, S., Boysen, J., Nelson, M., Secreto, C., Warner, S., L., Bearss, D., J., Lesnick, C., Shanafelt, T., D., Kay, N., E. and Ghosh, A., K. (2015). Axl Inhibition Primes Chronic Lymphocytic Leukemia B-Cells to Apoptosis and Show Synergistic/Additive Effects in Combination with BTK inhibitors. *Clin. Cancer Res.*, *21*(9): 2115–2126.

Soh, K., K., Kim, W., Lee, Y., S., Peterson, P., Jain, A., S., Warner, S., L., Bearss, D., J. and Whatcott, C., J. (2016). AXL inhibition leads to a reversal of a mesenchymal phenotype sensitizing cancer cells to targeted agents and immuno-oncology therapies. *Cancer Res., 76*(14): 235. doi:10.1158/1538-7445.AM2016-235.

Stockwin, L. H, Han, B., Yu, S., X., et al. (2009) Artemisinin dimer anticancer activity correlates with heme-catalyzed reactive oxygen species generation and endoplasmic reticulum stress induction. *International Journal of Cancer, 125*(6): 1266–1275.

Storz, P. (2005). Reactive oxygen species in tumor progression. *Front Biosci.*, *10* :1881–96.

Su, L., J., Zhang, J., H., Gomez, H., Murugan, R., Hong, X., Xu, D., Jiang, F. and Peng, Z., Y. (2019). Reactive Oxygen Species-Induced Lipid Peroxidation in Apoptosis, Autophagy, and Ferroptosis. *Oxid. Med. Cell. Longev., 2019*: 5080843; doi: 10.1155/2019/5080843

Sundar, S., N., Marconett, C., N., Doan, V., B., Willoughby, J., A., S. and Firestone, G., L. (2008). Artemisinin selectively decreases functional levels of estrogen receptor-alpha and ablates estrogen-induced proliferation in human breast cancer cells. *Carcinogenesis, 29*(12), 2252-8.

Sundaresan, M., Yu, Z., X., Ferrans, V., J., Irani, K. and Finkel, T. (1995). Requirement for generation of H2O2 for platelet-derived growth factor signal transduction. *Science, 270*(5234): 296–9.

Takaku, M., Kainuma, T., Ishida-Takaku, T., Ishigami, S., Suzuki, H., Tashiro, S., van Soest, R., W., M., Nakao, Y. and Kurumizaka, H. (2011). Halenaquinone, a chemical compound that specifically inhibits the secondary DNA binding of RAD51. *Genes Cells.*, *16*: 427–436.

Tan, E. J., Kahata, K. , Idås, O. , Thuault, S. , Heldin, C.-H. , & Moustakas, A. (2015). The high mobility group A2 protein epigenetically silences the Cdh1 gene during epithelial-to-mesenchymal transition. *Nucleic Acids Research*, 43, 162–178.

Taverna, J., A. , Hung, C., N. , DeArmond, D., T. , Chen, M., Lin, C., L., Osmulski, P., A., Gaczynska, M., E., Wang, C., M., Lucio, N., D., Chou, C., W., Chen, C., L., Nazarullah, A., Lampkin, S., R., Qiu, L., Bearss, D.,J., Warner, S. et al. (2020). Single-Cell Proteomic Profiling Identifies Combined AXL and JAK1 Inhibition as a Novel Therapeutic Strategy for Lung Cancer. *Cancer Res.*, *80*(7):1551-1563. doi: 10.1158/0008-5472.CAN-19-3183.

Thompson, E., W., Paik, S., Brünner, N., Sommers, C., L., Zugmaier, G., Clarke, R., Shima, T., B., Torri, J., Donahue, S., Lippman, M., E., Martin, G., R., Dickson, R., B. (1992). Association of increased basement membrane invasiveness with absence of estrogen receptor and expression of vimentin in human breast cancer cell lines. *Journal of Cellular Physiology, 150*(3).

Thuraia, A., A., Gauthier, R., Chidiac, R., Fukui, Y., Screaton, R., A., Gratton, J., P. and Côté, J., F. (2015). Axl Phosphorylates Elmo Scaffold Proteins To Promote Rac Activation and Cell Invasion. *Mol. Cell. Biol., 35*(1): 76–87. doi: 10.1128/MCB.00764-14

Tilló, E. S., Fanlo, L., Siles, L., Moreno, S., M., Moros, A., Blanch, G., C., Estruch, R., Martinez, A., Colomer, D., Győrffy, B., Roué, G. and Postigo, A. (2014). The EMT activator ZEB1 promotes tumor growth and determines differential response to chemotherapy in mantle cell lymphoma. *Cell Death and Differentiation, 21*: 247–257.

Tin, A., S., Sundar, S., N., Kalvin, Q., Tran, K., Q., Park, A., P., Poindexter, K., M. and Firestone, G., L. (2012). Antiproliferative effects of artemisinin on human breast cancer cells requires the downregulated expression of the E2F1 transcription factor and loss of E2F1-target cell cycle genes. *Anticancer Drugs*, *23*(4):370-9.

Tobar, N, Cáceres, M., Santibáñez, J., F., Smith, P., C. and Martínez, J. (2008). RAC1 activity and intracellular ROS modulate the migratory potential of MCF-7 cells through a NADPH oxidase and NFkappaB-dependent mechanism. *Cancer Lett., 267*(1):125–32.

Tomimatsu, N., Fujimura, K., Matsumura, Y., Umehara, H., Mouritsen, L., Warner, S., L. and Bearss, D., J. (2019). Targeting AXL kinase with TP-0903 successfully reverses the mesenchymal phenotype and extends survival in preclinical models of advanced ovarian cancer. *Tumor Biology, 79*(13).

Tomková, V., Sandoval-Acuña, C., Torrealba, N. and Truksa, J. (2019). Mitochondrial fragmentation, elevated mitochondrial superoxide and respiratory supercomplexes

disassembly is connected with the tamoxifen-resistant phenotype of breast cancer cells. *Free Radic. Biol. Med., 143*: 510-521. doi: 10.1016/j.freeradbiomed.2019.09.004.

Trebinska-Stryjewska, A., Swiech, O., Opuchlik, L. J., Grzybowska, E. and Bilewicz, R. (2020). Impact of Medium pH on DOX Toxicity toward HeLa and A498 Cell Lines. *ACS Omega*, *14*; 5(14): 7979–7986; doi: 10.1021/acsomega.9b04479

Truong P., T., Yong C., M., Abnousi, F., Lee, J., Kader, H., A., Hayashi, A. and Olivotto, I., A. Lymphovascular invasion is associated with reduced locoregional control and survival in women with node-negative breast cancer treated with mastectomy and systemic therapy. (2005). *J Am Coll Surg., 200*(6):912-21. doi: 10.1016/j.jamcollsurg.2005.02.010.

Turchick, A., Hegan, D., C., Jensen, R., B. and Glazer, P., M. (2017). A cell-penetrating antibody inhibits human RAD51 via direct binding. *Nucleic Acids Res., 45*: 11782–11799

Turchick, A., Liu, Y., Zhao, W., Cohen, I. and Glazer, P., M. (2019). Synthetic lethality of a cell-penetrating anti-RAD51 antibody in PTEN-deficient melanoma and glioma cells. *Oncotarget, 10*:1272–1283.

Vandewalle, C., Van Roy, F. and Berx, G. (2009). The role of the ZEB family of transcription factors in development and disease. *Cell Mol. Life Sci. ,66*:773–787. doi: 10.1007/s00018-008-8465-8

Vendrell, J., A., Thollet, A., Nguyen, N., T., Ghayad, S., E., Vinot, S., Bieche, I., Grisard, E., Josserand, V., Coll, J., L., Roux, P., et al. (2012). ZNF217 is a marker of poor prognosis in breast cancer that drives epithelial-mesenchymal transition and invasion. *Cancer Res., 72*:3593–606.

von Hagens, C., Walter-Sack, I., Goeckenjan, M., Osburg, J., Storch-Hagenlocher, B., Sertel, S., et al. (2017). Prospective Open Uncontrolled Phase I Study to Define a Well-Tolerated Dose of Oral Artesunate as Add-On Therapy in Patients with Metastatic Breast Cancer (ARTIC M33/2). *Breast Cancer Res. Treat. 164*(2), 359–369. doi:10.1007/s10549-017-4261-1

Vuoriluoto, K., Haugen, H., Kiviluoto, S., Mpindi, J., P., Nevo, J., Gjerdrum, C., Tiron, C., Lorens, J., B. and Ivaska, J. (2011). Vimentin regulates EMT induction by Slug and oncogenic H-Ras and migration by governing Axl expression in breast cancer. *Oncogene, 30*: 1436–48.

Wang, C., Jin, H, Wang, N., Fan, S, Wang, Y., Zhang, Y., Wei, L., Tao, X., Gu, D., Zhao, F., Fang, J., Yao, M. and Wenxin, Q., W. (2016). Gas6/Axl axis contributes to

chemoresistance and metastasis in breast cancer through Akt/GSK-3β/β-catenin signaling. *Theranostics, 6*(8): 1205–19.

Wang, J., S., Wang, M., J., Lu, X., Zhang, J., Liu, Q., X., Zhou, D., Dai, J., G. and Zheng. H. (2020). Artesunate inhibits epithelial-mesenchymal transition in non-small-cell lung cancer (NSCLC) cells by down-regulating the expression of BTBD7. *Bioengineered, 11*(1): 1197–1207. doi: 10.1080/21655979.2020.1834727.

Wang, J., Zhang, J., Shi, Y., Xu, C., Zhang, C., Wong, Y., K., Lee, Y.,M., Krishna, S., Yingke, He, Y., Kwang, L., T., K., Sim, W., Hua, Z., C., Shen, H., M. and Lin, Q. (2017). Mechanistic investigation of the specific anticancer property of artemisinin and its combination with aminolevulinic acid for enhanced anticolorectal cancer activity. *ACS Cent. Sci., 3*: 743−750.

Wang, M., He, S., F., Liu, L., L., Sun, X., X., Yang, F., Ge, Q., Wong, W., K. and Meng, J., Y. (2017). Potential role of ZEB1 as a DNA repair regulator in colorectal cancer cells revealed by cancer-associated promoter profiling. *Oncolgy Reports*, *38*(4): 1941-1948. https://doi.org/10.3892/or.2017.5888

Wang, M., Kirk, J., S., Venkataraman, S., Domann, F., E., Zhang, H., J., Schafer, F., Q., Flanagan, S., W., Weydert, C., J., Spitz, D., R., Buettner, G., R. and Oberley, L., W. (2005). Manganese superoxide dismutase suppresses hypoxic induction of hypoxia-inducible factor-1alpha and vascular endothelial growth factor. *Oncogene, 24*(55): 8154-66. doi: 10.1038/sj.onc.1208986.

Wang, N., Zeng, G., Z., Yin, J., L. and Bi, Z., X. (2019). Artesunate activates the ATF4-CHOP-CHAC1 pathway and affects ferroptosis in Burkitt's Lymphoma. *Biochemical and Biophysical Research Communications, 519*(3): 533-539. Doi:10.1016/j.bbrc.2019.09.023.

Wang, S., J., Sun, B., Cheng, Z., X., Zhou, H., X., Gao, Y., Kong, R., Chen, H., Jiang, H., C., Pan, S., H., Xue, D., B. and Bai, X., W. (2011). Dihydroartemisinin inhibits angiogenesis in pancreatic cancer by targeting the NF-κB pathway. *Cancer Chemother Pharmacol.*, *68*(6): 1421-30. doi: 10.1007/s00280-011-1643-7.

Wang, X., Saso, H., Iwamoto, T., Xia, W., Gong, Y., Pusztai, L., Woodward, W., A., Reuben, J., M., Warner, S., L., Bearss, D., J., Hortobagyi, G., N., Hung, M., C. and Ueno, N., T. (2013). TIG1 promotes the development and progression of inflammatory breast cancer through activation of Axl kinase. *Cancer Research*, *73*(21): 6516–6525.

Weifeng, T., Feng, S., Xiangji, L., Changqing, S., Zhiquan, Q., Huazhong, Z., Peining, Y., Yong, Y., Mengchao, W, Xiaoqing, J. and Yee, L., W. (2011). Artemisinin inhibits in

vitro and in vivo invasion and metastasis of human hepatocellular carcinoma cells. *Phytomedicine, 18*(2-3): 158-62. doi: 10.1016/j.phymed.2010.07.003.

Welsh, J., W., Mahadevan, D., Ellsworth, R., Cooke, L., Bearss, D. and Stea, B. (2009). The c-Met receptor tyrosine kinase inhibitor MP470 radiosensitizes glioblastoma cells. *Radiat. Oncol. 4*:69.

West, J., D. and Marnett, L., J. (2006). Endogenous reactive intermediates as modulators of cell signaling and cell death. *Chem. Res. Toxicol., 19*: 173-194

Weydert, C., J., Waugh, T., A., Ritchie, J., M., Iyerc, K., S., Smith, J., S., Li, L., Spitz, D., R. and Oberley, L., W. (2006). Overexpression of manganese or copper–zinc superoxide dismutase inhibits breast cancer growth. *Free Radical Biology and Medicine, 41*(2): 226-237.

Weydert, C., J., Zhang, Y., Sun, W., Waugh, T., A., Teoh, M., L., T., Andringa, K., K., Burns, N., A., Spitz, D., R., Smith, B., J. and Oberley, L., W. (2008). Increased oxidative stress created by adenoviral MnSOD or CuZnSOD plus BCNU (1,3-bis(2-chloroethyl)-1-nitrosourea) inhibits breast cancer cell growth. *Free Radical Biology and Medicine, 44*(5): 856-867.

WHO. *WHO,* Guidelines for the Treatment of Malaria (2006).

Wiegmans, A., P., Al-Ejeh, F., Chee, N., Yap, P., Y, Gorski, J., J., Da Silva, L., Bolderson, E., Trench, G., C., Anderson, R., Simpson, P., T., Lakhani, S., R. and Khanna, K. (2014). Rad51 supports triple negative breast cancer metastasis. *Oncotarget, 5*(10): 3261–3272.

Wilson, C., Ye, X., Pham, T., Lin, E., Chan, S., McNamara, E., Neve, R., M., Belmont, L., Koeppen, H., Yauch, R., L., Ashkenazi, A. and Settleman, J. (2014). AXL inhibition sensitizes mesenchymal cancer cells to antimitotic drugs. *Cancer Res., 74*(20): 5878-90. doi: 10.1158/0008-5472.CAN-14-1009.

Woo, M., Hakem, R., Soengas, M., S., Duncan, G., S., Shahinian, A., Ka, D., Hakem, A., McCurrach, M., Khoo, W., Kaufman, S., A., Senaldi, G., Howard, T., Lowe, S., W and Mak, T., W. (1998). Essential contribution of caspase-3/CPP32 to apoptosis and its associated nuclear changes. *Genes Dev., 12*: 806-819

Wu, H., T., Zhong, H., T., Li, G., W. Shen, J., X., Ye, Q., Q., Zhang, M., L. and Liu, J. (2020). Oncogenic functions of the EMT-related transcription factor ZEB1 in breast cancer. *Journal of Translational Medicine*, *18*(51).

Xu, Q., Li, Z., Peng, H., Sun, Z., Cheng, R., Ye, Z. and Li, W. (2011). Artesunate inhibits growth and induces apoptosis in human osteosarcoma HOS cell line In vitro and In vivo. *Biomedicine and Biotechnology*, *12*(4): 247–255.

Yamashita, N., Tokunaga, E., Kitao, H., Tanaka, K., Taketani, K., Aishima, H., S., S., Oki, E., Morita, M. and Maehara, Y. (2013). Significance of the vimentin expression in triple-negative breast cancer. *Journal of Clinical Oncology, 31*(15). doi: 10.1200/jco.2013.31.15_suppl.1056.

Yao, Y., Guo, Q., Cao, Y., Qiu, Y., Tan, R., Yu, Z., Zhou, Y. and Lu, N. (2018). Artemisinin derivatives inactivate cancer-associated fibroblasts through suppressing TGF-β signaling in breast cancer. *Journal of Experimental and Clinical Cancer Research*, 37(282).

Yata, K., Lloyd, J., Maslen, S., Bleuyard, J., Y., Skehel, M., Smerdon, S., J. and Esashi, F. (2012). Plk1 and CK2 act in concert to regulate Rad51 during DNA double strand break repair. *Mol. Cell.*, *45*: 371–383.

Yin, L., Duan, J., J., Bian, X., W. and Yu, S., C. (2020). Triple-negative breast cancer molecular subtyping and treatment progress. *Breast Cancer Research, 22*(61)

Youns, M., Efferth, T., Reichling, J., Fellenberg, K., Bauer, A. and Hoheisel, J., D. (2009). Gene expression profiling identifies novel key players involved in the cytotoxic effect of Artesunate on pancreatic cancer cells. *Biochemical Pharmacology*, *78*(3): 273–283.

Zeeshan, H., M., Lee, G., H., Kim, H., R. and Chae, H., J. (2016). Endoplasmic reticulum stress and associated ROS. *Int. J. Mol. Sci., 17*: 327-347

Zhang, J, Tian, X., J., Zhang, H., Teng, Y., Li, R., Bai, F., Elankumaran, S. and Xing, J. (2014). TGF-beta-induced epithelial-to-mesenchymal transition proceeds through stepwise activation of multiple feedback loops. *Sci Signal.*, *7*: ra91.

Zhang, P, Luo, H., Li, M. and Tan, S. (2015). Artesunate inhibits the growth and induces apoptosis of human gastric cancer cells by downregulating COX-2. *Onco Targets Ther*, *8:* 845-54. doi: 10.2147/OTT.S81041.

Zhang, P., Sun, Y., and Ma, L. (2015). ZEB1: at the crossroads of epithelial-mesenchymal transition, metastasis and therapy resistance. *Cell Cycle*, 14: 481–487. doi: 10.1080/15384101.2015.1006048

Zhang, P., Wei,Y., Wang, L., Debeb, B., G., Yuan, Y., Zhang, J., Yuan, J., Wang, M., Chen, D., Sun, Y., Woodward, W., A., Liu, Y., Dean, D., C., Liang, H., Hu, Y., Ang, K., K., Hung, M., C., Chen, J. and Ma. L. (2014). ATM-mediated stabilization of ZEB1

promotes DNA damage response and radioresistance through CHK1. *Nat Cell Biol.,* *16*(9): 864-75. doi: 10.1038/ncb3013.

Zhang, X., Zhang, Z., Zhang, Q., Sun, P., Xiang, R., Ren, G. and Yang, S. (2018). ZEB1 confers chemotherapeutic resistance to breast cancer by activating ATM. *Cell Death Dis.*, *9*:57.

Zhang, Y., Arner, E., N., Rizvi, A., Toombs, J., E., Huang, H., Warner, S., L., Foulks, J., M. and Brekken, R., A. (2022). AXL inhibitor TP-0903 reduces metastasis and therapy resistance in pancreatic cancer. *Mol. Cancer Ther., 21*(1): 38–47. doi: 10.1158/1535-7163.MCT-21-0293.

Zhang, Z., Yin, J., Lu, C., Wei, Y., Zeng, A. and You, Y. (2019). Exosomal transfer of long non-coding RNA SBF2-AS1 enhances chemoresistance to temozolomide in glioblastoma. *Journal of Experimental and Clinical Cancer Research*, *38*(166).

Zhao, Z., Sun, Y., Chen, W., Lv, L. and Li, Y. (2016). Hispolon inhibits breast cancer cell migration by reversal of epithelial-tomesenchymal transition via suppressing the ROS/ERK/Slug/E-cadherin pathway. *Oncology Reports.*, *35*: 896-904, 2016. doi: 10.3892/or.2015.4445.

Zhou, J., Chen, Y., Lang, J., Y., Lu, J., J. and Ding, J. (2008). Salvicine inactivates beta 1 integrin and inhibits adhesion of MDA-MB-435 cells to fibronectin via reactive oxygen species signaling. *Mol. Cancer Res., 6*(2): 194–204.

Zhou, Y., Zhu, Y., Fan, X., Zhang, C., Wang, Y., Zhang, L., et al. (2017). NID1, a new regulator of EMT required for metastasis and chemoresistance of ovarian cancer cells. *Oncotarget*, *8:* 33110–33121. doi: 10.18632/oncotarget.16145

Zhou, Z., Zhang, P., Hu, X., Kim, J., Yao, F., Xiao, Z., Zeng, L., Chang, L., Sun, Y. and Ma, L. (2017). USP51 promotes deubiquitination and stabilization of ZEB1. *Am. J. Cancer Res.*, *7*:2020–31.

Gastric cancer

Lung cancer
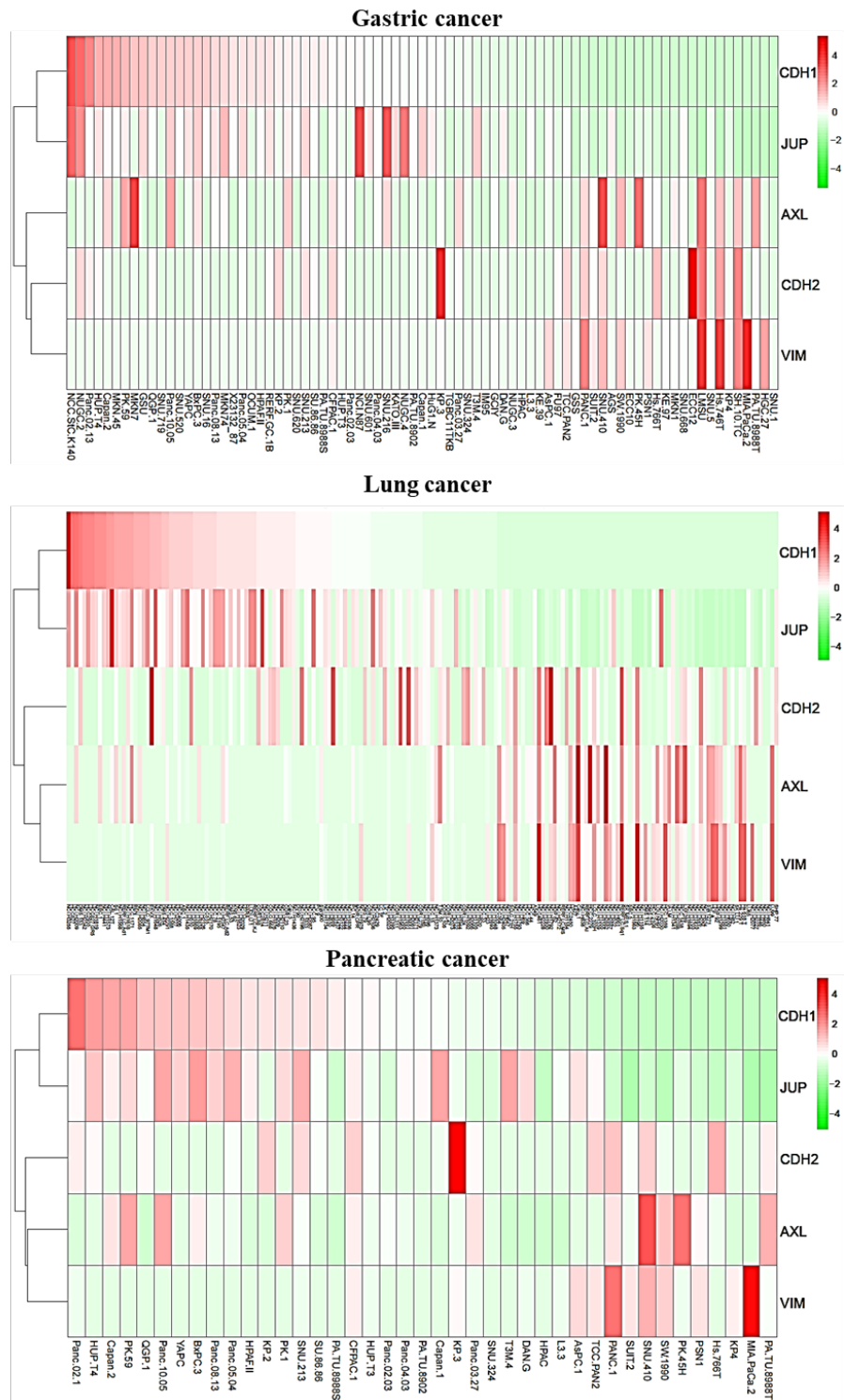
Pancreatic cancer

Supplementary Figure S7A. Heat Map analysis. The relative gene expression of *AXL, CDH1, CDH2, VIM* and *JUP* in gastric, lung and pancreatic cancer cell lines is shown. *AXL* co-clustered with mesenchymal markers. Genes are hierarchical clustered using Euclidean distances. Data was downloaded from in silico experiments conducted in EMBL-EBI database. Data are z-scored.
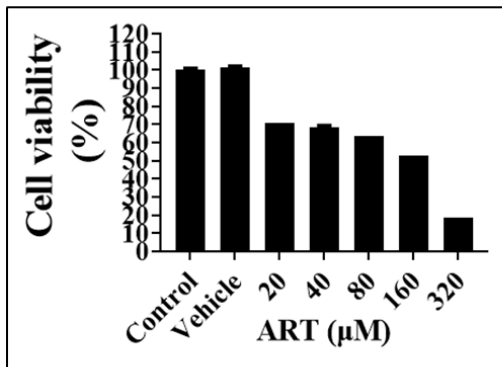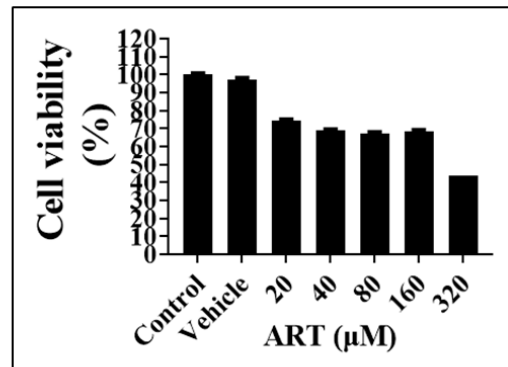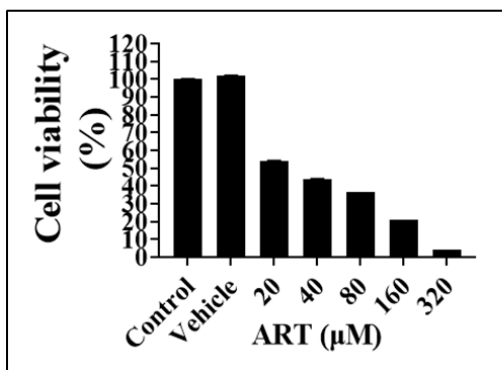
TNBC

BT-549
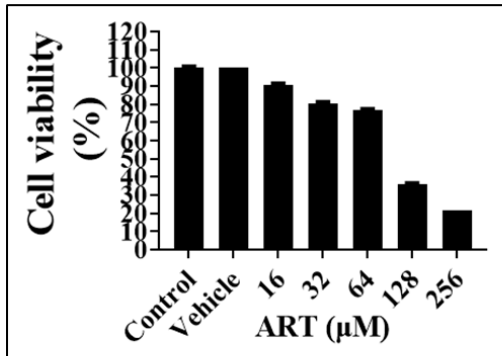
MDA-MB-231
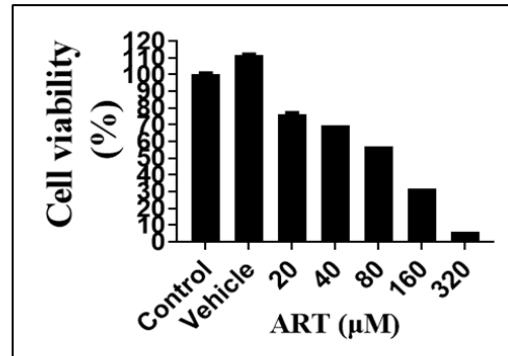
MDA-MB-436

Hs 578-T

NON TNBC

T-47D

MCF-7
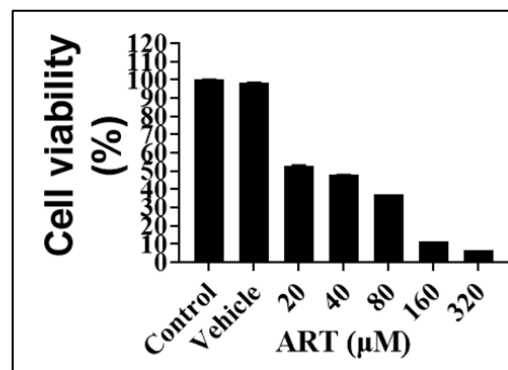
Supplementary Figure S8. MTT results after treatment of TNBC and non TNBC cell lines with ART at different concentrations. The cell viability is shown in a linear scale. TNBC cells were more resistant to ART cytotoxicity.

	MCF-7/ZEB1 (-) Dox	
1	Raw Data{Wavelength:570.0}	
2		1
3	A	2,564
4	B	2,024
5	C	1,975
6	D	1,993
7	E	2,24
8	F	2,802
9	G	0,037
10	H	0,038
11		
12		
13		Control
14		Average
15		2,266333
16		SEM
17		0,140778

	MCF-7/ZEB1 (+) Dox	
1	Raw Data{Wavelength:570.0}	
2		1
3	A	1,586
4	B	1,522
5	C	1,577
6	D	1,524
7	E	1,544
8	F	1,611
9	G	0,037
10	H	0,037
11		
12		Control
13		Average
14		1,560667
15		SEM
16		0,046905

Supplementary Figure S9C. MTT absorbance values of MCF-7/ZEB1 (-) Dox and (+) Dox control cells. MCF-7/ZEB1 (+) Dox cells had lower absorbance values compared to (-) Dox cells indicating a lower proliferation of (+) Dox cells.
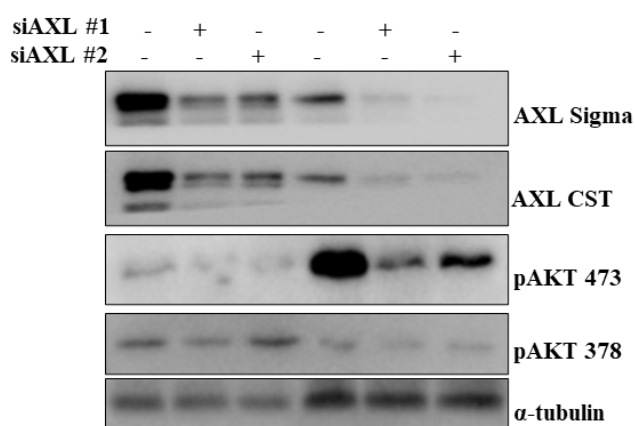
Supplementary Figure S10A/1. AXL and pAKT in TNBC. Removal of AXL by two siRNA AXL decreased protein expression of pAKT 473 in MDA-MB-231 and BT-549 cells. The impact was higher on BT-549 cells. AXL was detected by two different antibodies (from Sigma and Cell Signaling Technology).

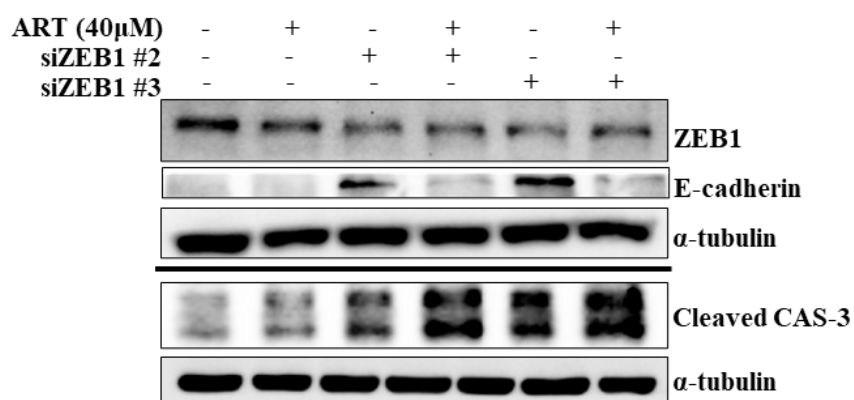| ART (40μM)	-	+	-	+	-	+	-	+	-	-
si AXL	-	-	+	+	-	-	+	+	-	-
si ZEB1 #1	-	-	-	-	+	+	+	+	-	-
Staurosporine	-	-	-	-	-	-	-	-	+	+

ZEB 1

AXL

E-cad

P-cad

Cleaved CAS-3

α-tubulin
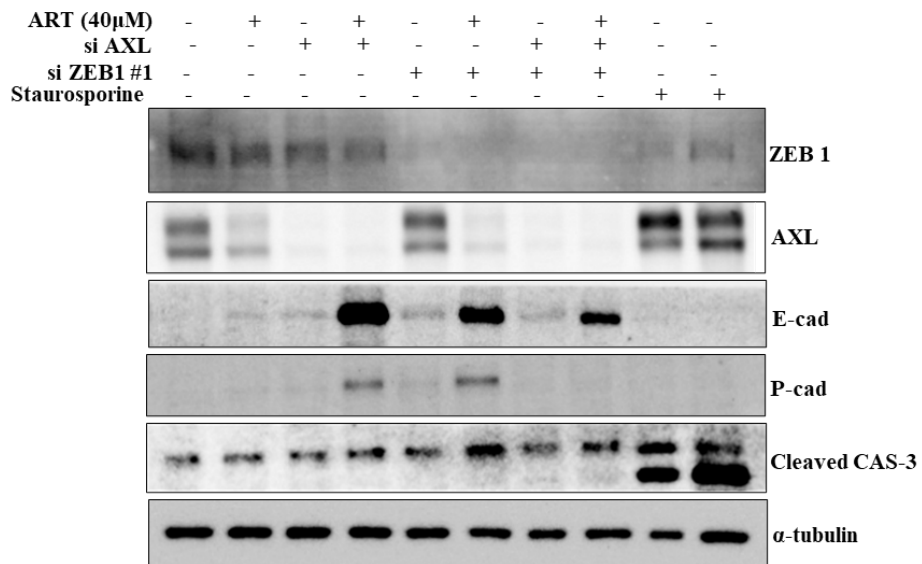
Supplementary Figure S10A/2. Effect on apoptosis after AXL and ZEB1 removal in ART treated cells. MDA-MB-231 cells were treated with ART 40 μM, siRNA AXL and ZEB1 #1 and a combination of siRNA AXL, ZEB1 and ART for 72 h. Western Blot results shows that removal of ZEB1 and not AXL sensitised cells to ART induced cleaved caspase 3. The positive control for apoptosis, that is staurosporine, is included.

ART (40 μM)	-	-	+	-	+	-	+	-	+
siZEB1 #2	-	-	-	+	+	-	-	-	-
siZEB1 #3	-	-	-	-	-	-	-	+	+
Staurosporine	-	+	-	-	-	-	-	-	-

ZEB1

E-cadherin

P-cadherin

Cleaved CAS-3

α-tubulin
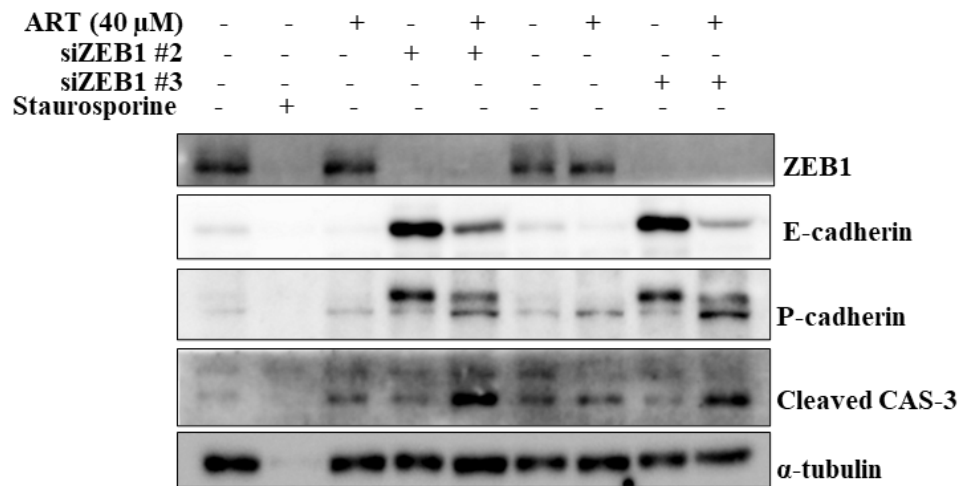
Supplementary Figure S10A/3. Effect on apoptosis after ZEB1 removal in ART treated cells. MDA-MB-231 cells were treated with ART 40 μM, siRNA ZEB1 #2 and #3 and a combination of siRNA ZEB1 and ART for 72 h. Western Blot results shows that removal of ZEB1 increased E-cadherin and P-cadherin and sensitised cells to ART induced cleaved caspase 3.
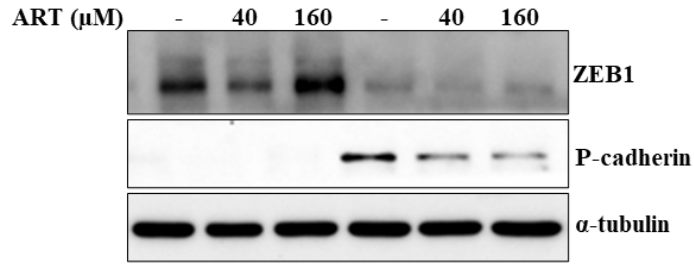
Supplementary Figure S10B/1. ZEB1 and P-cadherin expression in MDA-MB-231/cntrl and shZEB1 cells. In shZEB1 cells, ZEB1 was almost absent while P-cadherin present compared to MDA-MB-231/cntrl cells. ART induced ZEB1.
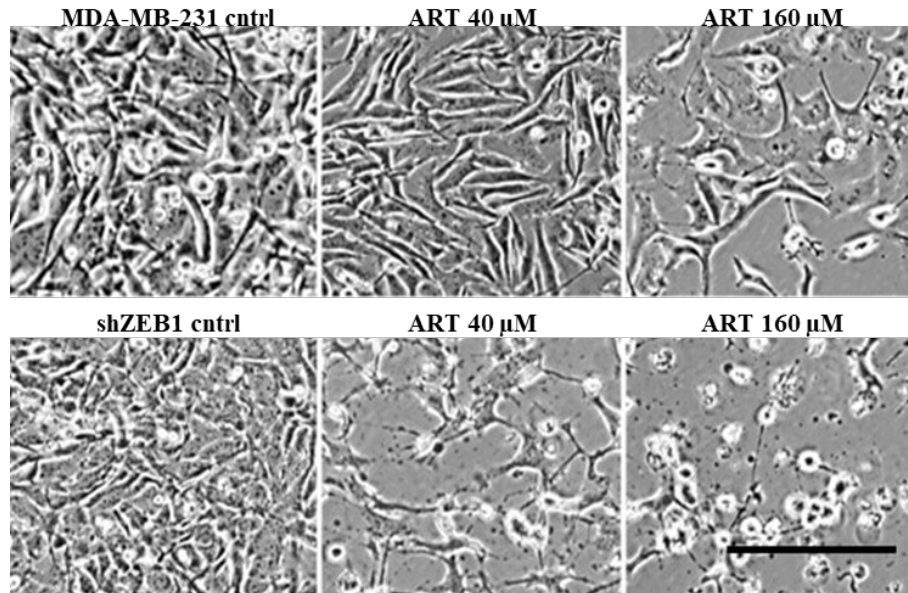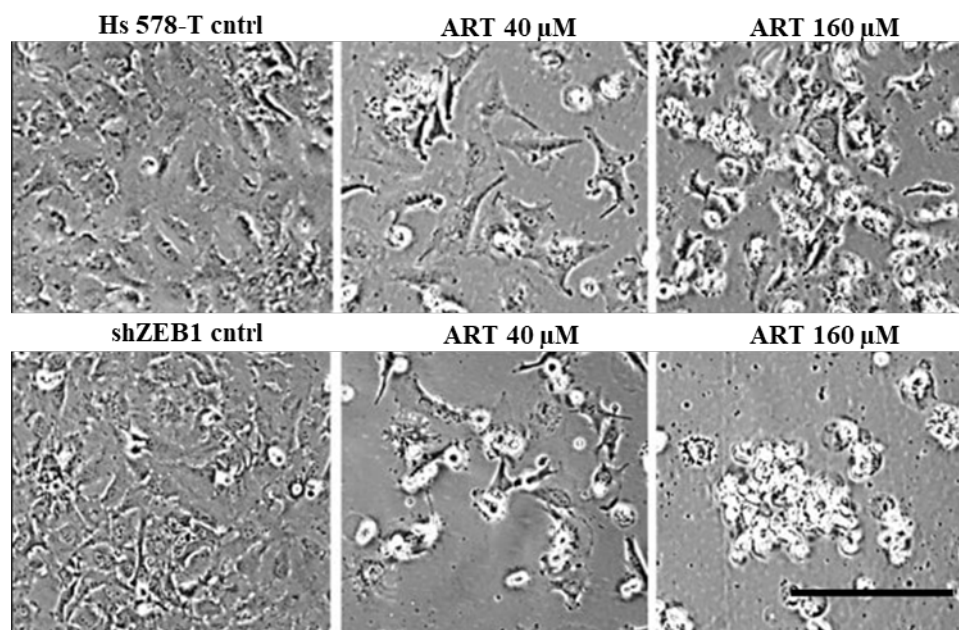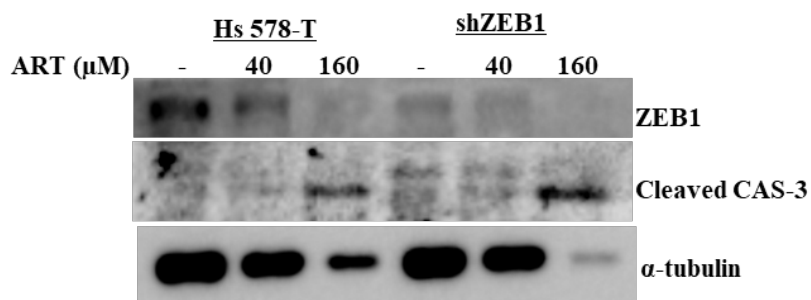

Supplementary Figure S10B/2. ART treatment of MDA-MB-231/cntrl and shZEB1 cells. Phase contrast images show that ART 160 μM for 72 h was more cytotoxic, in terms of cell viability, in shZEB1 cells. The fields of cells shown are a zoom of pictures taken at 10x magnification; scale bar 100 μm.

ART (40µM)	-	+	-	+	-	+
siZEB1 #2	-	-	+	+	-	-
siZEB1 #3	-	-	-	-	+	+

ZEB1

E-cadherin

α-tubulin

Cleaved CAS-3

α-tubulin

Supplementary Figure S10C. Effect on apoptosis after ZEB1 removal in ART treated cells. MDA-MB-2436 cells were treated with ART 40 µM, siRNA ZEB1 #2 and #3 and a combination of siRNA ZEB1 and ART for 72 h. Western Blot results shows that removal of ZEB1 increased E-cadherin and sensitised cells to ART induced cleaved caspase 3. The black line indicates that samples were analysed in two different days (related tubulin is indicated)

| | Hs 578-T | | | shZEB1 | | |
| ART (µM) | - | 40 | 160 | - | 40 | 160 |

ZEB1

α-tubulin
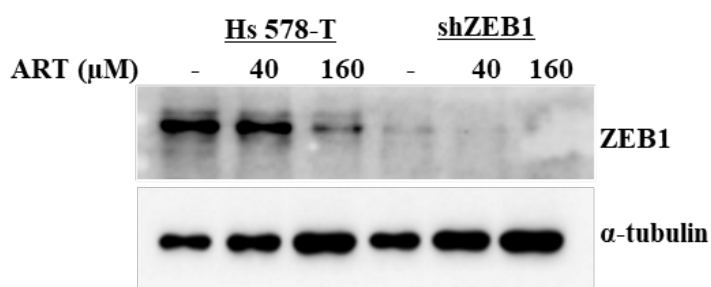
Supplementary Figure S10D/1. ZEB1 expression in Hs 578-T/cntrl and shZEB1 cells. ZEB1 was expressed in Hs 578-T while almost absent in shZEB1 cells. ART suppressed ZEB1.

Supplementary Figure S10D/2. ART treatment in Hs 578-T/cntrl and shZEB1 cells. Phase contrast images show that ART for 72 h was more cytotoxic, in terms of cell viability, in shZEB1 cells compared to Hs-578/cntrl cells. The fields of cells shown are a zoom of pictures taken at 10x magnification; scale bar 100 μm.

Supplementary Figure S10D/3. ART treatment for 72 h in Hs 578-T/cntrl and shZEB1 cells. Western Blot results show that ART induced higher cleaved caspase 3 expression in shZEB1 compared to Hs 578-T/cntrl cells**.**
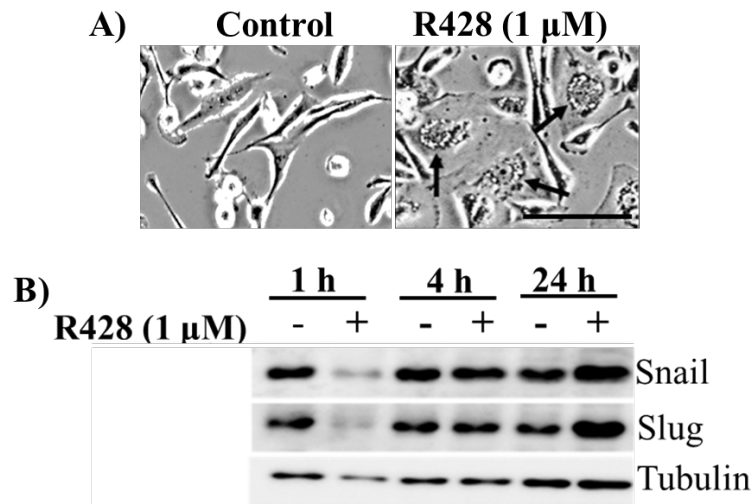
Supplementary Figure S11A/1. A) R428 effect on phenotype. Phase contrast images show that R428 did not change phenotype and induced high intracellular vesiculation (in the arrows) after 24 h in MDA-MB-231 cells. The fields of cells shown are a zoom of pictures taken at 10x magnification; scale bar 100 μm. **B)** Wetsern Blotting. R428 increased Snail and Slug protein expression after 24 h in MDA-MB-231 cells.

Supplementary Figure S11A/2. TP-0903 effect on phenotype. Phase contrast images show that cells lost their mesenchymal phenotype after TP-0903 treatment for 24 h. The fields of cells shown are a zoom of pictures taken at 10x magnification; scale bar 100 μm.

Simultaneous treatment

CI Data for Non-Constant Combo: AT2.5 (A+T)

Dose A	Dose T	Effect	CI
2.5	0.015	0.26631	1.91085
2.5	0.03	0.43044	1.27789
2.5	0.06	0.49427	1.71714
2.5	0.125	0.57120	2.24952
2.5	0.25	0.87795	0.38625
2.5	0.5	0.88941	0.65251
2.5	1.0	0.87234	1.64781
2.5	2.0	0.87141	3.33035

CI Data for Non-Constant Combo: AT5 (A+T)

Dose A	Dose T	Effect	CI
5.0	0.015	0.22703	2.77553
5.0	0.03	0.44985	1.20116
5.0	0.06	0.55156	1.26989
5.0	0.125	0.57821	2.19151
5.0	0.25	0.85784	0.50472
5.0	0.5	0.89876	0.56942
5.0	1.0	0.91373	0.87499
5.0	2.0	0.92167	1.49577

CI Data for Non-Constant Combo: AT 10 (A+T)

Dose A	Dose T	Effect	CI
10.0	0.015	0.31449	1.71215
10.0	0.03	0.44755	1.33850
10.0	0.06	0.52150	1.59756
10.0	0.125	0.59243	2.07665
10.0	0.25	0.82739	0.72077
10.0	0.5	0.83684	1.27703
9.0	1.0	0.88973	1.30630
10.0	2.0	0.90821	1.93158

CI Data for Non-Constant Combo: AT20 (A+T)

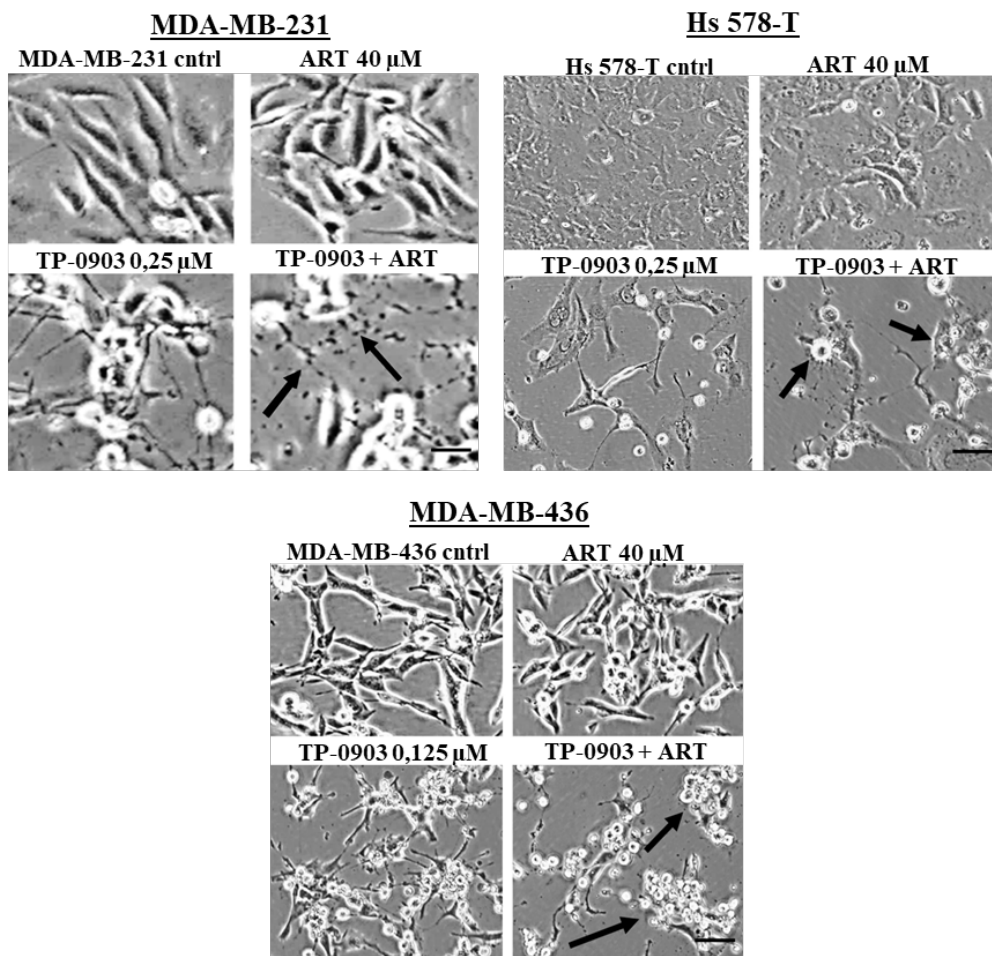| Dose A	Dose T	Effect	CI
20.0	0.015	0.26956	2.89177
20.0	0.03	0.45636	1.50696
20.0	0.06	0.56298	1.40469
20.0	0.125	0.60727	2.01809
20.0	0.25	0.84351	0.63777
20.0	0.5	0.88543	0.72528
20.0	1.0	0.87059	1.72517
20.0	2.0	0.91359	1.76808

Sequential treatment

CI Data for Non-Constant Combo: AT2.5 (A+T)

Dose A	Dose T	Effect	CI
2.5	0.015	0.36785	0.83497
2.5	0.03	0.52184	0.67033
2.5	0.06	0.54260	1.17272
2.5	0.125	0.58557	1.89675
2.5	0.25	0.88752	0.34273
2.5	0.5	0.86290	0.93776
2.5	1.0	0.87690	1.57639
2.5	2.0	0.93193	1.26647

CI Data for Non-Constant Combo: AT5 (A+T)

Dose A	Dose T	Effect	CI
5.0	0.015	0.27130	1.66605
5.0	0.03	0.49698	0.79698
5.0	0.06	0.58146	0.95713
5.0	0.125	0.63698	1.41377
5.0	0.25	0.84721	0.56296
5.0	0.5	0.90225	0.55080
5.0	1.0	0.90297	1.08684
5.0	2.0	0.92204	1.55427

CI Data for Non-Constant Combo: AT10 (A+T)

Dose A	Dose T	Effect	CI
10.0	0.015	0.41052	0.78175
10.0	0.03	0.47389	0.96794
10.0	0.06	0.60318	0.87309
10.0	0.125	0.66180	1.23435
10.0	0.25	0.88367	0.36574
10.0	0.5	0.90650	0.51630
10.0	1.0	0.90212	1.10382
10.0	2.0	0.89299	2.53080

CI Data for Non-Constant Combo: AT20 (A+T)

| Dose A	Dose T	Effect	CI
20.0	0.015	0.37473	1.18330
20.0	0.03	0.59880	0.53687
20.0	0.06	0.62838	0.80200
20.0	0.125	0.64828	1.38577
20.0	0.25	0.91070	0.24629
20.0	0.5	0.91764	0.42860
20.0	1.0	0.92002	0.81350
20.0	2.0	0.93316	1.23666

Supplementary Figure S12A. TP-0903 plus ART synergism in a simultaneous and sequential treatment. A representative Compusyn report after simultaneous/sequential treatment of MDA-MB-231 cells with TP-0903 at 0.015 μM -2 μM plus ART 2.5 μM - 20 μM for 72 h. The cells were pre-treated with TP-0903 for 24 h. The number of CIs values showing synergism was higher in the sequential treatment. Dose A= ART; Dose T= TP-0903; Effect= growth inhibition; CI= Combination Index. CI<1 indicates synergism. Effect and CI were calculated after performing the MTT assay on four technical replicates.

| TP-0903 (1 µM) | - | + | - | - | - | + | + | + |
| ART (µM) | - | - | 1 | 4 | 16 | 1 | 4 | 16 |

Cleaved CAS-3

α-tubulin
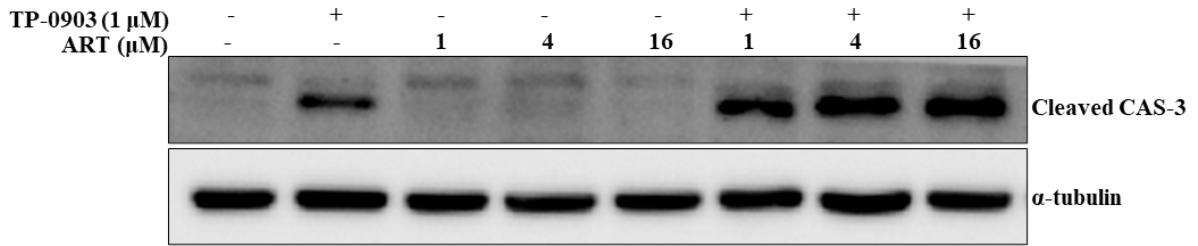
Supplementary Figure S13/1. TP-0903 plus ART effect on apoptosis. Western Blot. MDA-MB-231 cells were treated with TP-0903 at 1 µM, ART 1 µM, 4 µM and 16 µM and a combination of TP-0903 plus ART for 24 h. TP-0903 plus ART synergised to increase cleaved caspase 3 compared to control and drugs alone.
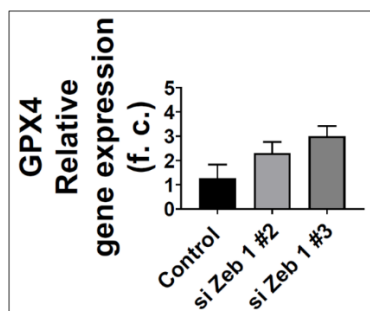

MDA-MB-231

MDA-MB-231 cntrl   ART 40 µM

TP-0903 0,25 µM   TP-0903 + ART

Hs 578-T

Hs 578-T cntrl   ART 40 µM

TP-0903 0,25 µM   TP-0903 + ART

MDA-MB-436

MDA-MB-436 cntrl   ART 40 µM

TP-0903 0,125 µM   TP-0903 + ART

Supplementary Figure S13/2. TP-0903 plus ART effect on TNBC phenotype. Top left) MDA-MB-231 cells were pre-treated with TP-0903 at 0,25 µM and then further treated for 48 h with ART 40 µM, TP-0903 at 0,25 µM and a combination of the two. TP-0903 plus ART rendered cells smaller and with broken protrusions (arrows) compared to TP-0903. Top right and bottom) Hs 578-T and MDA-MB-436 cells were pre-treated and treated as MDA-MB-231 cells. TP-0903 plus ART induced apoptotic bodies (arrows) at higher extent than TP-0903 in both cell lines. The fields of cells shown are a zoom of pictures taken at 10x magnification; scale bar 100 µm.
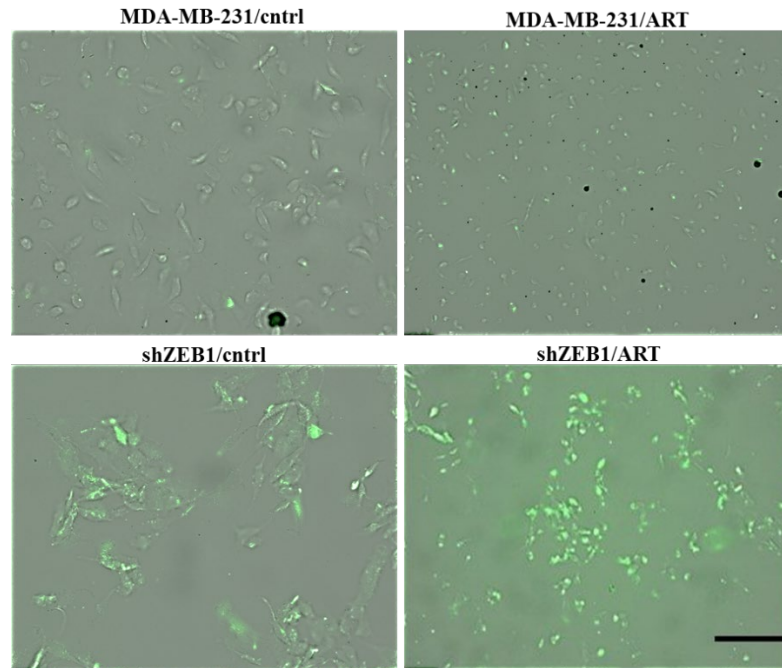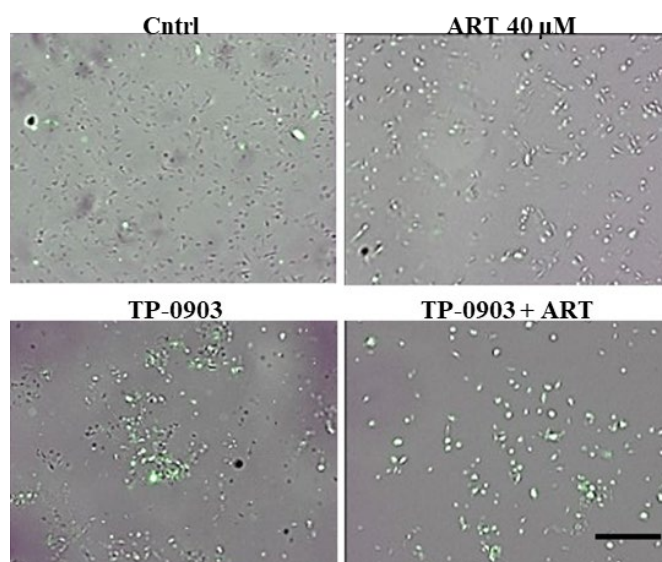
Supplementary Figure S15A/1. Total ROS assay in MDA-MB-231/cntrl and MDA-MB-231/shZEB1 cells treated or not with ART. cells. Merged pictures of the treatments of Fig. 15A. The microscope images were taken at 10x magnification; scale bar 100 μm.
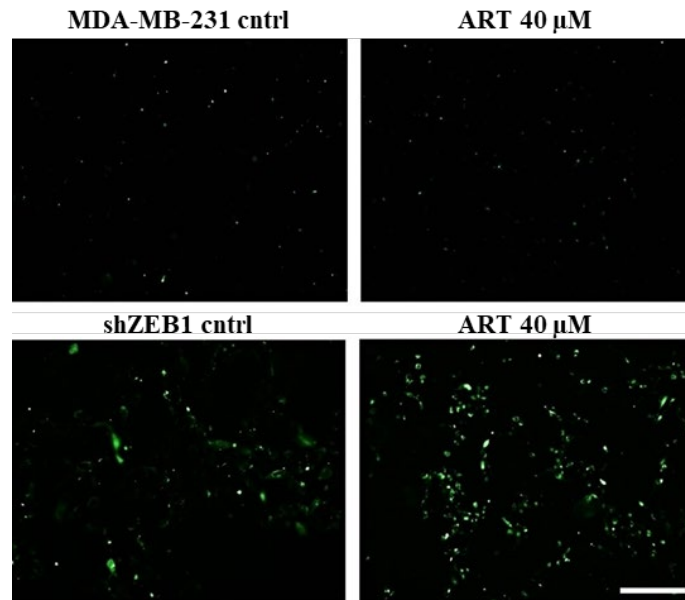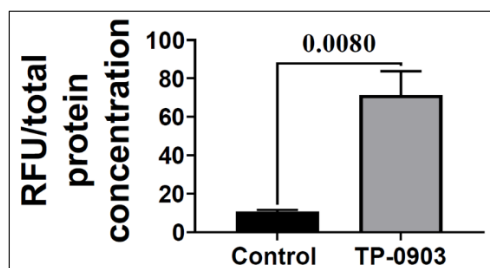

Supplementary Figure S15A/2. Total ROS assay of an addtional field of cells after that MDA-MB-231 and shZEB1 cells were treated with ART. MDA-MB-231 and shZEB1 cells were treated with ART 40 μM for 2 days before doing the CM-DCFH DA test. The fluorescence emitted from the probe was detected by a fluorescent microscopy. Total ROS were higher in shZEB1/cntrl compared to MDA-MB-231/cntrl and in shZEB1/ART compared to MDA-MB-231/ART. The images were taken at 10x magnification; scale bar 100 μm.
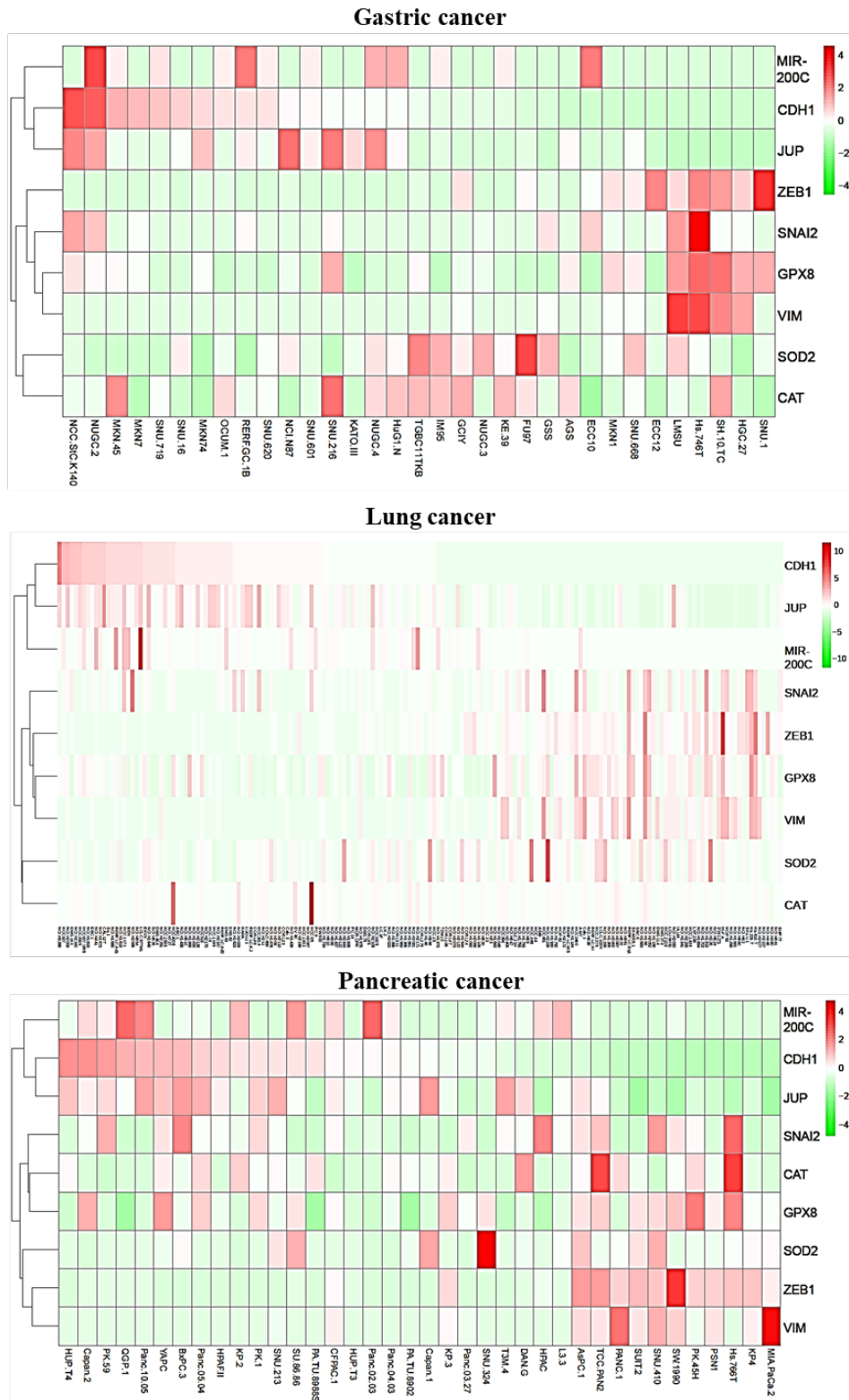
Supplementary Figure S15A/3. qPCR analysis. MDA-MB-231 cells depleted for ZEB1 by siRNA #2 and #3 had increased GPX4 expression compared to control cells. The Dunnett's test was used to check significance between control and treatment groups; significant p-value lower than or equal to 0,05. Results are expressed as mean ± SEM of a technical triplicate.


Supplementary Figure S16A/1. Total ROS assay in MDA-MB-231 cells. Merged pictures of treatments of Fig. 15A. The microscope images were taken at 10x magnification; scale bar 100 μm.


Supplementary Figure S16A/2. TP-0903 significantly increased total ROS levels compared to control cells after comparison of control and TP-0903 in MDA-MB-231 cells. The unpair t-test was performed and significant p-value loer than or equal to 0,05. Results are expressed as mean ± SEM of three different fields taken from the same coverslip.

Supplementary Figure S17. Heat Map analysis. The relative expression of *SOD2, CAT, GPX8, CDH1, JUP, mir 200c, VIM, ZEB1* and *SNAI2* in gastric, lung and pancreatic cell lines is shown. *ZEB1* co-clustered with antioxidant enzymes. Genes are hierarchical clustered using Euclidean distances. Data was downloaded from in silico experiments conducted in EMBL-EBI database. Data are z-scored.

A)
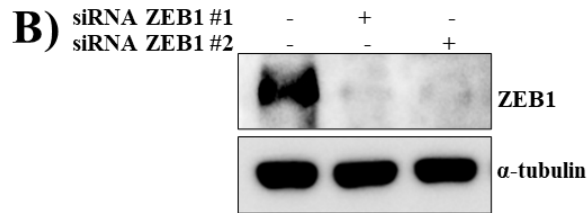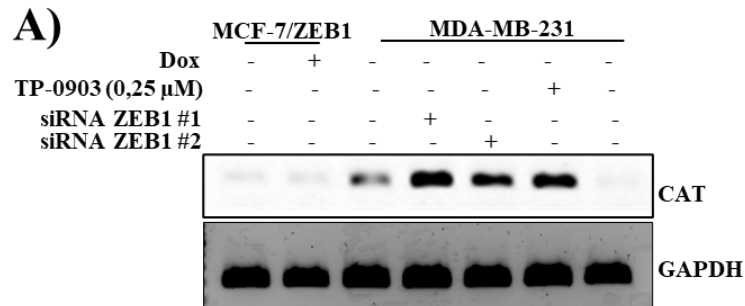
Supplementary Figure S18. Dox, siRNA ZEB1 and TP-0903 effect on *CAT* gene expression. **A)** PCR analysis. Dox treatment did not affect *CAT* in MCF-7/ZEB1 cells while siRNA ZEB1 increased *CAT*. TP-0903 abrogated *CAT* expression. **B)** Efficiency of siRNA ZEB1 in MDA-MB-231 cells.
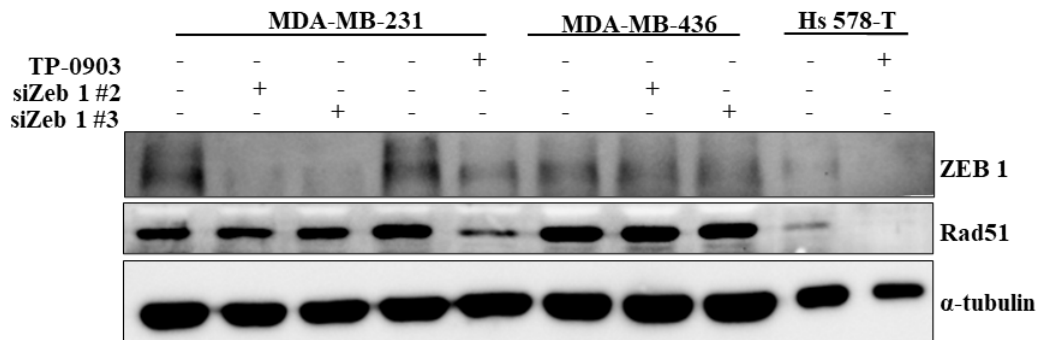
Supplementary Figure S20. TP-0903 and siRNA ZEB1 effect on Rad51. Removal of ZEB1 in MDA-MB-231 and MDA-MB-436 did not affect Rad51. TP-0903 treatment after 72 h suppressed Rad51 in both MDA-MB-231 and Hs 578-T cells.